National Library of Canada
Bibliothèque nationale du Canada

Canadian Theses Service
Service des thèses canadiennes

Ottawa, Canada
K1A 0N4

NOTICE

The quality of this microform is heavily dependent upon the quality of the original thesis submitted for microfilming. Every effort has been made to ensure the highest quality of reproduction possible.

If pages are missing, contact the university which granted the degree.

Some pages may have indistinct print especially if the original pages were typed with a poor typewriter ribbon or if the university sent us an inferior photocopy.

Previously copyrighted materials (journal articles, published tests, etc.) are not filmed.

Reproduction in full or in part of this microform is governed by the Canadian Copyright Act, R.S.C. 1970, c. C-30.

AVIS

La qualité de cette microforme dépend grandement de la qualité de la thèse soumise au microfilmage. Nous avons tout fait pour assurer une qualité supérieure de reproduction.

S'il manque des pages, veuillez communiquer avec l'université qui a conféré le grade.

La qualité d'impression de certaines pages peut laisser à désirer, surtout si les pages originales ont été dactylographiées à l'aide d'un ruban usé ou si l'université nous a fait parvenir une photocopie de qualité inférieure.

Les documents qui font déjà l'objet d'un droit d'auteur (articles de revue, tests publiés, etc.) ne sont pas microfilmés.

La reproduction, même partielle, de cette microforme est soumise à la Loi canadienne sur le droit d'auteur, SRC 1970, c. C-30.

NL-339 (r. 88/04)

Canada

THE UNIVERSITY OF ALBERTA

Dynamics of the fcc-hcp ^{4}He Transformation

by

K.A. McGreer

A THESIS
SUBMITTED TO THE FACULTY OF GRADUATE STUDIES AND RESEARCH
IN PARTIAL FULFILMENT OF THE REQUIREMENTS FOR THE DEGREE
OF Doctor of Philosophy

Department of Physics

EDMONTON, ALBERTA
Spring 1988

Permission has been granted to the National Library of Canada to microfilm this thesis and to lend or sell copies of the film.

The author (copyright owner) has reserved other publication rights, and neither the thesis nor extensive extracts from it may be printed or otherwise reproduced without his/her written permission.

L'autorisation a été accordée à la Bibliothèque nationale du Canada de microfilmer cette thèse et de prêter ou de vendre des exemplaires du film.

L'auteur (titulaire du droit d'auteur) se réserve les autres droits de publication; ni la thèse ni de longs extraits de celle-ci ne doivent être imprimés ou autrement reproduits sans son autorisation écrite.

ISBN 0-315-42869-4

THE UNIVERSITY OF ALBERTA

RELEASE FORM

NAME OF AUTHOR K.A. McGreer

TITLE OF THESIS Dynamics of the fcc-hcp ^{4}He Transformation

DEGREE FOR WHICH THESIS WAS PRESENTED Doctor of Philosophy

YEAR THIS DEGREE GRANTED Spring 1988

Permission is hereby granted to THE UNIVERSITY OF ALBERTA LIBRARY to reproduce single copies of this thesis and to lend or sell such copies for private, scholarly or scientific research purposes only.

The author reserves other publication rights, and neither the thesis nor extensive extracts from it may be printed or otherwise reproduced without the author's written permission.

(SIGNED) Ken McGreer

PERMANENT ADDRESS:

202-10625-81 Ave
Edmonton Alberta
T6E 1Y1

DATED ....Jan.4........1988

THE UNIVERSITY OF ALBERTA

FACULTY OF GRADUATE STUDIES AND RESEARCH

The undersigned certify that they have read, and recommend to the Faculty of Graduate Studies and Research, for acceptance, a thesis entitled Dynamics of the fcc-hcp ^{4}He Transformation submitted by K.A. McGreer in partial fulfilment of the requirements for the degree of Doctor of Philosophy in Physics.

Franck
....
Supervisor

Oler
....

Michael L. Wayman

Goott
....

Horst Meyer
....
External Examiner

Date.....Dec 16 1987.....................

DEDICATION

To Anna,

ABSTRACT

This thesis is an investigation into the dynamics of the fcc-hcp transformation in ^{4}He. The dynamics was investigated by studying the morphology of the transformation, the kinetics of the transformation, transverse sound velocity changes preceding the hcp→fcc transformation, and attenuation of transverse sound near the transformation.

The transformation morphology was visually observed. Observed interactions between the interface and defects in the solid provided the most direct evidence that the transformation is martensitic. Observations of the transformation occurring by the migration of a single planar interface across the entire sample provided strong evidence that the transformation is a thermoelastic martensitic transformation. This also indicated that the samples were likely single crystals. The single planar interfaces had a preferred orientation. Some transformations occurred in which an interface rotated around a pivot. A model of the interface structure is presented and used to explain the above results. In this model, the interface consists of an array of coupled Shockley partial dislocations. Bands of different variants of the hcp phase were produced during rapid heating or cooling.

In a study of the fcc-hcp ^{4}He transformation kinetics, it was demonstrated that small temperature oscillations could produce small oscillations of the fcc-hcp interface.

This, along with the observation that little elastic force accumulated to oppose the transformation, indicated that the transformation was a Class I thermoelastic transformation. The transformation kinetics was dominated by the driving force that was required to activate an interface.

The velocity of transverse sound was measured as a function of temperature in ^{4}He at 1.1 and 1.5 kbar. As predicted by the quasi-harmonic approximation, the elastic constant decreased linearly with the thermal component of the internal energy. The rate of decrease was similar to that in other hcp materials. The transverse sound velocity did not soften sufficiently for a soft mode to play a role in the dynamics of the transformation.

The attenuation of transverse sound was measured at 1.5 kbar. The attenuation was generally higher in the fcc phase than in the hcp phase.

ACKNOWLEDGMENTS

I thank Dr. Franck for his enthusiasm, financial support, advice and supervision. Technical assistance and interest of Allan O'Shea was greatly appreciated. Kent Lundgren made valuable and appreciated contributions by video taping some of the transformations. The editorial assistance of Dawn McArthur was greatly appreciated. I thank my parents for their support and I thank Anna Cerri for her generous encouragement.

Scholarships from the National Research Council of Canada were gratefully acknowledged.

Table of Contents

Chapter Page

I. INTRODUCTION 1

A. DEFINITION OF MARTENSITIC PHASE TRANSFORMATION .. 1

B. FEATURES OF MARTENSITIC TRANSFORMATIONS 2

C. THERMOELASTIC MARTENSITE 6

D. PREVIOUS OBSERVATIONS ON THE fcc-hcp ^{4}He TRANSFORMATION 7

E. THIS STUDY 9

F. BIBLIOGRAPHY 11

II. OBSERVATIONS ON KINETICS OF THE fcc-hcp ^{4}He TRANSFORMATION 13

A. INTRODUCTION 13

Athermal Transformation Kinetics 13

Hysteresis 13

Stabilization 14

Previous Observations of the fcc-hcp Transformation Kinetics in ^{4}He 15

This Study 16

B. EXPERIMENT 16

High Pressure Cell 16

Crystal Preparation 18

Optical Method 18

Temperature Measurement and Control 21

C. RESULTS 22

D. DISCUSSION 25

E. SUMMARY 30

F. BIBLIOGRAPHY 42

III. OBSERVATIONS OF THE fcc-hcp ^{4}He TRANSFORMATION MORPHOLOGY 43

A. INTRODUCTION 43

B. THEORY 43

  Dislocations in fcc Crystals 43

  Dislocations in hcp Crystals 45

  The Fundamental Agent of the fcc-hcp Transformation 46

  Stacking Fault Formation 47

  Dislocation Models of the Interface Structure 48

  Array of Identical Shockley Partials as an Interface Model 49

  Array of Coupled Shockley Partials as an Interface Model 52

C. EXPERIMENT 57

  Visual Method 57

D. RESULTS 61

  Sample 1 62

  Sample 2 68

  Other Samples 73

E. DISCUSSION 74

F. SUMMARY 84

G. BIBLIOGRAPHY 128

IV. STUDY OF PRETRANSITION ACOUSTIC EFFECTS NEAR THE fcc-hcp ^{4}He TRANSFORMATION 130

A. INTRODUCTION 130

B. THEORY 131

  Acoustic Mode Softening and Homogeneous Nucleation 131

  Anomalous Dispersion and Heterogeneous Nucleation 140

C. EXPERIMENT 143

Introduction 143
The Acoustic High Pressure Cell 143
Ultrasonic Method 145
Data Acquisition 149
Sample Preparation 150
Calculation of Internal Energy 151
D. RESULTS 153
E. DISCUSSION 159
F. SUMMARY 165
G. BIBLIOGRAPHY 204
V. ATTENUATION OF TRANSVERSE SOUND AND THE fcc-hcp ^{4}He TRANSFORMATION 207
A. INTRODUCTION 207
B. EXPERIMENT 207
C. RESULTS 209
D. DISCUSSION 210
E. SUMMARY 211
F. BIBLIOGRAPHY 213
VI. CONCLUSIONS 214
VII. APPENDIX: Energy of a Dislocation Assembly 218

List of Tables

Table	Description	Page
3.1	S-N Relation	88
3.2	Visually Observed Transformations Sample 1	109
4.1	Measured Values of $\hat{C}_0$ and Γ in ^{4}He	197
4.2	Values of $\Gamma_{\alpha\beta}$ in hcp Materials	202

List of Figures

Figure	Description	Page
1.1	^{4}He fcc-hcp Phase Diagram	10
2.1	Ellipse of Polarization	31
2.2	Thermal Cycling in ^{4}He at 1.2 kbar a) (top) run 1 b) (bottom) run 2	32
2.3	Thermal Cycling in ^{4}He at 1.2 kbar a) (top) run 3 b) (bottom) run 4	33
2.4	Thermal Cycling in ^{4}He at 1.2 kbar a) (top) run 5 b) (bottom) run 6	34
2.5	Thermal Cycling in ^{4}He at 1.2 kbar a) (top) runs 1-6 b) (bottom) small transformation loops	35
2.6	Thermal Cycling in ^{4}He at 1.3 kbar a) (top) run 1 b) (bottom) run 2	36
2.7	Thermal Cycling in ^{4}He at 1.3 kbar a) (top) run 3 b) (bottom) run 4	37
2.8	Thermal Cycling in ^{4}He at 1.3 kbar a) (top) run 5 b) (bottom) run 6	38
2.9	Thermal Cycling in ^{4}He at 1.3 kbar a) (top) run 7 b) (bottom) run 8	39
2.10	Traces of the Transformation Driven by Elastic Forces a) (top) in ^{4}He at 1.2 kbar b) (bottom) in ^{4}He at 1.3 kbar	40
2.11	Activation Barrier Dependence on Time	41
3.1	a) Thompson Tetrahedron b) hcp Double-tetrahedron	87
3.2	Kink Migration in Dislocations	90
3.3	Model of Identical Partials	92

3.4 ISPA Model of Interface Structure Accommodated by
a) surface relief 94
b) elastic stress 96
c) slip 98
d) twinning 100
e) band formation 102

3.5 Model of Coupled Partials 104

3.6 CSPA Model of Interface Structure 106

3.7 Advance of a CSPA by Kink Formation 108

3.8 Transformations Occurring at 12:40 & 12:42 110

3.9 Transformations Occurring at 12:44 & 12:46 111

3.10 Transformations Occurring at 12:48 & 12:51 112

3.11 Transformation Occurring at 12:53 113

3.12 Transformations Occurring at 12:59 & 1:05 114

3.13 Transformations Occurring at 1:10 & 1:18 115

3.14 Transformations Occurring at 1:29 & 1:31 116

3.15 Transformations Occurring at 1:32, 1:33 & 1:42 117

3.16 Transformations Occurring at 1:45 & 1:47 118

3.17 Eight Interfaces in the Preferred Orientation 119

3.18 Planar Interface in Sample 2 120

3.19 Defect Pinning of the Interface 121

3.20 Rotating Interface 122

3.21 Partial Transformation Preceding the Formation of Bands 123

3.22 Formation of Bands 124

3.23 Continued Formation of Bands 125

3.24 Fading of Bands 126

3.25 Bands in Two Orientations 127

4.1 Acoustic High Pressure Cell 166

4.2 Electronics for Absolute Velocity Measurement 167

4.3 Electronics for Relative Velocity Measurement 168

4.4 Internal Energy Dependence on Temperature 169

4.5 Velocity Dependence on Temperature in Sample 1A run1 170

4.6 $\hat{C}$ Dependence on u(T) in Sample 1A run1 171

4.7 $\hat{C}$ Dependence on u(T) in Sample 1A run2 172

4.8 $\hat{C}$ Dependence on u(T) in Sample 1B 173

4.9 $\hat{C}$ Dependence on u(T) in Sample 2A 174

4.10 $\hat{C}$ Dependence on u(T) in Sample 3A 175

4.11 $\hat{C}$ Dependence on u(T) in Sample 4A 176

4.12 $\hat{C}$ Dependence on u(T) in Sample 4B 177

4.13 $\hat{C}$ Dependence on u(T) in Sample 5A 178

4.14 $\hat{C}$ Dependence on u(T) in Sample 5B 179

4.15 $\hat{C}$ Dependence on u(T) in Sample 5C 180

4.16 $\hat{C}$ Dependence on u(T) in Sample 5D run1 181

4.17 $\hat{C}$ Dependence on u(T) in Sample 5D run2 182

4.18 $\hat{C}$ Dependence on u(T) in Sample 5E 183

4.19 $\hat{C}$ Dependence on u(T) in Sample 6A 184

4.20 $\hat{C}$ Dependence on u(T) in Sample 6B 185

4.21 $\hat{C}$ Dependence on u(T) in Sample 6C 186

4.22 $\hat{C}$ Dependence on u(T) in Sample 7A 187

4.23 $\hat{C}$ Dependence on u(T) in Sample 7B 188

4.24 $\hat{C}$ Dependence on u(T) in Sample 8A 189

4.25 $\hat{C}$ Dependence on u(T) in Sample 9A 190

4.26 $\hat{C}$ Dependence on u(T) in Sample 9B run1 191

4.27 $\hat{C}$ Dependence on u(T) in Sample 9B run2 192

4.28 $\hat{C}$ Dependence on u(T) in Sample 10A 193

4.29 $\hat{C}$ Dependence on u(T) in Sample 10B 194

4.30 $\hat{C}$ Dependence on u(T) in Sample 10C run1 195

4.31 $\hat{C}$ Dependence on u(T) in Sample 10C run2 196

4.32 Distribution of Values of $\hat{C}_0$ in ^{4}He at 1.5 kbar 198

4.33 Distribution of Values of Γ in ^{4}He at 1.5 kbar 199

4.34 Transverse Mode Elastic Constant in ^{4}He at Several Pressures 200

4.35 $\hat{C}_0$ Dependence on Γ in ^{4}He at 1.1 and 1.5 kbar 201

5.1 Distribution of Measured Values of Attenuation of Transverse Sound a) in hcp ^{4}He b) in fcc ^{4}He 212

I. INTRODUCTION

A. DEFINITION OF MARTENSITIC PHASE TRANSFORMATION

H.M. Howe coined the term "martensitic transformation" to honor the pioneering work of Adolf Martens on martensitic steels.[1] Since then, "martensitic transformation" has taken on a more general meaning and a variety of definitions have been proposed. The following definition, adopted from Nishiyama[2] and Wayman[3], encompasses the core of all definitions of "martensitic transformation": a solid-solid structural transformation that occurs by the cooperative displacement of atoms.[4] Here, "cooperative displacement" suggests that the displacements are spatially correlated to some extent and occur in some kind of orderly sequence. To emphasize the cooperative nature of the displacement by way of a metaphor, Frank[5] described martensitic transformations as "military transformations" and transformations in which the atomic displacements are relatively independent as "civilian transformations".

While the above definition imposes restrictions only on microscopic features (namely the correlation and sequence of the atomic displacements), other proposed definitions have included restrictions on the macroscopic features of morphology and the kinetics. Cohen, *et al.* ‘ and Owen’ suggested that the definition require that the transformation kinetics be dominated by strain energy and that the shear strain be large. Christian‘ suggested that the definition explicitly prohibit transformations with kinetics requiring thermal activation. The complexity and variety of kinetics and morphology of martensitic transformations make it difficult and undesirable to incorporate such features into the definition.’ Consequently, the concise definition used by Wayman and by Nishiyama is considered to be the most suitable.

---

[1] E.R. Petty, "Introduction", in Martensite - Fundamentals and Technology, E.R. Petty ed., (Longman, London, 1970).

[2] Z. Nishiyama, Martensitic Transformations, (Academic Press, New York, 1978).

[3] C.M. Wayman, "Martensitic Transformations" Encyclopedia of Materials Science and Engineering, M.B. Bever ed., (MIT Press, Cambridge Massachusetts, 1986), P. 2736.

[4] The only change is my usage of "displacement of atoms", which I believe to describe the intended meaning more precisely than "movement of atoms".

[5] F.C. Frank, NPL Conf. Relation Between Structure Stength Met. Alloys, (H.M. Stationary Office, London, 1963). P. 248

B. FEATURES OF MARTENSITIC TRANSFORMATIONS

The cooperative nature of the atomic displacements causes certain features to appear in martensitic transformations. It is generally agreed that the following features are present in all martensitic transformations: a diffusionless transformation process, a lattice orientation

---

‘ M. Cohen, G.B. Olson, P.C. Clapp, Proc. ICOMAT-79, Cambridge Mass, P. 1 (1979).

’ W.S. Owen, "Martensitic Transformation" in Encyclopedia of Materials Science and Engineering, M.B. Bever ed., (MIT Press, Cambridge Massachusetts, 1986), P. 2736.

‘ J.W. Christian,"Martensitic Transformations: Crystallography", in Encyclopedia of Materials Science and Engineering, M.B. Bever ed., (MIT Press, Cambridge Massachusetts, 1986), P. 3496.

’ C.M. Wayman, "Martensitic Transformations: An Overview" in Proc. Intl. Conf. Solid→Solid Phase Transformations, H.I. Aaronson, D.E. Laughlin, R.F. Sekerka, C.M. Wayman eds., (The Metallurgical Society of AIME, 1981) P. 1119.

relation between parent and product crystals, a planar, coherent or semicoherent parent-product interface in the early stages of the transformation, and an invariant plane strain relation between the lattices. These features are discussed in turn below.

Martensitic transformations must be diffusionless in the sense that the displacement of atoms over distances larger than a lattice spacing must not be required. This is so because diffusion is regarded as a process that cannot occur cooperatively. This means that a martensitic transformation can have no change in chemical composition. While absence of diffusion in the transformation is a necessary characteristic of a martensitic transformation, it is not an exclusive characteristic. A massive transformation is diffusionless but not martensitic. Structural phase transformations in elemental solids are diffusionless.[10]

By lattice orientation relation or lattice correspondence it is meant that the crystallographic axes of the parent crystal have a definite relation to the axes of the product crystal. In cobalt, for example, the orientation relation for the hcp-fcc transformation has been shown to be:

$$\{111\}||\{0001\} \text{ and } [1\bar{1}0]||[11\bar{2}0]$$

This is called the Shoji-Nishiyama relation (S-N relation).

---

[10] G.A. Chadwick, *The Metallography of Phase Transformations*, (Butterworth, London, 1972).

It should be noted that this relation describes four distinct possible orientations of the hcp phase relative to the fcc phase that produces it. Each of the different orientations is called a "variant".

In the early stages of the transformation, interfaces between parent and product crystal have been observed to be semicoherent or fully coherent. The fact that atomic displacement must be cooperative along the interface seems to require coherent semicoherent planar interfaces. The plane of the interface is called the "habit plane". The habit plane is not necessarily the plane of lattice correspondence and the habit plane may have irrational indices.

A structural phase transformation can be described crystallographically as the formation of a product lattice through the application of a deformation tensor to the parent lattice. Homogeneous deformation can be described as the application of the same deformation tensor to every unit cell. When the unit cell has more that one atom, each atom within the unit cell may have a different displacement, but each atom must have the same displacement as the corresponding atom in another cell. The relative atomic displacement within a unit cell is called an "atomic shuffle".

An invariant plane strain is a strain in which there is at least one lattice plane that does not get distorted or rotated by the transformation. An invariant plane strain is required in a martensitic transformation in order to preserve the coherency of the interface without involving diffusion. Ideally, a martensitic transformation would have a coherent parent-product interface that would correspond to an invariant plane. Usually, a lattice invariant deformation (which need not be an invariant plane strain) is required in addition to the lattice distortive deformation (which is, at least approximately, an invariant plane strain). Thus, the habit plane is usually only semicoherent and lies close to the invariant plane of the lattice distortive deformation. Due to the lattice invariant strain (which may be slip or twinning), the macroscopic strain is different from the lattice distortive strain

The homogeneous deformation required to produce an fcc→hcp transformation in which the S-N relation holds is relatively simple. The required strain is a shear of ~19.5° in a $[11\bar{2}]$ direction. This is an invariant plane strain (the {111}||{0001} plane is invariant) and no lattice distortive strain is required if the hcp axis ratio is the ideal ratio. Atomic shuffles are required on every second {111}||{0001} plane. It should be kept in mind that a description of the deformation required in a martensitic transformation does not entail a description of a mechanism for the transformation.

The following kinetic features are common, but not essential, properties of martensitic transformation: athermal transformation kinetics, hysteresis, and the occurrence of stabilization (both mechanical and thermal).

C. THERMOELASTIC MARTENSITE

In its original usage by Kurdjumov and Khandros[11] thermoelastic martensite (TEM) referred to an isolated martensitic plate whose chemical driving force was balanced by an opposing elastic stress such that when the reverse transformation was conducted the interface would retrace its course without hysteresis. Present usage of "TEM transformation" has relaxed from the ideal of a transformation without hysteresis to a tranformation with little hysteresis. Olson and Cohen[12] maintain that elastic and chemical forces must at least be nearly in balance for the term "TEM" to apply. Nishiyama[13] ascribed the essential feature of TEM to be the presence of a reversible interface during the martensitic transformation. Wayman[14] ascribed the essential features of TEM to be a mobile interface (during formation and reversal) and a low driving force. It was recognized that materials that frequently had mobile interfaces did not *always* have mobile interfaces; low cooling rates, interruption of the progress of the interface, or self-accomodation processes could immobilize the interface (*i.e.* stabilization can occur). Nevertheless, these materials were considered to be TEM materials. Wayman ascribed the following characteristics to be associated with TEM: small hysteresis, reversibility of a specific interface in consecutive transformations, and reproduction of crystallographic orientation in consecutive transformation. Dunne and Wayman[15] divided TEM tranformations into two classes, namely: "Class I" and "Class II". In Class II, the athermal width is large because accumulated elastic strain energy opposes the chemical driving force and it is likely important for the material to have a high elastic limit (sometimes ascribed to the fact that the material is ordered). In Class I, the athermal width is small and the following factors appear to be requirements for TEM: small chemical driving force, small shear strain, and small volume change. According to Olson and Cohen's definition of TEM, only Class II TEM can be properly called TEM. Wayman's terminology will be used in this thesis.

---

[11] G.V. Kurdjumov and L.G. Khandros, Dokl. Acad. Naak SSSR, 66, 211 (1949).

[12] G.B Olson and M. Cohen, Scripta Met., 10, 359 (1976).

[13] Z. Nishiyama, Martensitic Transformations, (Academic Press, New York, 1978).

[14] C.M. Wayman, "Martensitic Transformations: An Overview" in Proc. Intl. Conf. Solid→Solid Phase Transformations, H.I. Aaronson, D.E. Laughlin, R.F. Sekerka, C.M. Wayman eds., (The Metallurgical Society of AIME, 1981), P. 1119.

D. PREVIOUS OBSERVATIONS ON THE fcc-hcp ^{4}He TRANSFORMATION

The fcc-hcp phase transformation was first observed by Dugdale and Simon[16]. They attributed a specific heat anomaly to a first order phase transition, and traced the phase line between the 1.1 kbar and 2.2 kbar. The low temperature phase, hcp, had been identified in an earlier x-ray study by

---

[15] D.P. Dunne and C.M. Wayman, Metall. Trans., 4, 147 (1973).

[16] J.S. Dugdale and F.E. Simon, Proc. R. London Ser. A, 218, 291 (1953).

Keesom and Taconis[17]. Dugdale and Simon speculated that the high temperature phase was the fcc phase. This was later established to be true through the x-ray diffraction studies of Mills and Schuch.[18]. Theoretical predictions of the phase line by Holian *et al.*[19] stimulated interest in determining the phase line with greater accuracy and extending it to higher pressures. Franck[20] extended the phase line to 4 kbar and Franck and Daniels[21] extended it further to 9 kbar. The phase diagram showing the region investigated in this study is shown in fig. 1.1.

In a calorimetric study of the transformation, Franck noted that the transformation had an athermal transition width and hysteresis. These kinetic factors suggested that the transformation was a martensitic transformation. Franck and Daniels found that consecutive fcc→hcp transformations produced hcp crystals that appeared to be in the same orientation (provided that the transitions went to completion and that the fcc crystal was not allowed to anneal). The reproducibility of the c-axis was direct evidence for the existence of an orientation relation between the parent and product crystals. This supported the assertion that the transformation was martensitic.

---

[17] W.H. Keesom and K.W. Taconis, Physica, 5, 161 (1938).
[18] R.L. Mills and A.F. Schuch, Phys. Rev. Lett., 6, 263 (1961).
[19] B.L. Holian, W.D. Gwinn, A.C. Luntz, and B.J. Alder, J. Chem. Pysys., 59, 5444 (1973).
[20] J.P. Franck, Phys. Rev. B, 22, 4315 (1980).
[21] J.P. Franck and W.B. Daniels, Phys. Rev. B, 24, 2456 (1981).

The phase line and kinetics of the fcc-hcp ^{3}He transformation is similar to that in the fcc-hcp ^{4}He transformation.[22] [23] The triple point of ^{3}He is 17.65 K and 1.56 kbar. The hysteresis is 160 mK near the triple point and 900 mK at 6.35 kbar.

E. THIS STUDY

This thesis was dedicated to learning more about the dynamics of the fcc-hcp phase transformation. Although microscopic observations were impossible, inferences of the microscopic dynamics of the transformation were made possible through careful investigations of the kinetics of the transformation, the morphology of the transformation, and the temperature dependence of the transverse sound velocity preceding the transformation.

---

[22] J.P. Franck, Phys. Rev. Lett, 7, 435 (1961).
[23] M.G. Ryschkewitch, J.P. Franck, B.J. Duch and W.B. Daniels, Phys. Rev. B, 26, 5276 (1982).

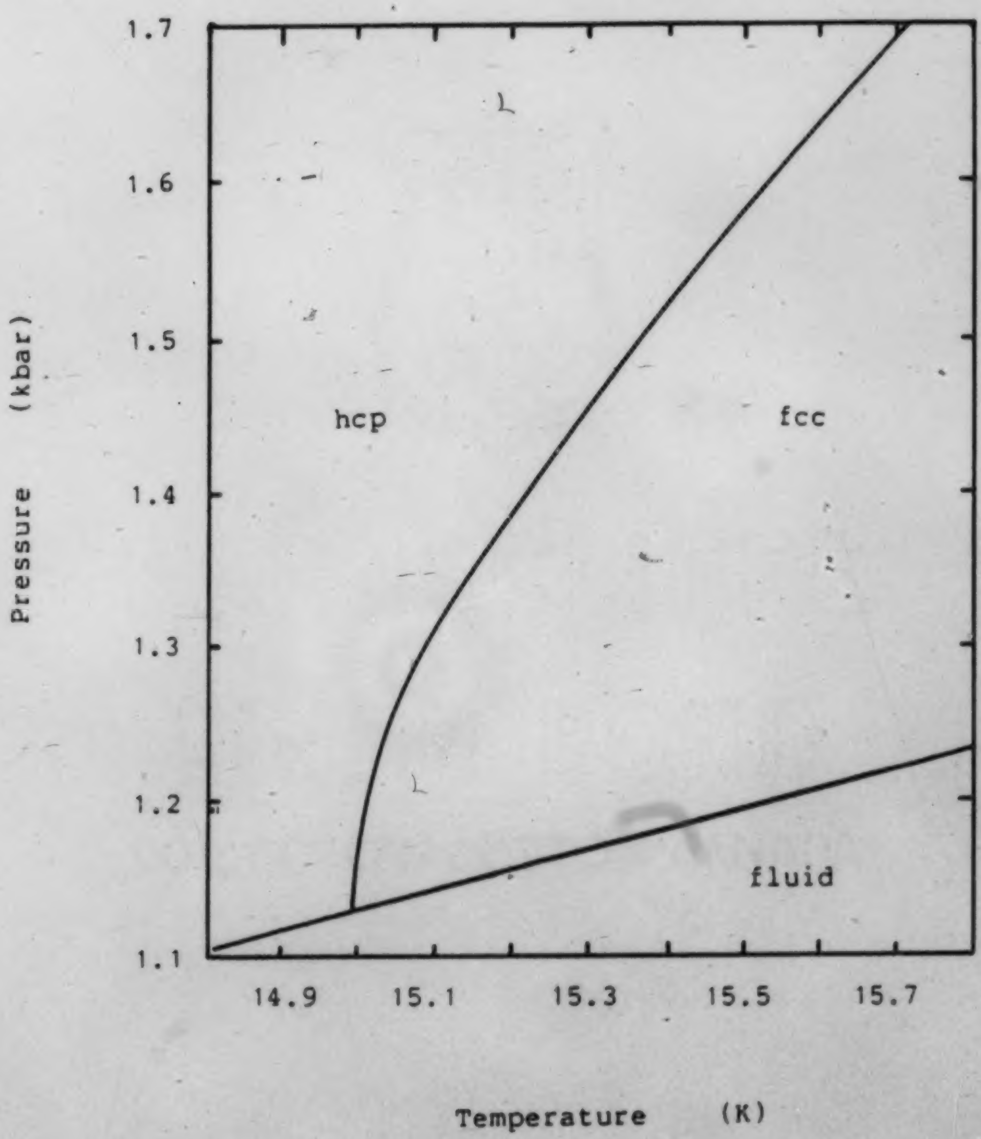

Fig. 1.1 ⁴He fcc-hcp Phase Diagram

F. BIBLIOGRAPHY

Chadwick, G.A., The Metallography of Phase Transformations, (Butterworths, London, 1972).

Christian, J.W.,"Martensitic Transformations: Crystallography", in Encyclopedia of Materials Science and Engineering, M.B. Bever ed., (MIT Press, Cambridge Massachusetts, 1986), P. 3496.

Christian, J.W.,The Theory of Transformations in Metals and Alloys, (Pergamon Press, New York, 1965).

Christian, J.W., Proc. Roy. Soc. A, 206, 51 (1951).

Cohen M., Olson G.B., Clapp P.C., Intl. Conf. on Martensitic Transformations, Cambridge Mass, P. 1 (1979).

Dugdale, J.S., and Simon, F.E., Proc. R. London Ser. A, 218, 291 (1953).

Dunne, D.P. and Wayman, C.M., Metall. Trans, 4, 147 (1973).

Franck, J.P., Phys. Rev. Lett, 7, 435 (1961).

Franck, J.P. and Daniels, W.B, Phys. Rev. B, 24, 2456 (1981).

Franck, J.P., Phys. Rev. B, 22, 4315 (1980).

Frank, F.C., NPL Conf. Relation Between Structure Stength Met. Alloys, (H.M. Stationary Office, London, 1963) P. 248.

Holian, B.L., Gwinn, W.D., Luntz, A.C., and Alder, B.J., J. Chem. Phys., 59, 5444 (1973).

Keesom, W.H., and Taconis, K.W., Physica, 5, 161 (1938).

Kuhlmann-Wilsdorf, D., "Dislocations", in Physical Metallurgy, R.W. Cahn ed, (John-Wiley & Sons, New York, 1965).

Mills, R.L., and Schuch, A.F., Phys. Rev. Lett., 6, 263 (1961).

Nishiyama, Z.,Martensitic Transformations, (Academic Press, New York, 1978).

Petty, E.R., "Introduction", in Martensite - Fundamentals and Technology, E.R. Petty ed., (Longman, London, 1970).

Olson, G.B. and Cohen, M., Scripta Met., 10, 359 (1976).

Owen W.S., "Martensitic Transformation" in Encyclopedia of

Materials Science and Engineering, M.B. Bever ed., (MIT Press, Cambridge Massachusetts, 1986), P. 2736.

Ryschkewitch, M.G., Franck, J.P., Duch, B.J. and Daniels, W.B., Phys. Rev. b, 26, 5276 (1982).

Wayman, C.M., "Martensitic Transformations: An Overview" in Proc. Intl. Conf. Solid→Solid Phase Transformations, H.I. Aaronson D.E. Laughlin, R.F. Sekerka, and C.M. Wayman eds., (The Metallurgical Society of AIME, 1981), P. 1119.

Wayman, C.M., "Martensitic Transformations" Encyclopedia of Materials Science and Engineering, M.B. Bever ed., (MIT Press, Cambridge Massachusetts, 1986), P. 2736.

II. OBSERVATIONS ON KINETICS OF THE fcc-hcp ^{4}He TRANSFORMATION

A. INTRODUCTION

Athermal Transformation Kinetics

A typical feature of martensitic transformations is that growth of the martensitic product is not thermally activated. In an athermal transformation, the temperature determines the fraction of the material transformed. Typically, no material transforms during cooling until the sample reaches a particular temperature (the martensitic start temperature, M_s) which is lower than the equilibrium temperature (T_0). The transformation continues only with continued cooling and is complete when the martensitic final temperature (M_f) is reached. The difference between these temperatures is called the athermal width.

Hysteresis

If the reverse transformation occurs by a martensitic transformation as well, the kinetics are similar; the reverse transformation starts at the Austenitic start temperature (A_s) and completes at the Austenitic final temperature (A_f). The requirement of supercooling and superheating leads to a temperature hysteresis associated with the transformation. While there are martensitic transformations that do not have athermal transformation kinetics (*i.e.* isothermal martensitic transformation), a structural transformation with athermal kinetics is likely to be a martensitic transformation.

The hysteresis is due to the fact that there are impediments to the progress of the transformation. These impediments may include the following: a nucleation barrier, an interface activation barrier, or friction on a moving interface. Superheating/supercooling may be required to start the growth of a nucleus resting in the parent phase. Superheating/supercooling may be required to pull an interface away from pinning sites -that is, to overcome an interface activation barrier. Superheating/supercooling may be required to overcome the loss of energy if the moving interface dissipates energy (if there is friction[1] [2]).

Stabilization

Stabilization in some martensitic materials can occur when the temperature is held constant after the transformation has started but before the transformation has completed. After a time at constant temperature, continuation of the cooling/heating does not cause the immediate continuation of the transformation; rather, a degree of supercooling/superheating is required. This is referred to as thermal stabilization.

---

[1] H.C. Tong and C.M. Wayman, Scripta Met., 11, 341 (1977).
[2] G.B. Olson and M. Cohen, Scripta Met., 10, 359 (1976).

Previous Observations of the fcc-hcp Transformation Kinetics in ^{4}He

In a calorimetric study of the transformation, Franck[3] noted that the transformation had an athermal transition width and hysteresis. The hysteresis was measured as a function of pressure. It was found to increase from 30 mK at the triple point (1.1 kbar) to 1 K at 3.9 kbar. The athermal transition width was also found to increase from ~20 mK at 1.1 kbar to 100 mK at 3.9 kbar. These studies were done with heating and cooling rates of typically 10 to 17 mK/min. Franck and Daniels[4] used an optical method of observing the transformation to extend the results to higher pressures and higher heating/cooling rates. It was found that both the transition hysteresis and the athermal width of the transformation were independent of the heating/cooling rates within the range between .1 K/min and 6 K/min. At higher pressures both the hysteresis and the athermal width continued to increase with pressure; at 8.7 kbar the hysteresis was 2.8 K and the athermal width was 2 K. Thermal stabilization was observed. It was also observed that the transformation could occur isothermally over the course of several hours provided that the temperature was below M_s (for the fcc→hcp transformation) or above A_s (for the hcp→fcc transformation). The mechanism involved in this isothermal transformation was assumed to be different than the mechanism involved in the athermal transformation (the transformation that appeared to require an athermal width to be traversed). Furthermore, the isothermal transformation was assumed to not interfere with the athermal transformation provided that the heating/cooling rates were "not-too-small". The kinetic factors observed in these two studies suggested that the transformation was a martensitic transformation.

---

[3] J.P. Franck, Phys. Rev. B, 22, 4315 (1980).
[4] J.P. Franck and W.B. Daniels, Phys. Rev. B, 24, 2456 (1981).

This Study

Typically, experiments on martensitic transformations follow the transformation to completion in both cooling and heating. The result is an experimentally obtained hysteresis curve. Information about the kinetics of the fcc-hcp ^{4}He transformation that could not be obtained by the aforementioned approach was obtained in this study by the following experimental approach: after the transformation was started (by supercooling or superheating as usual) and before the transformation went to completion, temperature oscillations about the equilibrium temperature were produced.

B. EXPERIMENT

High Pressure Cell

The high pressure cell used for this experiment followed the design of Franck and Daniels[5]. The cell had an an aluminum outer body. A stainless steel cylindrical tube (with inside diameter of 2 cm) was pressed into the aluminum body. The solid helium was contained within a beryllium-copper cylindrical tube (with inside diameter of .48 cm) that was pressed into the stainless steel tube. The space for the helium inside the beryllium-copper tube was 1.3 cm long and was closed off at the end with cylindrical sapphires that served as optical windows. The windows were .24 cm thick and .63 cm in diameter and had their c-axis aligned parallel to the optical path within five minutes of arc to minimize the birefringence in the windows. Steel push pieces held the windows in place and sealed the ends of the cell. The push pieces restricted the optical aperture to .16 cm. The push pieces and the beryllium-copper rings they pressed against were coated with indium to seal the high pressure cell. The initial seal between the windows and the push pieces was provided by the force of springs inside the cell that pushed the windows against the push pieces. The seal was an unsupported area seal that was self-sealing at high pressures. The helium was admitted to the cell through a capillary attached to the cell with a cone seal. The helium was pressurized with an Aminco high pressure pump. The cell was mounted on an optical cryostat (Cryogenics Associates).

---

[5] J.P. Franck and W.B. Daniels, Phys. Rev. B, 24, 2456 (1981).

Crystal Preparation

The samples were grown from isotopically pure, research grade helium (Linde ultra high purity 99.999% ^{4}He). The impurities were less than 1ppm and the ^{3}He impurities were less than .002ppm. The samples were slowly grown at constant volume with the capillary blocked and annealed for two to four hours.

Optical Method

Phase changes in the solid helium were detected by an optical method that took advantage of the different optical properties of the two helium phases. The fcc phase is optically isotropic. An hcp crystal of ^{4}He is a uniaxial positive birefringent crystal with the optical axis along the c-axis. A light ray having an electric field normal to the optical axis is called an ordinary ray (o-ray) and the light has a velocity, v_o, that does not dependent on direction of ray. A light ray having an electric field in the principal plane (the plane containing both the optical axis and the light ray) is called an extraordinary ray (e-ray) and the light has a velocity, v_e, that depends on the direction of the ray. An arbitrary ray entering a plate of such a crystal will have its electrical field resolved onto two mutually perpendicular directions called "the principal axes" of the plate. Each electric field component will propagate at its own velocity so that the ray separates into an o-ray and an e-ray. The two rays emerging from such a plate will be out of phase. For this reason, such a plate is called a "retardation plate" or a "retarder". The phase difference, ϕ, of the two emerging rays is given by:

$$\phi=2\pi(n_e-n_o)_{max}(d/\lambda)\sin^2\gamma \tag{2.1}$$

where d is the thickness of the crystal, λ is the wavelength of the light, n_e is the index of refraction for the e-ray, n_o is the index of refraction for the o-ray, and $(n_e-n_o)_{max}$ is the maximum difference in the index of refraction (corresponding to propagation in the basal plane). The azimuthal angle, γ, is the angle between the c-axis and the z-axis (the direction of the optical path). The slow axis of the effective retardation plate is the projection of the c-axis onto the x-y plane. As linear polarized light passes through a retarder, it becomes elliptically polarized and the principal axes of the ellipse of polarization are parallel to the principal axes of the retarder.

In hcp ^{4}He, $(n_e-n_o)_{max}$ has been estimated for pressures between 1 kbar and 10 kbar by Franck and Daniels[6]. The estimate was based on low pressure measurements of Vos *et al.*[7] and theoretical expressions of Kronig and Sonnen[8]. The difference in indices of refraction at the densities used in this study was estimated to be 7×10^{-6}. The retardation for red light has a maximum (for $\gamma=\pi/2$) of about 50°.

---

[6] J.P. Franck and W.B. Daniels, Phys. Rev. B, 24, 2456 (1981).

[7] J.E. Vos, R.V. Kingma, F.J. van der Gaag, and B.S. Blaisse, Phys. Lett., 24A, 738 (1967).

[8] R. Kronig and R.K.M. Sonnen, Physica (Utrecht), 24, 432 (1958).

Linear polarized light from a helium-neon laser (Spectra Physics 145P) was passed through the solid helium in the cell. A polarizer placed immediately in front of the laser was used to control the intensity of the light entering the cell. The optical path (the z-axis) was along the axial direction of the cylindrical helium sample. The polarization state of the light emerging from the cell depended on the crystal structure and orientation as discussed above. The light emerging from the cell was passed through a linear polarizer (the analyzer). The transmitted intensity through a retardation plate between linear polarizers that make angles α and β with the slow axis of the retarder is given by[1]:

$$I=I_0[\ \cos^2(\alpha-\beta)\ -\sin(2\alpha)\sin(2\beta)\sin^2(\tfrac{1}{2}\phi)\ ] \qquad (2.2)$$

This light intensity was measured by a photodetector (Spectra Physics 404 power meter). The received light intensity depended on the amount of retardation and the orientation of the slow axis relative to the polarizers. The detector output (refered to as "the optical signal") was a linear function of the received light intensity and was plotted on a chart recorder.

Additional optical effects were produced by other objects in the optical path. The sapphire windows on the high pressure cell had their c-axes parallel to the z-axis to avoid birefringence; however, they exhibited stress birefringence and thus had an effect like that of retrardation plates. The glass cryostat windows, on the other hand, had no apparent optical effect. A more detailed calculation that accounted for the effect of the windows has been carried out by Crepeau, *et al*.[19].

---

[1] R.S. Longhurst, Geometric and Physical Optics, (Longman, London, 1973).

The relationship between the optical signal and the fraction of the helium in the hcp phase is extremely complex because it depends on the orientation of the interface. Polycrystalline samples are more complicated yet. However, during the transitions in which the optical signal changed monotonically with time, one could assume that the optical signal depended monotonically on the hcp fraction of helium.

Temperature Measurement and Control

Temperature was measured using a germanium resistance thermometer (Cryocal). The conductance of the thermometer was measured with a 4-point conductance bridge (SHE Potentiometric Conductance Bridge). The output of the bridge was plotted on the chart recorder (simultaneously with the optical signal) and later converted to a temperature from the calibration data provided by Cryocal.

Temperature control was done manually. Temperature was controlled through the current applied to a heater mounted on the cell. The task of producing an oscillation in the temperature about the equilibrium temperature during the progress of the transformation was very difficult. Before the transformation went to completion, the temperature had to be changed approximately 70 mK to reach the equilibrium temperature. Thermal delay times were often longer than the time the transformation took to complete. Thus, I had to anticipate the start of the transformation and initiate the temperature change very slightly in advance of the transformation. A further difficulty was the possibility of the transformation completing in the reverse direction after the temperature change had been initiated but before a complete temperature oscillation was completed. To prevent this, I had to accurately judge the magnitude as well as the timing of changes in applied heating power. Many attempts had to be made before a successful temperature oscillation was produced.

---

[19] R.H. Crepeau, O. Heybey, D.M. Lee, S.A. Strauss, Phys. Rev., 3A, 1162 (1971).

C. RESULTS

In two samples, temperature oscillations about the equilibrium temperature were produced while the transformation was in progress. The samples were solidified at pressures of 1.18 kbar and 1.31 kbar. The sample, at any instant in time, is represented by a point on a graph with the y-coordinate being the optical signal and the x-coordinate being the temperature. The curve on the graph is the locus of points representing the progress of the transformation. The progress of the transformation is illustrated in figures 2.1 to 2.4 (for the sample at 1.18 kbar) and in figures 2.5 to 2.8 (for the sample at 1.31 kbar).

In the sample at 1.18 kbar, the optical signal always increased during the fcc→hcp transformation and decreased during the hcp→fcc transformation. In the sample at 1.31 kbar, the optical signal always decreased during the fcc→hcp transformation and increased during the hcp→fcc transformation. This indicated that the optical signal depended monotonically on the amount of the hcp phase in both samples.

In each sample, small temperature oscillations produced oscillations in the amount of hcp phase. These small transformation cycles are illustrated by small closed loops in the curves in figures 2.1 to 2.8. For convenience, some of the loops from the sample at 1.18 kbar are plotted separately in fig. 2.4b. Transformation cycles could be produced with temperature cycles as small as 5 mK. Temperature oscillations only produced transformation cycles if the temperature oscillation was about a particular temperature (14.94 K for the 1.18 kbar sample and 15.01 K for the 1.31 kbar sample). This established the equilibrium temperature to be 14.94 K for the 1.18 kbar sample and 15.01 K for the 1.31 kbar sample. The equilibrium temperature is marked with a vertical line in figures 2.1 to 2.9. Transformation cycles were readily produced as long as the temperature cycling was not stopped.

Usually, the fcc→hcp transformation required the temperature to be below the equilibrium temperature and the hcp→fcc transformation required the temperature to be above the equilibrium temperature. This was true when the usual hysteresis curve was traversed; however, during the heating portion of a small transformation cycle, the hcp→fcc transformation sometimes started prior to heating to the equilibrium temperature. Similarily, the fcc→hcp transformation sometimes started prior to cooling to the equilibrium temperature. The sections of the curve illustrating this effect are shown in figure 2.9.

When the temperature was held constant for over one minute, superheating or supercooling was required to make the transformation continue. In fig. 2.10, the amount of superheating/supercooling required to start the transformation is plotted against the length of time since the end of the previous transformation. Longer holding times caused the sample to require more superheating/supercooling (*i.e.* the more stabilized it became). This was true whether the preceding transformation went to completion or not. Typically, after holding one phase for two minutes, superheating/supercooling by about 20 mK was required for the transition to proceed. After holding one phase for ten minutes the phase had to be superheated/supercooled by about 70 mK.

D. DISCUSSION

When the temperature is different from the equilibrium temperature, there is a chemical driving force that tends to drive the transition. The energy available to drive the fcc→hcp transformation is given by:

$$\Delta F = F_{fcc}-F_{hcp}, \qquad (3.2)$$

where F is the Helmholtz free energy. ΔF is zero at T_0 and since:

$$(\partial F/\partial T)_v = -S \qquad (3.3)$$

one gets:

$$\Delta F = -(S_{fcc}-S_{hcp})(T-T_0) \equiv -\Delta S(T-T_0) \qquad (3.4)$$

ΔS has been measured in solid helium[11] and is about 15 mJ/moleK in the pressure range from 1 to 2 kbar. This is about 1.2×10^4 erg/cm^{3}K for this pressure range.

The initial hcp→fcc transformation required superheating by 60 mK. This can be expressed as a chemical driving force of 7×10^2 erg/cm^3 or .7 mbar. It appears that the transition at these pressures generally requires a driving force on the order of 1 mbar to initiate the transformation.

---

[11] J.P. Franck, Phys. Rev. B, 22, 4315 (1980).

The transformation can progress only if the chemical driving force is greater than the frictional force. The difference between the driving force required for the fcc→hcp and the hcp→fcc portions of a cycle is an upper limit on twice the frictional force. Transformation cycles were produced with temperature oscillations as small as 5 mK. The difference between the driving force for the fcc→hcp and the hcp→fcc transformations in a cycle this small is .06 mbar. The friction force against the transformation in a cycle this small can be no more than .03 mbar. This is less than 5% of the driving force required to initiate the transformation. These results indicate that the frictional force on the interfaces during the progress of the transformation play a minor role (if any role at all) in the kinetics of the transformation. This implies that the activation barrier, rather than the friction force, plays the dominant role in the kinetics of the transformation.

To my knowledge, the only other transformation investigated by this proceedure has been the thermoelastic martensitic transformation in a Cu-Zn alloy[13]. The results for this Cu-Zn alloy are quite different than the results for solid helium; in Cu-Zn the transformation kinetics appear to be dominated by frictional forces.

The size of the activation barrier was found to depend on the history of the crystal. Once the transformation mechanism was active, it remained active even as the transformation was reversed. This was demonstrated by the fact that the transformation could be reversed with very little driving force. However, if the hcp fraction was held constant for ~~over a minute~~, the solid became stabilized and superheating or supercooling was required to reactivate the mechanism before the transformation continued. The amount of superheating/supercooling required to start the transformation increased with the length of time that the solid had been held before driving the transformation. This indicates that stabilization of the interface can occur when the interface is stationary and that the activation barrier energy increases with the time over which stabilization is allowed to occur. Figure 2.10 shows the activation energy increasing with stabilization time. The solid line is the exponential:

---

[13] I. Cornelis and C.M. Wayman, Scripta Met., 10, 359 (1976).

$$\left|\frac{\Delta F}{\Delta S}\right| = 70\,\mathrm{mK}\ [1-\exp(t/(5\ \mathrm{min.}))] \qquad (3.5)$$

This suggests that the time constant for the stabilization process is roughly 5 minutes. With sufficient time for stabilization, an interface required as large a driving force to drive it as the force required to initiate the transformation. This suggested that nucleation requires a "virtual interface" at the cell wall to surmount an activation barrier similar to the the activation barrier acting on an stabilized interface within the solid. The scatter of points in fig. 2.10 from a monotonic increasing function of time suggests that the the length of time that an interface has remained stationary is not the only factor influencing the energy of the activation barrier.

Stabilization may be due to the migration of defects to the interface. Stabilization due to the migration of impurity atoms to the interface has been been proposed as a mechanism for stabilization[13]. This appears unlikely to be the case here because the helium samples were exceptionally free of impurity atoms. However, dislocations may migrate to the interface and cause stabilization. Dislocations are known to cause stabilization in deformed materials.[14]

There were instances in which the transformation progressed a small amount when the chemical driving force was opposing the progress of the transformation. That is, in some cases, the fcc→hcp transformation started when the temperature was above T_0 and the hcp→fcc transformation started when the temperature was below T_0. This usually happened only very near the equilibrium temperature (*i.e.* when the chemical force opposing the transition was small) and during small temperature cycles that kept the interface mobile. These occurrences are illustrated in fig. 2.4b. Perhaps whenever the transformation progressed in one direction, it built up an elastic force that opposed it. As soon as the chemical driving force was reduced below the opposing elastic force, the elastic force caused the transformation to progress in the reverse direction in spite of the chemical driving force. The elastic driving force caused the transition only when the temperature was within 10 mK of the equilibrium temperature (where the chemical driving force had been reduced to .06 mbar). Elastic driving force was estimated to be equal to the chemical driving force at the point where the transformation started. It appears that the magnitudes of the elastic force only reached values of .06 mbar. This was 10% of the chemical driving force that was required to initiate the transformation. Since the chemical driving force is proportional to $T-T_0$, fig. 2.10 shows that the magnitude of the elastic force appeared to be largely independent of the amount of hcp phase.

---

[13] K.R. Kinsman and J.C. Shyne, Acta Met., 14, 1063 (1966): 15, 1527 (1967).

[14] Z. Nishiyama, Martensitic Transformations, (Academic Press, New York, 1978).

The elastic force did not accumulate greatly during the transition in solid helium. That is, the magnitude of the elastic force in the solid always remained a small fraction of the chemical driving force required to initiate the transformation. This was indicated by the fact that the elastic force was independent of the extent of the transformation that preceded the observation of the elastic force causing the transformation. Another indication of this was that the athermal width was often very small; that is, once the transformation was started it often progressed to completion rapidly and with little or no superheating/supercooling in addition to that required to start the transformation.

The high mobility of the interface in both directions of the fcc-hcp transformation is clearly indicated by the ability for very small chemical driving forces (.03mbar) to maintain the motion of the interfaces or to reverse the motion of a moving interface. This indicates that the fcc-hcp ^{4}He transformation is a thermoelastic martensitic phase transformation. Futhermore, since the elastic stress never accumulates sufficiently to dominate the kinetics, the transformation is a class I TEM phase transformation.

E. SUMMARY

The activation energy dominates the kinetics of the hcp-fcc transformation in ^{4}He and is an order of magnitude larger than the frictional force or the elastic force opposing the transformation. At 1.2 kbar, the driving force required to initiate the transformation is on the order of 1 mbar. The transformation is a class I thermoelastic martensitic phase transformation.

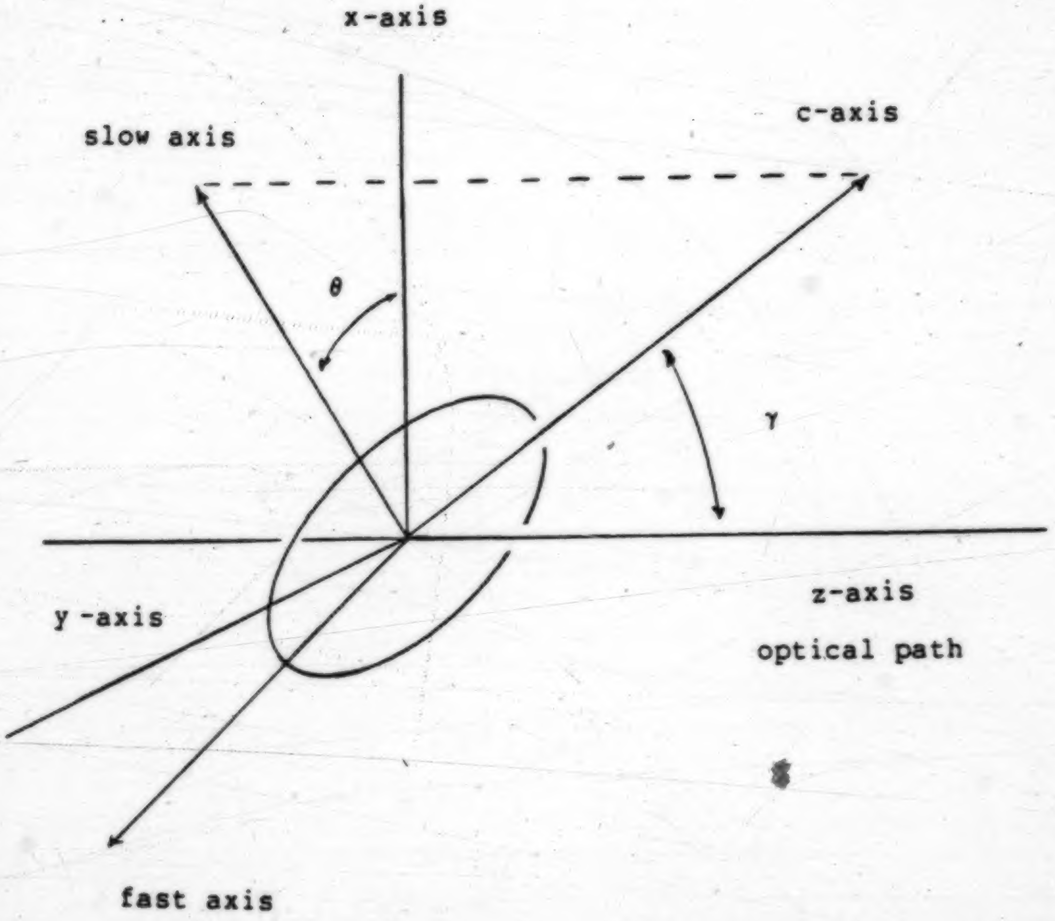
x-axis
slow axis
c-axis
θ
γ
y -axis
z-axis
optical path
fast axis

Fig. 2.1 Ellipse of Polarization

A retarder may be characterized by an ellispe of polarization. Light polarized along the semi-minor axis (the "slow axis") of the ellispe travels slower than light polarized along the semi-major axis (the "fast axis"). In hcp ⁴He, the slow axis is in the direction of the projection of the c-axis onto the plane that is perpendicular to the optical path (the z-axis in this figure).

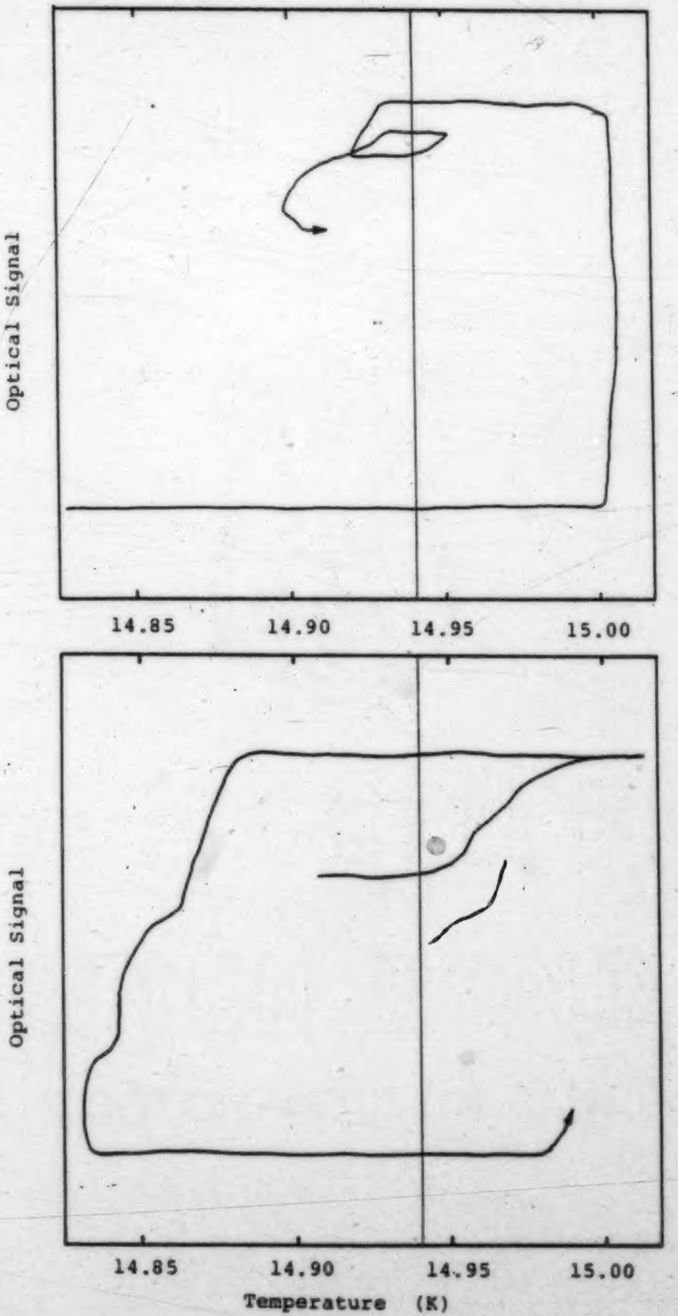

Fig. 2.2 Thermal Cycling in ^{4}He at 1.2 kbar
a) (top) run 1 b) (bottom) run 2

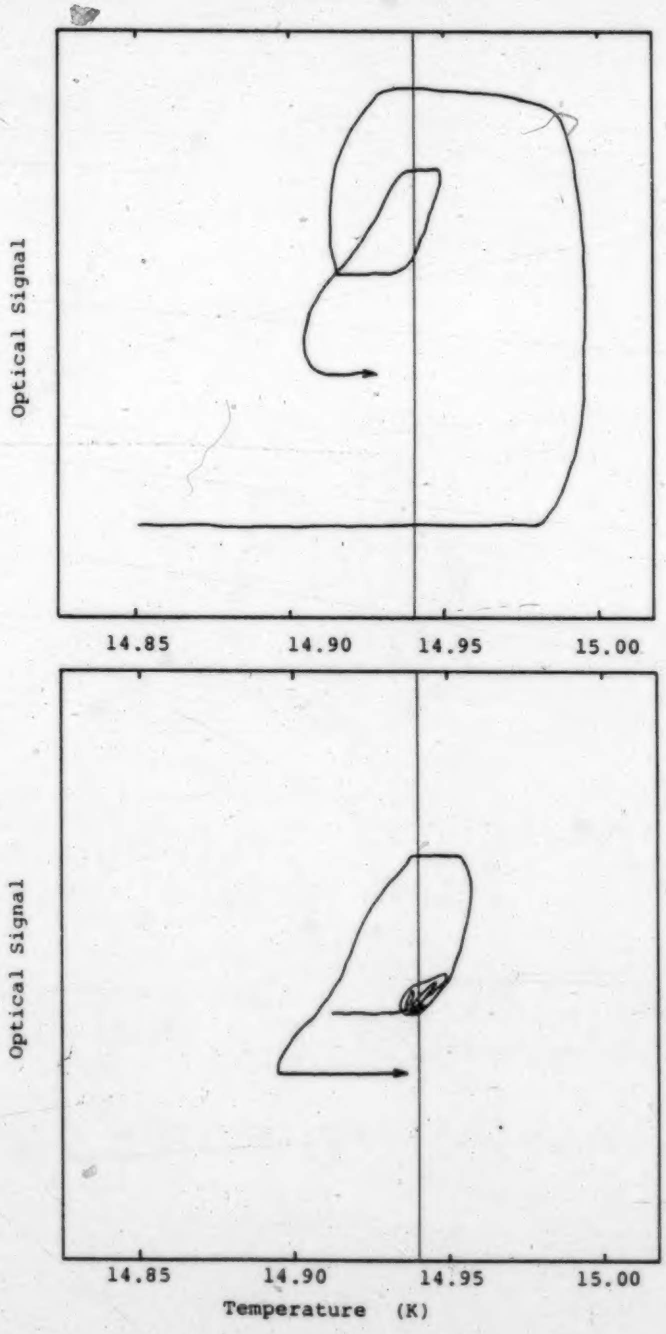

Fig. 2.3 Thermal Cycling in ^{4}He at 1.2 kbar
a) (top) run 3 b) (bottom) run 4

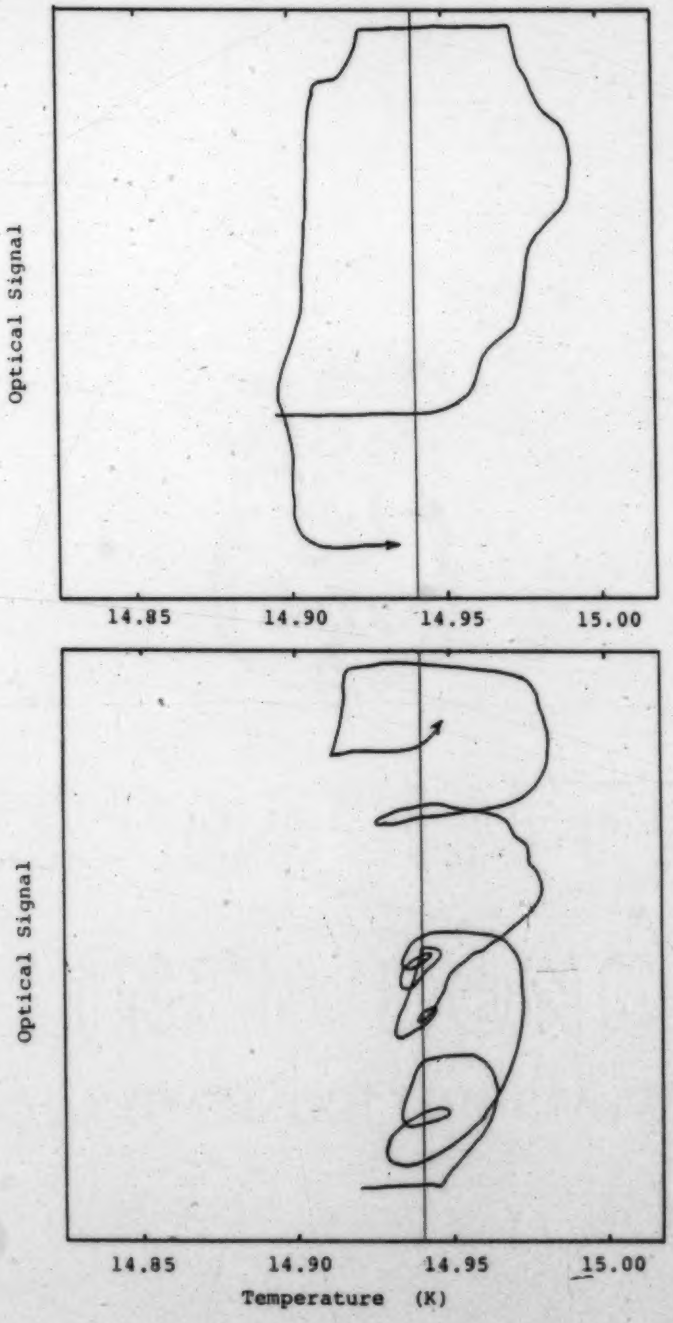

Fig. 2.4 Thermal Cycling in ⁴He at 1.2 kbar
a) (top) run 5 b) (bottom) run 6

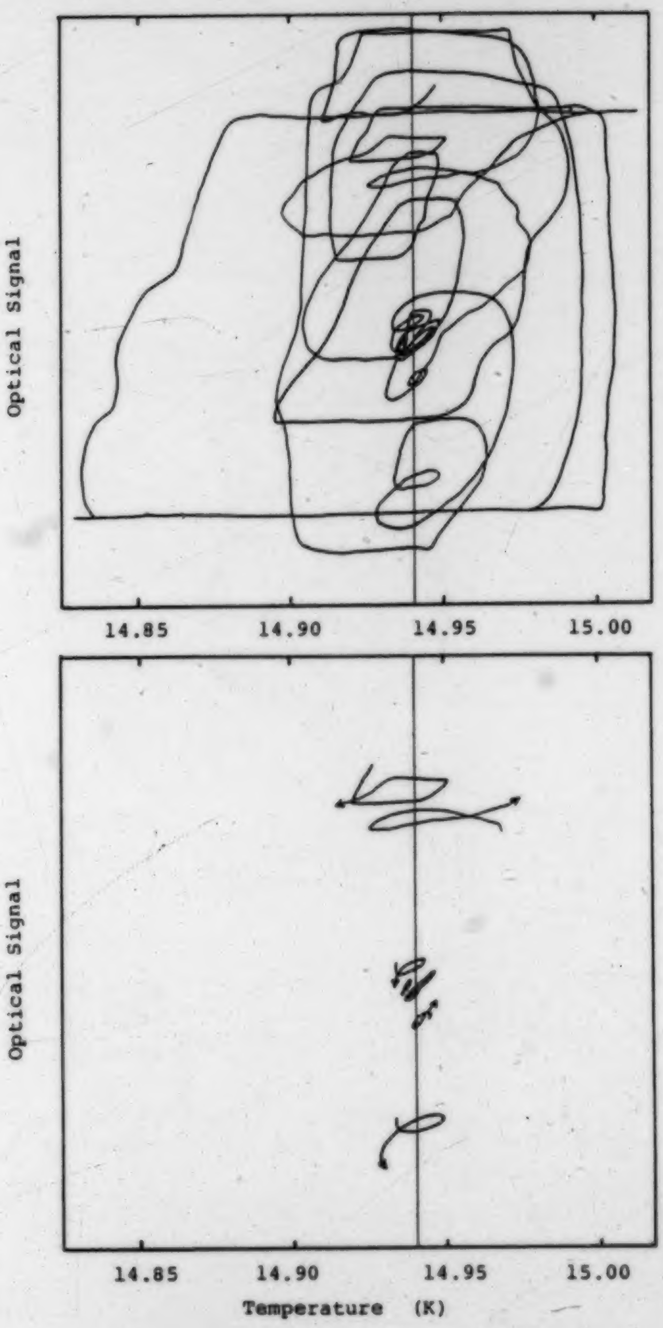

Fig. 2.5 Thermal Cycling in ^{4}He at 1.2 kbar a) (top) runs 1-6 b) (bottom) small transformation loops

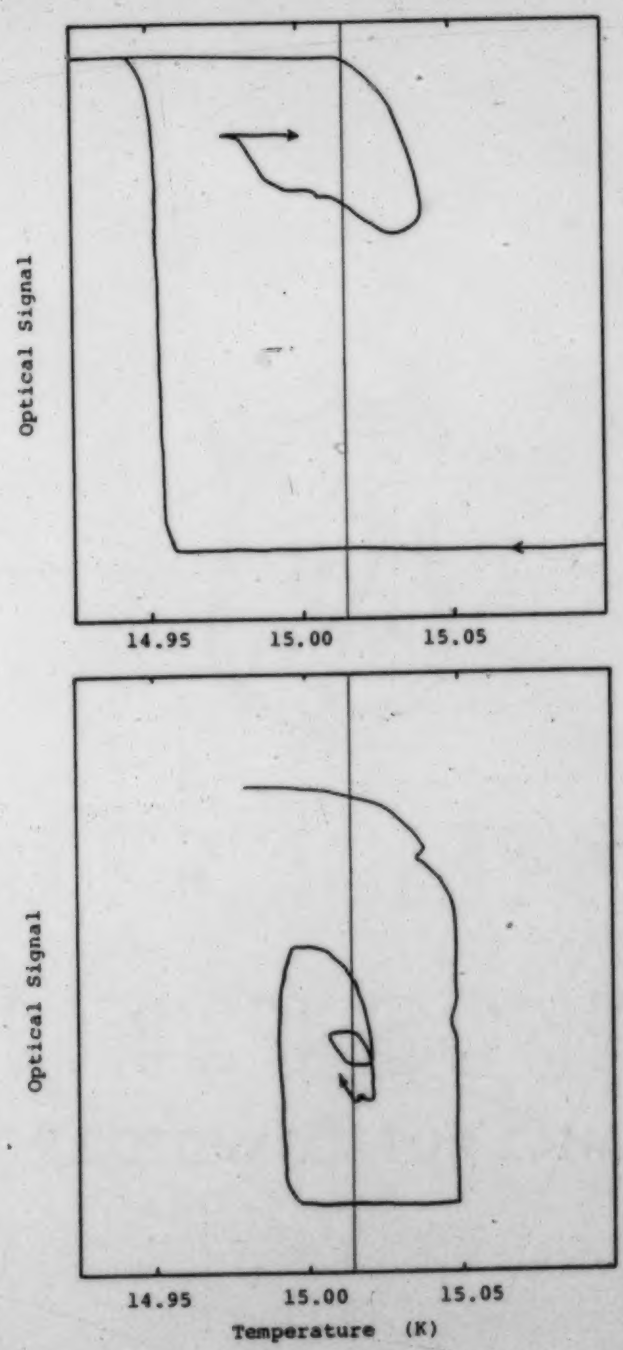

Fig. 2.6 Thermal Cycling in ^{4}He at 1.3 kbar
a) (top) run 1 b) (bottom) run 2

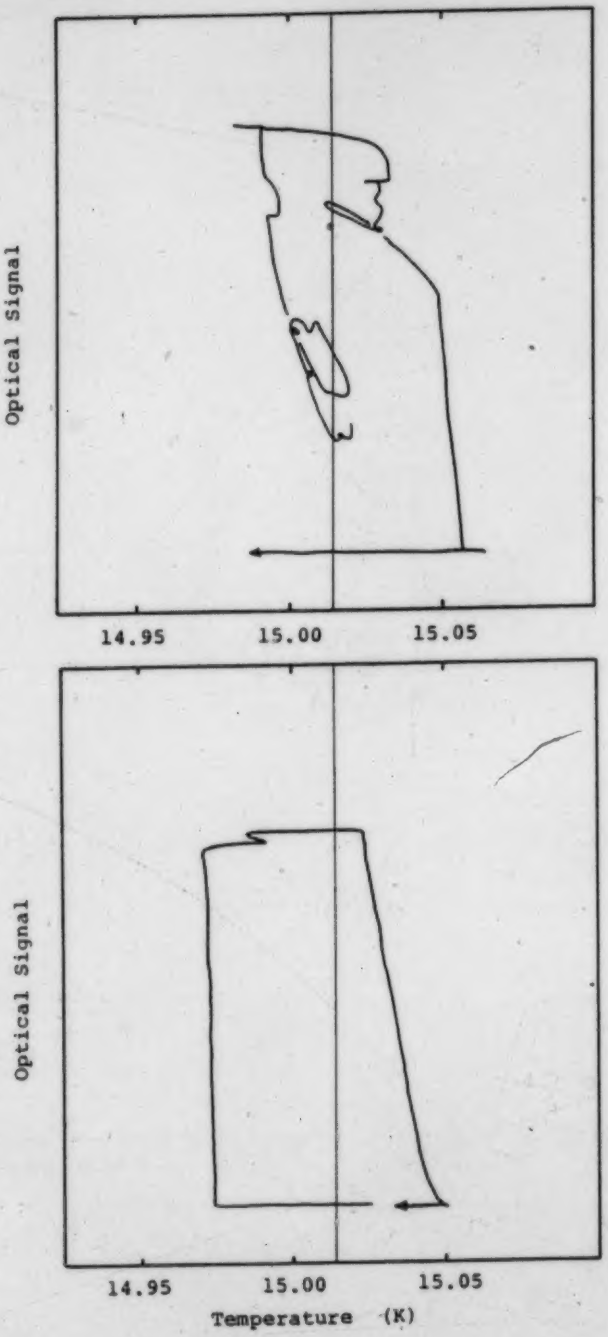

Fig. 2.7 Thermal Cycling in ^{4}He at 1.3 kbar
a) (top) run 3 b) (bottom) run 4

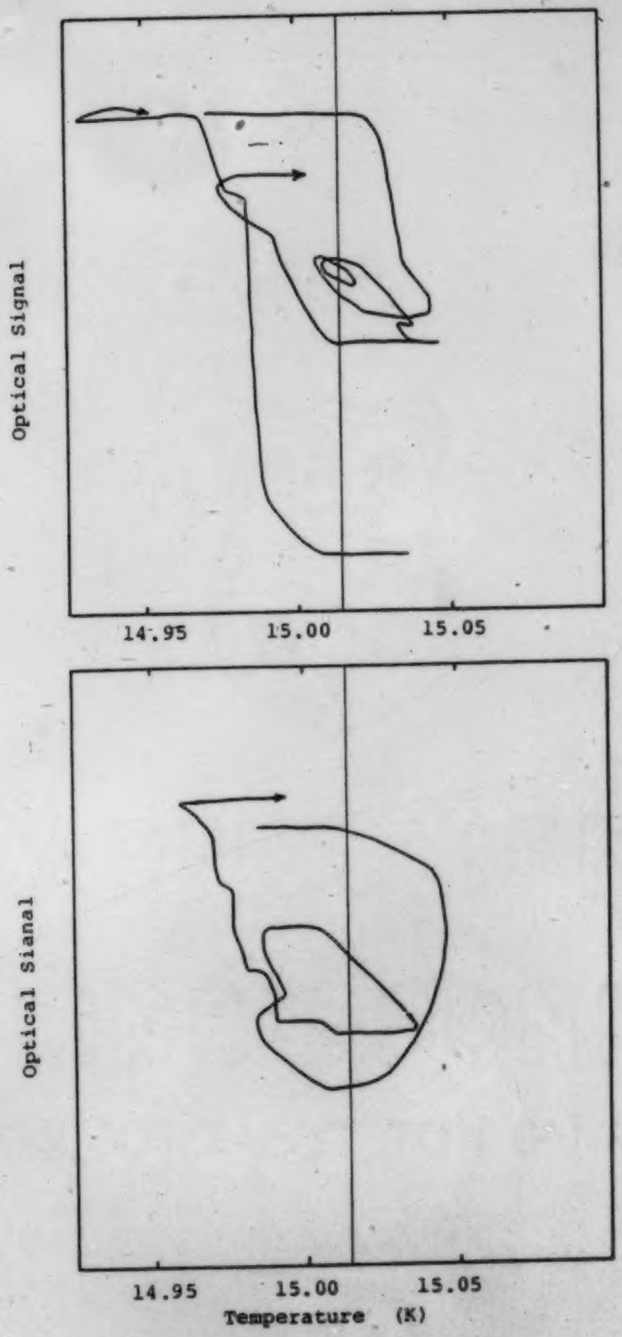

Fig. 2.8 Thermal Cycling in ^{4}He at 1.3 kbar
a) (top) run 5 b) (bottom) run 6

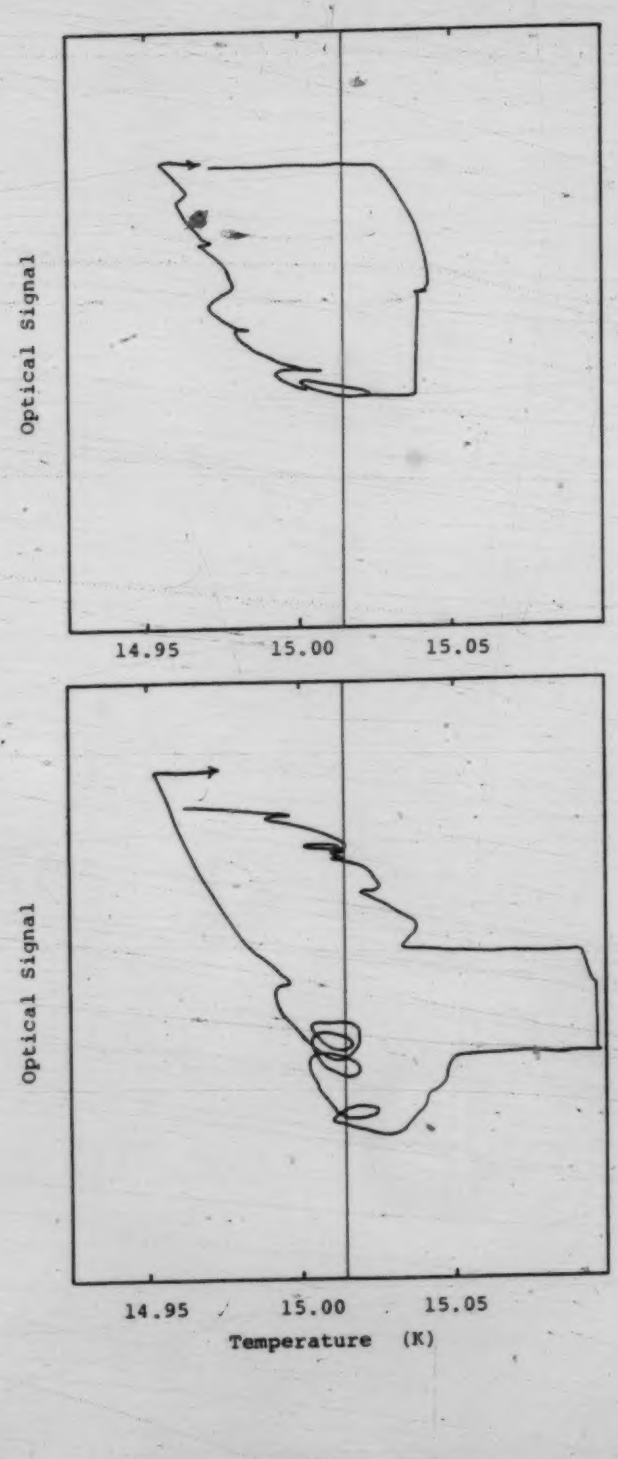

Fig. 2.9 Thermal Cycling in ^{4}He at 1.3 kbar
a) (top) run 7 b) (bottom) run 8

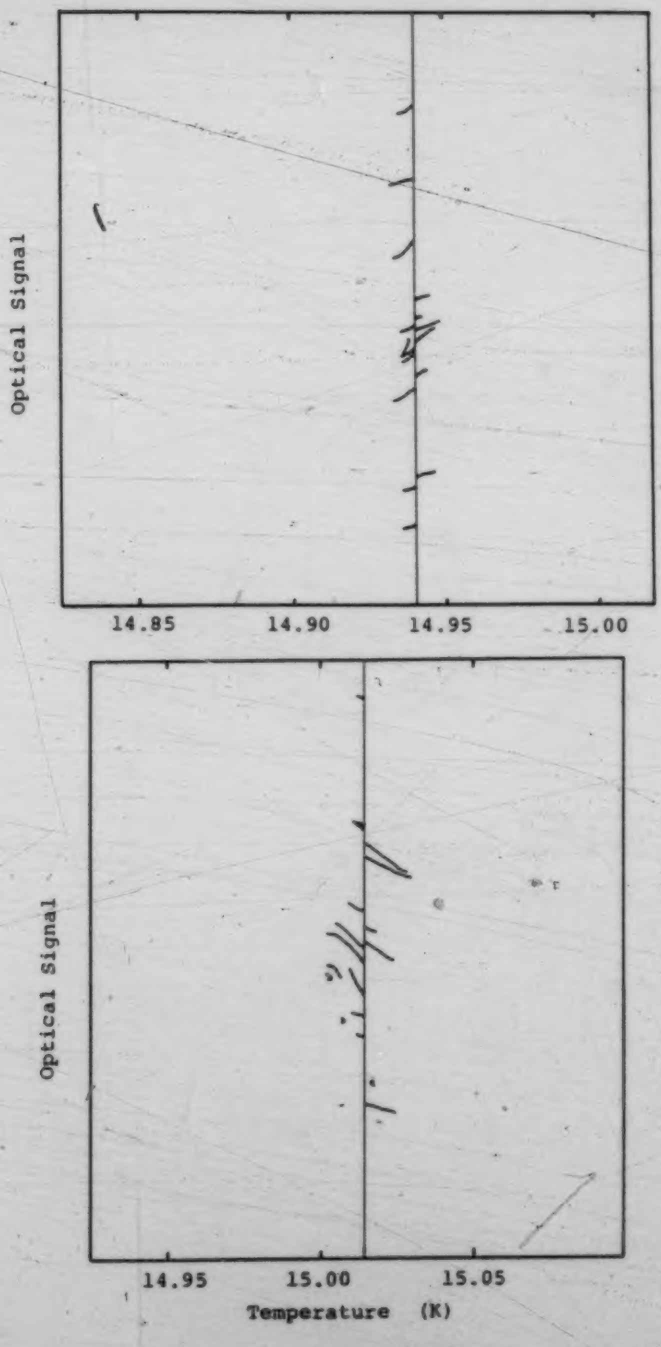

Fig. 2.10 Traces of the Transformation Driven by Elastic Forces
a) (top) in ⁴He at 1.2 kbar
b) (bottom) in ⁴He at 1.3 kbar

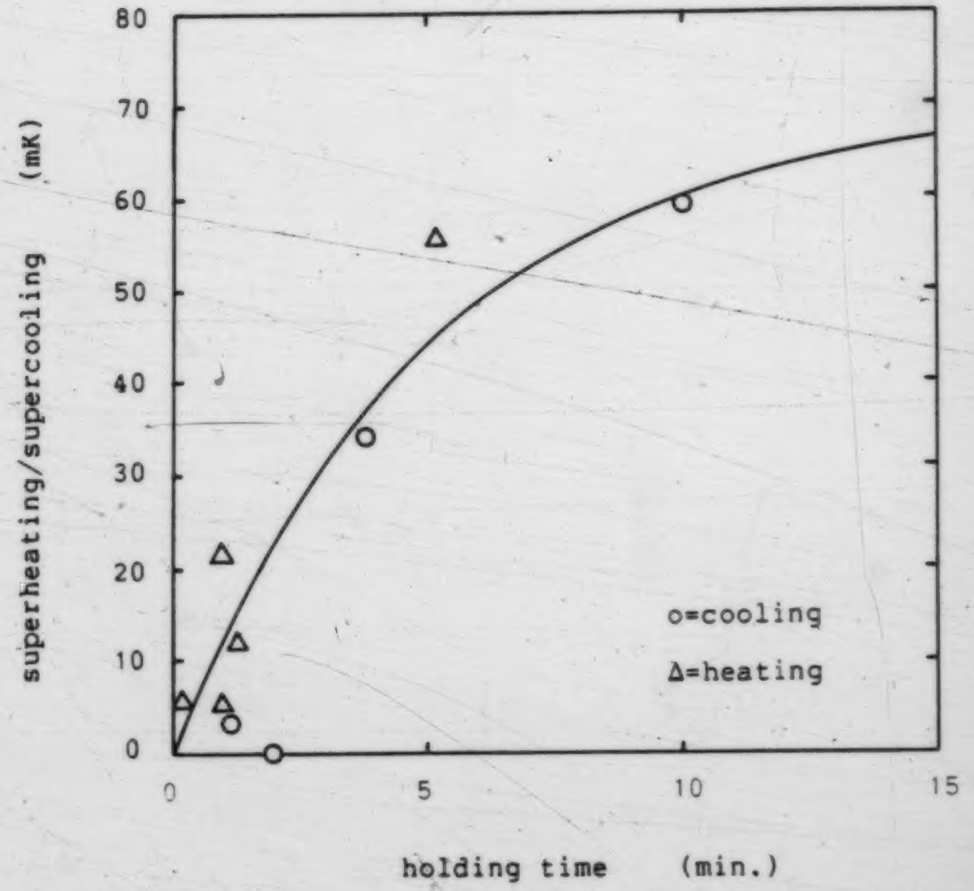

Fig. 2.11 Activation Barrier Dependence on Time

F. BIBLIOGRAPHY

Christian, J.W., The Theory of Transformations in Metals and Alloys, (Pergamon Press, New York, 1965).

Cornelis, I., and Wayman, C.M., Scripta Met., 10, 359 (1976).

Crepeau, R.H., Heybey, O., Lee, D.M., Strauss, S.A., Phys. Rev., 3A, 1162 (1971).

Franck, J.P., Phys. Rev. B, 22, 4315 (1980).

Franck, J.P., and Daniels, W.B., Phys. Rev. B, 24, 2456 (1981).

Kronig, R. and Sonnen, R.K.M., Physica (Utrecht), 24, 4322 (1958).

Longhurst, R.S., Geometric and Physical Optics, (Longman, London, 1973).

Nishiyama, Z., Martensitic Transformations, (Academic Press, New York, 1978).

Olson, G.B., and Cohen, M.,Scripta Met., 10, 359 (1976).

Tong, H.C. and Wayman, C.M., Scripta Met., 11, 341 (1977).

Vos, J.E., Kingma, R.V., van der Gaag, F.J. and Blaisse, B.S., Phys. Lett., 24A, 738 (1967).

Wayman, C.M., Scripta Met., 11, 341 (1977).

III. OBSERVATIONS OF THE fcc-hcp ^{4}He TRANSFORMATION MORPHOLOGY

A. INTRODUCTION

The morphology of interfaces involved in martensitic transformations make up a large part of metallurgical investigations into martensitic transformations. Metallurgical studies of the progress of an interface as it advances are generally restricted to studying thin foils or surface morphology. The ability to observe of the interface in the bulk solid is a unique advantage to this study of solid helium. This is the first reported study of the morphology of the martensitic transformation in solid helium. A new model of the interface is presented and shown to be consistent with the observations.

B. THEORY

Dislocations in fcc Crystals

The salient feature of a dislocation is the closure failure of a Burgers circuit around the dislocation. This is called the "Burgers vector". A Burgers vector is usually represented with its direction and magnitude in the standard Miller index notation. Thompson[1] developed a notation for Burgers vectors in fcc crystals that make it far easier to visualize the direction and magnitude of Burgers vectors and relations between different Burgers vectors.

---

[1] N. Thompson, Proc. Roy. Soc. B, 66, 481 (1953).

Thompson's notation refers to the Thompson tetrahedron (see fig. 3.1a), which has vertices labeled A,B,C,&D, faces opposite the vertices labeled α,β,γ,&δ respectively, and centroids of the faces labeled α,β,γ,&δ respectively. The four tetrahedron vertices represent nearest neighbor lattice sites. Each tetrahedron face represents an fcc close-packed plane (*i.e.* a {111} plane) and each tetrahedron edge represents an fcc close-packed line (*i.e.* a line in a $[1\bar{1}0]$ direction). A vector on the tetrahedron, labeled with the point at its head and the point at its tail in juxtaposition, can represent a Burgers vector or a displacement. If a Burgers vector goes from one lattice site to another, then the dislocation it represents is a perfect dislocation; otherwise, it is a partial dislocation. For example, AB is a perfect dislocation and Aδ is a partial dislocation (in this case, a "Shockley partial dislocation"). Table 3.1 shows some important fcc planes and vectors in both Miller and Thompson notations.

Dislocations generally glide in planes that contain both the Burgers vector of the dislocation and the dislocation line. In fcc crystals, the easy glide planes are the close-packed planes (tetrahedron faces). Thus the Thompson tetrahedron makes it immediately apparent that Aδ can glide in the δ plane provided that the dislocation line lies in that plane. A model of a Shockley partial gliding in a close-packed plane is illustrated in fig. 3.2.

A Burgers vector can also be thought of as a vector representing the displacement of material above the glide plane relative to material below the glide plane that occurs when the dislocation passes through the material. The passage of a perfect dislocation would shift atoms above the glide plane over to the next lattice site. The passage of a partial dislocation, on the other hand, would shift atoms to a site that is not a proper lattice site. This, happening on a single plane, would generate a stacking fault.

Dislocations in hcp Crystals

A notation similar to the Thompson notation, based on a double-tatrahedron (see fig. 3.1b), is useful in hcp crystals.[2] In this notation, the basal plane is the σ plane, the c-axis is along σs, and the close-packed directions are in the basal plane and in the directions of ab, bc and ca. In this notation the Burgers vectors of Shockley partials in the hcp phase are $a\sigma$, $b\sigma$ and $c\sigma$. Table 3.1 shows important hcp planes and vectors in both Miller and Thompson notations. Along with the each hcp plane and vector, table 3.1 shows the fcc plane or vector in the orientation dictated by the S-N relation.

---

[2] A. Berghezan, A. Fourdeux, and S. Amelinckx, Acta. Met., 9, 464 (1961).

The Fundamental Agent of the fcc-hcp Transformation

The fundamental agent of the fcc-hcp martensitic transformation mechanism is likely a Shockley partial dislocation. This idea originated from Christian.[3] A Shockley partial dislocation gliding on a fcc δ plane will change two close-packed layers of an fcc stacking arrangement into two layers of an hcp stacking arrangement with the hcp σ plane parallel to the fcc δ plane. The passage of a Shockley partial on every second δ plane would cause the fcc→hcp transformation. (See fig. 3.3) This would produce an hcp crystal in the orientation dictated by the S-N relation. The S-N relation would be maintained if the σ plane formed along any of the fcc close-packed planes; each hcp orientation is called a "variant". As a matter of convention, it will be assumed that the hcp σ plane will be along the δ plane. Conversely, the passage of a Shockley partial on every second σ plane will cause the hcp→fcc transformation.

The strongest evidence for the role of the Shockley partial as the fundamental agent of the fcc-hcp transformation comes from electron microscope observations of Shockley partials in materials in which the fcc-hcp transformation occurs. The materials observed in this way are cobalt alloys[4] [5], stainless steel[6] and high manganese steel.[7]

---

[3] J.W. Christian, Proc. Roy. Soc. A, 206, 51 (1951).
[4] E. Voltava, Acta Met., 8, 901 (1960).
[5] S. Mahajan *et al.*, Metall. Trans. A, 8, 283 (1977).
[6] H. Fujita and S. Ueda, Acta Met., 20, 759 (1972).

Transformation mechanisms based on Shockley partials are necessarily martensitic by their very nature. Since a single dislocation operates on a single layer, the displacement of each atom on that layer is identical. This satisfies the criterion that a martensitic transformation must have atomic displacements that are highly correlated in space. Additionally, each row of atoms along the dislocation line is displaced in sequence as the dislocation advances. Even *within* a row of atoms, the atoms are expected to be displaced in a sequence established by the migration of kinks along the partial (see fig. 3.2). A transformation occurring by this mechanism is necessarily martensitic even if it does not show features that are typical of other martensitic transformations.

Stacking Fault Formation

A two layer structure of hcp within an fcc lattice is called a stacking fault. The fcc-hcp transformation can be thought of as the formation of a stacking fault on every second close-packed plane.

The fcc→hcp transformation by irregular faulting starts with the generation of stacking faults at random positions within the crystal. The transformation progresses as the fault density increases. Eventually, as the fault density per close-packed layer approaches .5, the crystal structure becomes an hcp structure. This process is similar to a classical second order transformation and the order parameter is related to the fault density. Evidence for the fcc→hcp transformation occurring by irregular faulting in stainless steel has been presented by Dash & Otte[8] and Fujita & Ueda[9].

---

[7] Z. Nishiyama, Metal Physics, 7, 107 (1961).

If the fcc→hcp transformation is a conventional first order transformation, it occurs by a regular faulting process. A small region forms in which the stacking faults occur on every second close-packed plane; *i.e.* a small region of hcp forms. The transformation continues by the growth of the hcp phase at the expense of the fcc phase. During the process a well-defined interface separates the two phases. Evidence for the fcc→hcp transformation in cobalt by a regular faulting process has been presented by Venables[10].

Regular faulting may also produce a series of transformations from fcc, through various intermediate close-packed phases, and finally to hcp.

Dislocation Models of the Interface Structure

Unless the transformation occurs by an irregular faulting process, an interface will separate the two phases during the course of the transformation. If Shockley partials are the fundamental agent of the fcc-hcp transformation mechanism, then the interface must contain Shockley partials. If the structure of the interface can be modeled by partials, then the dynamics of the atomic displacements on the interface may be reduced to the simpler problem of the dynamics of the atomic displacements of the atoms along a partial dislocation. An array of Shockley partials may be used to explain the interface structure and dynamics.

---

[8] J. Dash and H.M. Otte, Acta Met., 11, 1169 (1963).
[9] H. Fujita and S. Ueda, Acta Met., 20, 759 (1972).
[10] J.A. Venables, Phil. Mag., 7, 35 (1962).

Some of the properties of an array of dislocations are due to elastic strain field of the dislocations. The elastic strain field of a dislocation in bulk material depends entirely on its Burgers vector and the elastic constants of the material. A number of dislocations in the bulk produce a strain field equal to the sum of the individual strain fields. To first order, as the group of dislocations change from an arrangement of close proximity to a widely spaced arrangement, the energy (multiplied by a proportionality constant) crosses over from the square of the sum of the Burgers vectors to the sum of the squares of the Burgers vectors (see appendix).

Two models of the fcc-hcp interface structure composed of Shockley partials are considered here.

Array of Identical Shockley Partials as an Interface Model

The interface may be modeled with an array of identical Shockley partial dislocations (eg. all $A\delta$ partials) situated on alternate close-packed planes. For example, the array may consist of partials in the following sequence:

$$\ldots A\delta \quad A\delta \quad A\delta \quad A\delta \quad A\delta \ldots$$

Such an array is illustrated in fig. 3.4. In this model, the square of the sum of the Burgers vectors of the partials is much larger than the sum of the squares; therefore, the energy of the array is lowest when the partials are widely separated. Maximun separation may be achieved if a single partial lies on an interface at any time. A single partial may cause an fcc-hcp transformation by travelling back and forth across its glide plane and climbing two close-packed layers at the end of each traverse.[11] Alternatively, a single partial may wind its way around a pole dislocation.[12] [13] Regardless of the details of the transformation, an interface with identical partials (or a single partial) must lie in the δ plane. The abreviation, "ISPA", will be used for "identical Shockley partial array".

Because the partials are widely separated, the interface will lie close to the glide plane of the partials (*i.e.* the δ plane). This plane happens to be the plane of invariant strain under the homogeneous deformation that produces the fcc→hcp transformation; therefore, this model follows the conventional crystallographic theories of martensitic transformations.[14]

---

[11] J.W. Christian, Proc. Roy. Soc. A, 206, 51 (1951).

[12] Z. Seeger, Metallk., 44, 247 (1953).

[13] Z.S. Basinski and J.W. Christian, Phil. Mag., 44, 791 (1953).

[14] J.W. Christian, The Theory of Transformations in Metals and Alloys, (Pergamon Press, New York, 1965).

The homogeneous deformation produced by the passage of an ISPA must be accommodated by the solid. Figure 3.4 schematically illustrates the hcp→fcc transformation according to the ISPA model. The figures show accommodation by surface relief (a), elastic acommodation (b), slip (c), twinning (d), and (as discussed in the next paragraph) band formation (e). In addition to the energy of the fcc-hcp interface, energy is required by each of these accommodation mechanisms (except for surface relief along a free surface).

The fcc→hcp transformation may produce hcp bands: one band may be created by the migration of Aδ Shockley partials on every second close-packed layer, the neighboring band on one side may be created by the passage of Bδ partials, and the neighboring band on the other side may be created by the passage of Cδ partials. It should be emphasized that these bands are not distinct variants; the orientation of the hcp phase is the same regardless of whether Aδ, Bδ or Cδ partials produce the transformation. Such bands have been observed in cobalt-nickel alloys.[15] [16] The width of the observed bands were on the order of 1μ and as small as 10-30 nm for pure cobalt. Since the sum of the Burgers vectors of the partials (Aδ+Bδ+Cδ) is zero, this type of banding will produce an average displacement of zero; however, each band will produce a local region of strain which must be accommodated (perhaps elastically), and therefore requires some energy for accommodation. The production of zero average displacement in this way is called self-accommodation. Similarily, the hcp→fcc transformation may produce fcc bands.

---

[15] S. Takeuchi and T. Honma, Sci. Rep. RITU, 9A, 492 (1957).

[16] H. Bibring, F. Sebilleau and C. Buckle, J. Inst. Met., 87, 71 (1958-59).

Array of Coupled Shockley Partials as an Interface Model

The interface may be modeled with an array of coupled Shockley partial dislocations. The array consists of equal numbers of the partials Aδ, Bδ, & Cδ, one of which is on every second δ layer. For example, the array may consist of partials in the following sequence:

... Aδ Bδ Cδ Aδ Bδ Cδ Aδ Bδ Cδ Aδ Bδ Cδ ...

Such an array is illustrated in fig. 3.5 and fig. 3.6.

It is reasonable to suppose that the formation of these arrays is energetically favorable. First, since the sum of the Burgers vectors of the partials is zero, the energy to the first approximation approaches zero as the partials become closer (see appendix). Since the sum of the squares of the partials is greater than the square of the sum of the Burgers vectors, the energy of the array is lowest when the partials are closest together. Futhermore, the energy in the first approximation of an ISPA does not approach zero and is, therefore, greater than the energy of a CSPA. Second, it is reasonable to suppose that it is energetically favorable for a long array of coupled partials to to remain intact rather than separate into sections, in spite of the possibility for each section to have a zero value for the sum of the Burgers vectors of the partials. Consider the array with the following sequence of partials:

... $A\delta_1$ $B\delta_1$ $C\delta_1$ $A\delta_2$ $B\delta_2$ $C\delta_2$ | $A\delta_3$ $B\delta_3$ $C\delta_3$ $A\delta_4$ $B\delta_4$ $C\delta_4$ ...

Subscripts have been added to the symbols for the partials to distiguish them from identical partials in other positions along the array. The section of the array to the left of the vertical bar (the "left section") has a $C\delta$ partial (the $C\delta_2$) at its end. The strain field of this partial is reduced by the $A\delta_2$ and $B\delta_2$ partials to its left and, therefore, is bound to the left section of the array. However, since the strain fields of the $A\delta_2$ and $B\delta_2$ partials are not centered exactly at the $C\delta_2$ partial, the cancelation of the $C\delta_2$'s strain field is not complete. Furthermore, the effectiveness of the $A\delta_2$ and $B\delta_2$ partials at canceling $C\delta_2$'s strain field is reduced because the strain field of the $A\delta_2$ and $B\delta_2$ partials are reduced by the $C\delta_1$ partial to the left of the $A\delta_2$ partial. For these reasons, a portion of the strain field due to the $C\delta_2$ partial remains uncanceled by the partials to the left of it. Similarily, the $A\delta_3$ and $B\delta_3$ partials at the end of the right section will have a portion of their strain field is not completely canceled by the strain field of the $C\delta_3$ partial. The remaining portion of $C\delta_2$'s strain field can be further reduced by the remaining portion of the strain field due to $A\delta_3$ and $B\delta_3$; therefore, the ends of the two sections will attract each other and it will be energetically favorable for the the array to remain intact. The attraction of the ends of the sections is reminiscent of the attraction between electric dipoles.

A formal proof for the attraction of the sections of the array was attempted. The attempt involved summing explicit expressions for the stress and strain fields due to each partial and calculating the energy of the net field. The calculation was found to be too involved for treatment here but would make an interesting theoretical study.

Coupled partial arrays with other sequences of partials may also be stable, but will likely have higher energies. Consider, for example, the following two sequences of partials:

... Aδ Bδ Cδ Aδ Bδ Cδ Aδ Bδ Cδ Aδ Bδ Cδ Aδ Bδ Cδ ...

... Aδ Bδ Cδ Aδ Bδ $\underline{C\delta}$ Bδ Aδ Cδ Bδ Aδ Cδ $\underline{B\delta}$ Cδ Aδ ...

In the first array, every partial has a different partial on each side of it so that any three adjacent partials has a zero value for the sum of the Burgers vectors. This a low energy configuration. The same can be said of most of the partials in the second array. However, this cannot be said of the underlined partials. The underlined Cδ partial in the second array is in a higher energy configuration because it is further separated from the Aδ that is required, along with the Bδ partial, to cancel its strain field. The underlined Bδ is similarily in a higher energy configuration. An array similar to the second array has many more possible configurations and may therefore occur even if its energy is higher.

Arrays with the following sequences of partials have partials that are less uniformly distributed than the arrays discussed in the last paragraph:

$$\ldots\ A\delta\ B\delta\ \underline{C\delta}\ \underline{B\delta}\ \underline{C\delta}\ B\delta\ \underline{A\delta}\ \underline{B\delta}\ A\delta\ C\delta\ B\delta\ A\delta\ C\delta\ \underline{A\delta}\ C\delta\ \ldots$$

$$\ldots\ A\delta\ B\delta\ C\delta\ A\delta\ B\delta\ \underline{\underline{C\delta}}\ \underline{\underline{C\delta}}\ B\delta\ A\delta\ C\delta\ B\delta\ \underline{\underline{A\delta}}\ \underline{\underline{A\delta}}\ C\delta\ B\delta\ \ldots$$

A single line under the symbol for the partial indicates that the partial is in a higher energy configuration, as discussed in the last paragraph. A double line under the symbol for the partial indicates that the partial is in a yet higher energy configuration because it is adjacent to an identical partial. These are less energetically favorable than the arrays discussed in the previous paragraph and are less likely to remain intact.

The partials are coupled with a binding force because the energy of the array decreases as the partials draw nearer to each other. The binding force between the partials provides the interface with surface tension. If the attractive force between the partials dominates even at separations as small as twice the separation of close-packed layers, then the array will tend to form perpendicular to the glide plane in order to minimize the separation between the partials. Repulsive forces between the partials at close proximity or noncentral components of the forces may favor another orientation of the array. Any preferred orientation of the array may be considered in macroscopic terms as an anisotropy in the surface tension.

The deformation in this model is not homogeneous because adjacent δ layers deform differently due to the different partials gliding on them. The deformation averaged over a small region of the interface in this model is zero because the sum of the Burgers vectors of the partials is zero. Every plane is an invariant plane of the transformation. This means that a transformation mechanism with a CSPA requires almost no energy to accommodate the product phase after the transformation (this is in contrast to a transformation mechanism with an ISPA). Because of this, accommodation energy considerations in solids (except for thin foils, whiskers and unrestrained single crystals, in which surface relief readily occurs) favor the mechanism with a CSPA.

The partials in the array glide along the δ plane as the interface advances. The glide of each partial may occur by the formation and migration of kinks in the partial. These kinks may form and move independently of each other, or, since the partials are coupled, a kink in one partial may be coupled to a kink in the adjacent partial. Figure 3.7 shows how kinks in the partials of a CSPA may form and migrate to advance the interface.

Although interface models consisting of dislocation arrays have been proposed for transformations other than the fcc-hcp transformation[17], the model shown here, to my knowledge, has not been suggested before. The abreviation,

---

[17] G.B. Olson and M. Cohen, Met. Trans, 79, (1981): Part I, 1897; Part II, 1905; Part III, 1915.

"CSPA", will be used for "coupled Shockley partial array". According to the above arguments, a CSPA requires less energy for the interface and less accommodation energy following the passage of the interface than an ISPA.

C. EXPERIMENT

Optical detection of the fcc-hcp transformation inspired efforts to make visual observations of the fcc-hcp interface. The visual method of observation was designed as a modification to the optical method. The high pressure cell, high pressure system, cryogenic system and helium supply was the same as described in chapter II.

Visual Method

As described in the chapter II, the birefringence of the hcp phase made it act as a retardation plate. The fcc phase was opticallly isotropic. Thus the two phases were optically distinguishable. With modifications to the optical method, visual images of the transformation could be produced.

Solid helium was formed between linear polarizers. A video camera, without the lens attached, was placed about one meter from the sample and a lens was placed about halfway between the camera and the sample. The camera and lens positions were adjusted to provide enough magnification to let the image of the sample nearly fill the camera's field of view and to bring the image into focus. A white light source was provided by a slide projector and diffused with a ground glass plate. The light was polarized with a linear polarizer that followed the diffusing screen. Video images were recorded on a time lapse video casette recorder. A potentiometric conductance bridge measured the conductance of a germanium thermometer attached to the cell. The digital display of the bridge was monitored by a second video camera. A special effects generator (Panasonic WJ-4600A) mixed this video image with the video image of the sample to produce an image of the bridge's digital display in a corner of the recorded video image.

Two variations of the visual method were used: the intensity contrast method and the color contrast method. The color contrast method distinguished between the two phases by the different color of the light that emerged from each phase. The amount of retardation, ϕ, experienced by the light depends on its wavelength, λ, according to eq. 2.1. When white light passes through a retardation plate situated between linear polarizers, it may emerge with a color called the "tint of passage".[18] The reason for the color is that the analyzer (the second polarizer in the light path) diminishes the intensity of light of some wavelengths more than others (see eq. 2.2). The tint of passage obtained for the special cases of parallel and perpendicular polarizers are listed by Bergmann and Schaefer[19]. The color of the emerging light is most sensitive to the amount of retardation if only the light near the center of the visible spectrum (yellow light) is extinguished. This condition is met for parallel polarizers 45° to one of the principal axes when the retardation is π, 3π or 5π and for perpendicular polarizers 45° and 135° to the slow axis when the total retardation is 2π or 4π (see eq. 2.2). A mica plate was inserted between the polarizers to raise the retardation for yellow light so that one of the above conditions for optimum sensitivity could be met.

---

[18] R.S. Longhurst, Geometric and Physical Optics, (Longman, London, 1973).

[19] L. Bergmann and C. Schaefer, Optik, (Walter de Gruyter, Berlin, 1966).

The light intensity that is transmitted through a retarder that is placed between two parallel polarizers is given by:

$$I=I_0\left(1 - \sin^2(2\alpha) \sin^2(\phi/2) \right) \qquad (3.1)$$

where ϕ is the retardation (see eq. 2.2) and α is the angle between the polarization direction and the retarder's slow axis direction. Maximum variation of the intensity for light of different wavelenghts occurs when α is 45°. Assume that the polarizers are adjusted to meet this optimum condition. The first extinction occurs when ϕ equals π. When ϕ is between 160° and 200°, the transmitted intensity will be less than 3% of the maximum intensity. If the mica plate causes a retardation of 135° to red light, it will cause a retardation of 200° to blue light (see eq. 2.1). The fcc phase will produce no additional retardation. In this case, the image will appear red because the transmitted light intensity at the blue end of the spectrum will be very low relative to the transmitted intensity at the red end of the spectrum. With an hcp crystal present, additional retardation will occur due to the birefringence of the hcp phase. For example, the c-axis may be in an orientation that will cause an additional 35° of retardation on red light. The retardation on red light will then be 170° and the retardation on blue light will be 255°. This light will produce a blue image. In this case, the different phases may easily be distinguished. The hcp phase at the pressures studied may add or subtract up to 60° of nominal retardation from the nominal retardation of the mica plate. In general, the color of the hcp image will depend on the hcp orientation through the following factors: the retardation (ϕ) (which depends on the c-axis azimuthal angle, γ) and the slow axis orientation (which depends on the c-axis polar angle). The colors may be changed by changing the mica plate and polarizer orientations.

The intensity contrast method is done without the mica plate. With the fcc phase present, no retardation occurs (except that caused by the slight amount of stress birefringence in the sapphire windows) and the image is achromatic. With the hcp phase present, the retardation is small and transmitted light of all wavelengths are changed by approximately the same amount. The color of the image is washed out or unsaturated and hard to distinguish from the achromatic fcc image; however, the phases may be distinguished by the fact that the transmitted light intensity, integrated over all wavelengths, is changed in the hcp phase. The optical arrangement with the mica plate removed is more suited to the intensity contrast method. The relative intensities of the images of the two phases depends on the hcp orientation and the polarizer orientations.

The camera used for the color contrast method (Panasonic 5600) had a feature that allowed the time and date to be superimposed onto the video image. For the intensity contrast method, a black and white Panasonic 1550 was used because it was more sensitive to small intensity changes.

Photographs were produced from the video recording by photographing the video monitor. A shutter speed of ¼ second was used to reduce the effect of the blanking signal that swept across the monitor thirty times per second. When black and white reproductions of color photographs were required, the color photographs were illuminated with red light and rephotographed onto black and white film. In these photographs, the light grey region in the photograph was red on the video image and the dark grey region was blue.

D. RESULTS

Visual observations of the fcc-hcp transformation in many samples of solid ^{4}He were made. Visual observation revealed a variety of features.

Sample 1

Sample 1 was solidified over the course of a few hours at a pressure of 1.4 kbar and annealed overnight in the fcc phase. The color contrast method was used to record the transformation. Along with the image of the solid helium, the conductance of the germanium resistance thermometer attached to the cell was recorded by a video camera and was displayed in the bottom right corner of the video frame. Over a 1 K range, the thermometer calibration curve near the transition temperature was linear within 5 mK. The temperature (T) depended on the conductance (c) approximately as:

$$T = (c - 42.41 \text{ mMho})(.506 \text{ K/mMho}) + 15.000 \text{ K} \qquad (3.2)$$

Visual observations of eighteen consecutive transformations were made. Table 3.2 lists the transformations along with data on the transformations and the figure number in which photographs of the transformations are displayed (figures 3.8 to 3.25). The time at which the transformation was half complete is used to indentify the transformation. The tabulated data on the transformations will be commented on later.

Figure 3.9 shows a sequence of photographs that illustrate the fcc→hcp transformation that occurred at 12:46. The sequence starts with the photograph in the top left corner, follows with the photographs below it, and continues with the photographs in the next column from top to bottom. The diameter of the aperture that restricted the field of view of these images was 1.6 mm. Small dark spots that are present in all the photographs of this sample are due to impurities that had precipitated onto the windows of the cell. The cooling rate during this transformation was 3.4 mK/sec. The first photograph of the sequence shows the fcc phase at the first sign of the transformation. The optics had been adjusted in such a way that the isotropic fcc phase produced a blue image. The temperature of the sample in this photograph was 14.838 K. The next photograph in the sequence shows the sample at the slightly lower temperature of 14.833 K. A region of red appeared in the lower left corner of the image. The optics had been adjusted in such a way that the birefringent hcp phase produced a red image. In subsequent images in this sequence, the hcp region (red) grew and eventually replaced the fcc region (blue). During the course of the transition, the image was clearly divided into two distinct regions (the red and blue regions). The boundary separating the two regions in the image was the projection of the fcc-hcp interface onto a plane perpendicular to the z-axis. Since the boundary in this transformation was very sharp, the fcc-hcp interface was nearly parallel to the z-axis. Had the interface been less parallel to the z-axis, the boundary separating the two regions would have more diffuse. The boundary separating the regions of color was a straight line, indicating that the fcc-hcp interface was planar. The line separating the two regions remained in its original orientation as one region grew and the other dimininshed. This indicated that the interface did not rotate as it progressed. The interface migrated the entire width of the field of view with an average velocity of .1 mm/sec. The interface did not advance with a constant velocity; rather, the velocity seemed to vary by a factor of two or more during different stages of its advance. No other interfaces appeared in this transformation. The horizontal streaks that appeared in the video images are due to an artifact of the video recorder. No event other than the migration of a single planar unrotating interface was observed in this transformation.

Figure 3.10 shows the subsequent hcp→fcc transformation (the reverse transformation) which occurred at 12:48. The first picture of the sequence (top left) shows the red image of the hcp phase. Upon heating (at 3.2 mK/sec), the fcc phase began to grow producing a blue region (fcc) in the bottom left corner of the image. The transformation progressed by the migration of a single planar unrotating interface that was in the same orientation as the interface in the preceding fcc→hcp transformation.

Although a sharp boundary was observed in over half of the transformations in this sample, some transformations were observed in which no sharp boundary appeared. These transformations were produced with the same heating/cooling rates and occurred at the same temperature as the transformations in which a sharp boundary did appear. One such transformation occurred at 12:51. The region was never sharply separated into two different colors. At each point in the image, the color gradually changed from blue to red. This contrasts with observations of other fcc→hcp transformations in which the color at a point in the image changed abruptly as a boundary crossed the point. The color change did not occur simultaneously at every point in the image and, at a particular time (see the seventh photograph of the transformation that occurred at 12:51), a gradient in the color could be seen across the image. The gradient of the color can be described as a highly diffuse boundary separating regions of different color. Similar examples of diffuse boundaries occurred at 12:59 and 1:45. In other cases, the transformation appeared to occur partly with a sharp boundary and partly with a diffuse boundary. Examples of this occurred at 1:05, 1:32, and 1:47. The likely interpretation of the events that produced a diffuse boundary is the migration of an interface that is well defined but not sufficiently parallel to the z-axis to produce a sharp boundary.

Almost all interfaces that were parallel to the z-axis, first appeared at the edge of the field of view and presumably originated at the cell wall. When the migration of one such interface produced the majority of the transformation, the interface usually (but not always) started from the bottom left portion of the cell regardless of whether the transformation was the fcc→hcp transformation or the hcp→fcc transformation (the exceptions were at 12:44 and 1:31). When two interfaces were observed that were parallel to the z-axis, each appeared from edges of the field of view that were on opposite sides of the image. Two exceptions to this generalization were the transformations that occurred at 1:05 and 1:47. A blue band appeared within the red region at 1:05. The band was very faint at first (as shown in the second photograph of the sequence), gradually became clearer, and eventually became very apparent (sixth photograph). The band indicated the growth of the fcc phase. At 1:47, a red band (due to the formation of hcp) faintly appeared as shown in the sixth photograph of the sequence. This band gradually became clearer until it joined the red region produced by the hcp phase in the rest of the cell.

Over half the transformations in this sample occurred by the migration of an interface that was parallel to the z-axis. In these transformations, the interface were planar and advanced without rotating. Figure 3.17 shows eight interfaces that were observed in different transformations in this sample (namely the transformations that occurred at 12:40, 12:42, 12:44, 12:46, 12:48, 12:53, 1:42, and 1:47). Remarkably, all of these interfaces were in the same orientation. There were many transformations in which two interfaces were parallel to the z-axis. In such cases, both interfaces were in the same orientation as the interfaces shown in fig 3.17. All interfaces that were parallel to the z-axis were in the orientation shown in fig. 3.17.

The color of the image of the hcp phase depends on the direction of the c-axis. Since the color of the hcp image is different from the color of the fcc image, the hcp c-axis is not parallel to the z-axis. Furthermore, nearly the same hue of red appeared with each hcp phase. This suggested that the hcp orientation and the crystal thickness was the same after each fcc→hcp transformation.

The transformation at 1:18 was started by heating to 14.97 K. Heating was interrupted when the temperature reached 14.98 K. The interruption of heating coincided with the interruption of the advance of the interface. The temperature was held constant and the interface remained stationary for three minutes. As soon as the heating was resumed, the interface began to advance and, with continued heating, the interface advanced to the end of the sample.

Table 3.2 contains information about the transformations illustrated in figures 3.8 to 3.16, To each transformation, a number from one to five was assigned that indicated the sharpness of the boundary separating the two regions of different color: "1" was assigned to transformations having very sharp boundaries and "5" was assigned to transformations having very diffuse boundaries (*i.e.* to transformations showing a gradient in the color rather than a sharp boundary). Since it was difficult to determine precisely when the transformation started and finished, the athermal width was taken as the temperature change over the course of the majority of the transformation and the temperature at which the sample was half transformed was tabulated rather than the conventional temperatures (M_s and A_s). The rate at which the temperature was changing was also tabulated.

Sample 2

Sample 2 was solidified at 1.5 kbar. This sample was prepared in a very different way than sample 1. Solidification was started by slowly cooling at constant volume as usual. When the cell was about two thirds filled with solid, heat was applied to the sample. The heat melted the solid in the capillary, allowing more fluid to enter the cell. This raised the pressure in the cell suddenly and caused completion of the solidification. The cell was immediately cooled again to prevent a rising temperature from melting the solid. The result of this process was a solid sample with a large visible defect at the center. The defect was in the shape of a crescent opening downwards and was visible in all the images of this sample. The intensity contrast method was used for this sample. The conductance of the germanium resistance thermometer attached to the cell was recorded on the video tape and was displayed in the top right corner of the video frame. Over a 1 K range, the thermometer calibration curve near the transition temperature was linear within a few mK. The temperature (T) depended on the conductance (c) approximately as:

$$T = (c - 11.880 \text{ mMho})(.561 \text{ K/mMho}) + 15.000 \text{ K} \quad (3.3)$$

As in sample 1, observations were made of transformations produced by the migration of a single planar unrotating interface nearly parallel to the z-axis. An example of such a transformation is shown in fig. 3.18. The cooling rate during this transformation is 3.3 mK/sec. The transition started at a temperature of 14.91 K. The athermal width was 100 mK. This transformation (except for the orientation of the interface) was similar to the observations of transformations in sample 1. In most of the transformations that had interfaces parallel to the z-axis, the interface appeared in the same orientation as the interface illustrated in fig. 3.18.

Many transformations occurred in which no sharp boundary appeared in the image. These transformations were similar to those in sample 1 that had diffuse boundaries and were likely due to the fact that the interface was not parallel to the z-axis.

In many transformations, the progress of the interfaces appeared to be hindered by the defect at the center of the solid. An example of such a transformation is shown in fig. 3.19. The column on the left contains photographs of the transformation and the column on the right contains drawings that were traced from the photographs. The drawings point out the interface of interest. The interface advanced only on the left side of the defect. The section of the interface that advanced remained planar and in the same orientation as the interface in fig. 3.11. Another section extended from defect to the section of the interface that had advanced. It appeared that the defect interrupted the interface at one point yet did not stop the rest of the interface from advancing. It is noteworthy that a rounded corner (rather than a sharp corner) joined the section that advanced to the section that was pinned to the defect. This transformation started at 14.91 K during cooling at a rate of 3.6 mK and had an athermal width of 6 mK.

Another transformation in which the defect in the solid affected the progress of the interface is shown in fig. 3.20. The column on the right contains drawings illustrating the same interfaces as shown in the photographs on the left. The photographs only faintly show the interfaces; however, the video tape clearly shows the interface motion and was used as a guide to drawing the illustrations on the right. Each of the interfaces shown can be described as a nearly planar interface that rotates about a pivot. The pivot appears to be a line lying along the z-axis and located at or near one of the defects at the center of the solid. It is not clear whether the pivot is located at the crescent shaped defect or the smaller defect below it. This transformation started at 14.99 K during cooling at a rate of .8 mK/sec and had an athermal width of 15 mK.

Some observations were made of the transformation occurring by the passage of curved interfaces. These interfaces sometimes changed shape as the transformation progressed. These transformations appeared so faintly on the video image that they could not be seen on the monitor once the video was held in freeze frame. This made it impossible for them to be displayed with photographs.

Rapid cooling sometimes produced results that were very different from those already discussed. When sample 2 was cooled at 60 mK/sec to 14.50 K, parallel bands of light and dark regions began to appear. Figure 3.21 shows images of the sample preceding the formation of the bands. The transformation appeared to take place (at least to some extent) at 14.6 K. This was indicated by the changes of light intensity in the image as shown in fig. 3.21. The last six photographs in figure 3.21 were taken over an interval of 3.0 seconds during cooling at a rate of 66 mK/sec. The formation of the bands is illustrated in the sequence of photographs shown in figures 3.22 to 3.23. Figure 3.22 shows eight photographs of the sample over a 1.6 second interval during cooling at an average rate of 43 mK/sec. Figure 3.23 shows eight photographs over a 2.6 second interval during cooling at a rate of 23 mK/sec. Figure 3.24 shows eight photographs over a 2.8 second interval during cooling at a rate of 5 mK/sec. Both bands that were lighter than the original shade of grey and bands that were darker appeared. A light band and an adjacent dark band usually appeared simultaneously. Each band appeared first as a thin faint band and, with time, became wider and more distinct. The arrow in the first photograph of fig. 3.24 points to a thin faint line as it first appeared. As shown in subsequent photographs, the band became wider and more distinct (first six photographs), but eventually became faint again (seventh photograph). The distinctness and number of bands increased until the temperature reached 14.39 K. Below 14.39 K, the bands began to fade away and at 14.34 K there was very little trace of the bands. As the bands faded, most appeared to fade on the right side of the image before they faded on the left. This is shown clearly in fig. 3.24. It appeared that the bands faded away by reducing their length more so than by reducing their width. It is noteworthy that these bands were aligned parallel to the orientation of the single planar interface shown in fig. 3.18.

Another occurrence of the formation of bands in this sample is illustrated in fig. 3.25. The sample was cooled at a rate of 100 mK/sec to 14.42 K before the bands started to appear. Bands aligned in two different orientations. One set of bands was aligned in the same orientation as the bands in the case discussed above. The other set of bands was aligned at an angle of 69°±4° to this orientation. The first six photographs in fig. 3.25 were taken over a time interval of 3.4 seconds during an average cooling rate of 95 mK/sec. As before, the bands faded away with continued cooling.

Other Samples

In another sample at 1.5 kbar, similar bands appeared just prior to the hcp→fcc transformation. The sample had no observable defects as in sample 2. The heating rate that produced this result was 45 mK/sec and the temperature that it started at was 15.01 K. The helium supply used in this sample was not isotopically pure as in most of the samples.

Transformations were observed in many other samples. Transformations with diffuse boundaries (similar to the one that occurred in sample 1 at 12:51) were by far the type most commonly observed. Very many samples had to be observed in order to find a few that had interfaces that were nearly parallel to the z-axis.

E. DISCUSSION

Many transformation interfaces were observed with the visual method. The presence of a well defined interface indicated that the transformation occurred by a regular faulting process; *i.e.* it is a conventional first order phase transformation. Because interfaces could not be observed unless they were nearly parallel to the z-axis, transformations in which no interface was observed did not indicate that an interface was not involved in that transformation. It may be suggested that, when no interface was observed, an irregular faulting process occurred; however, this suggests that the transformation alternately occurred by regular and by irregular faulting. Although there is no direct evidence against this, the introduction of two mechanisms is unwarranted since one mechanism (regular faulting) can explain all the results. It may also be suggested that, when no interface was observed, nucleation and growth occured at many sites, producing grains too small to be resolved; however, this suggests that consecutive transformations alternately produced a single crystal and many fine grains, and although this may be possible it this entails a more significant variation in the progress of consecutive transformations than is warranted. The simplest explanation is that a regular faulting process occurred and that the phases were separated by an interface whether it was observed or not.

Since the migration of only one interface was sufficient to transformation the sample, there are no intermediate phases in the fcc→hcp or the hcp→fcc transformation.

The transformation appears to be heterogeneously nucleated. In sample 1, the transformation usually started from outside the field of view. It is reasonable to assume that the transformation started at the cell wall; *i.e.* it was heterogeneously nucleated. Nucleation did not occur at an embryo consisting of a remnant of the parent phase of the preceding transformation. This is clear because consecutive transformations often occurred by the migration of an interface in the same direction (usually from the left to right). In two cases in sample 1, a region of a new color appeared in the image without coming from outside the field of view. Although it is possible that homogeneous nucleation occurred in these two cases, it is also possible that the transformation started at the window in these cases. Since the majority of transformations appeared to start at the cell wall, there is visual evidence (albeit weak evidence) that the transformation is heterogeneously nucleated.

The fact that the clearly visible interfaces were usually planar is significant. The tendency of the interface to remain planar was stronger than the tendency of the chemical driving force to make the interface follow isothermal surfaces. (Isothermal surfaces in this sample are approximately concentric cylinders.) Furthermore, the observation that most of the transformations observed in sample 1 occurred by the migration of an interface in the same orientation indicated that the interface has a preferred orientation. Sample 2 also appeared to have a preferred orientation for the interface. The existence of a preferred orientation (*i.e.* a "preferred habit plane") is very convincing evidence that the transformation is indeed martensitic. Furthermore, the reproducibility of the habit plane orientation and the reproducibility of the product crystal orientation (both of which were observed in this sample) are features that are associated with martensitic transformations.[20] This is a good indication that the transformation is a martensitic transformation.

A preferred habit plane may be understood in terms of either of the two interface models discussed in the theory section. The ISPA model predicts the interface to be the δ plane[21]. In the CSPA interface model, the preferred habit plane depends on the details of the interactions between the partials. Without detailed calculations, one can predict only that the preferred habit plane will not be the δ plane, and perhaps that it contains one close-packed direction on the δ plane. The habit plane is expected to contain at least one close-packed line because the core energy of the partials is lowest in a close-packed direction. Normally, the core energy is much smaller than the elastic strain energy and thus may not affect the partial dislocation orientation significantly; however, in a CSPA, the elastic strain energy of the partials nearly cancel each other and the partials in the array are expected to be oriented along a close-packed direction to reduce the core energy. This habit plane will have two other habit planes that are equivalent to it; *i.e.* the habit plane will have a three-fold degeneracy. For example, if α is a preferred habit plane, then β and γ must be equally preferred habit planes.

---

[20] C.M. Wayman, "Martensitic Transformations: An Overview" in Proc. Intl. Conf. Solid→Solid Phase Transformations, H.I. Aaronson, D.E. Laughlin, R.F. Sekerka, C.M. Wayman eds., (The Metallurgical Society of AIME, 1981), P. 1119

[21] In this discussion, the S-N relation is assumed to hold and the δ fcc plane is parallel to the σ plane as a matter of convention.

Since the color of the hcp image was reproducible with each fcc→hcp transformation in sample 1, the c-axis orientation (and, therefore the δ plane orientation) was likely the same during each transformation. Since the δ plane is not degenerate, the observations on sample 1 which showed at least two interface orientations (parallel and not parallel to the z-axis) indicated that the interface was not always along the δ plane. If the preferred habit plane is the δ plane, the interface did not consistently lie in the preferred habit plane. Although there is no evidence to suggest that the interface must always lie in the preferred orientation, the idea that the interface behaves inconsistently is somewhat unsatisfying. Furthermore, the observation that the interface is not always parallel to the δ plane is inconsistent with the ISPA model. Any other preferred habit plane will have a three-fold degeneracy. If (as the CSPA model predicts) the preferred habit plane has three-fold degeneracy and one of the planes is parallel to the z-axis, then generally neither of the other two planes will be parallel to the z-axis.[22] Thus the interface may consistently lie in a preferred habit plane and yet not always lie parallel to the z-axis. The observation that the interface orientation has a preferred orientation and yet is not always parallel to the z-axis suggests that the preferred orientation has three-fold degeneracy. This supports the CSPA model and is inconsistent with the ISPA model.

The S-N relation predicts that a hcp crystal may be produced in one of four orientaions relative to the parent fcc crystal. Many observations showed the hcp crystal being reproduced in a particular orientation much more than 25% of the time. This suggests that there is a preferred hcp orientation. The preference for a particular orientation is explained in some materials by the growth of one phase from a remnant of the parent phase of the preceding transformation. Since the transformation did not start from such a remnant (as discussed earlier), the high reproducibility of the hcp orientation must have another explanation. The preference for a particular orientation (above the restrictions impossed by the S-N relation) may be related to the mechanism by which an interface is generated at the cell wall. For example, suppose that the wall prefers to generate partials that lie along the close-packed direction that is closest to being parallel to the wall. This will restrict the glide plane of the partials (and therefore the hcp σ plane) to two planes (the planes that contain the line that the partials lie along). Additionally, once a partial is formed, it may prefer to glide away from the wall in a direction that is closest to the normal of the wall. This will cause one of the two possible glide planes for a partial to be selected in preference to the other.

---

[22] If the z-axis happens to be along AD, BD or CD, then two of the preferred habit planes will be parallel to the z-axis.

Generally, grain boundaries interrupt the progress of the interface in a martensitic transformation. The migration of an interface across the entire width of sample 1 indicated that no grain boundaries were in the path of the interface. If the interface extended the entire length of the sample (from the front window to the back window), the interface swept through the entire sample without encountering a grain boundary; *i.e.* the sample was a single crystal. If the interface had not extended between the front and back windows, one would have expected to observe effects of the transformation occurring in the rest of the solid. Since no sign of the transformation in other grains was observed and the interface traversed the width of the sample, it is very likely that sample 1 was a single crystal.

It is significant that many of the transformations observed occurred by the migration of a single planar interface across an entire crystal. This is uncommon for martensitic transformations. Commonly, strains associated with the transformation process accumulate until they cause sufficient plastic deformation to destroy the interface coherency conditions that are necessary for the progress of the interface. This commonly occurs before a grain boundary is reached. The martensitic transformations that can occur by the migration of a single planar interface across the sample (Au-Cd[23], In-Th[24] [25] and Cu-Al-Ni[26] alloys) are thermoelastic martensitic transformations and have a small shape strain associated with the transformation. The migration of a single planar interface across an entire crystal in solid helium indicates that it is a thermoelastic transformation with small shape strain.

A transformation with an interface of identical partials would produce strain as it advanced. The accumulation of the strain can be restricted if self-accommodation occurs by band formation as described in the theory section and illustrated in fig. 3.4e. Self-accommodation in this way is not complete because each band has strain associated with it. The transformation with an interface of coupled partials is completely self-accommodating because it produces no strain as it advances.

---

[23] L.C. Chang and T.A. Read, Trans. AIME, 191, 47 (1951).

[24] M.W. Burkart and T.A. Read, Trans. AIME, 196, 1516 (1953).

[25] Z.S. Basinski and J.W. Christian, Acta Met., 2, 148 (1954).

[26] K. Otsuka, M. Takahashi, and K. Shimizu, Metall. Trans., 4, 2003 (1973).

The kinetics of the transformation in sample 1 were typical of martensitic transformations. The average fcc→hcp transformation temperature was 14.8 K and the average hcp→fcc transformation temperature was 15.0 K. There was a hysteresis of .2 K. The athermal nature of the transformation was best illustrated by the transformation at 1:18, in which the interface remained stationary for three minutes when the temperature was held constant. This indicated that the transformation required the temperature to increase; *i.e.* the transformation required an athermal width. No stabilization took place on this interface.

In sample 2, transformations occurred in which one interface traversed the entire width of the sample and yet other interfaces were observed during the same transformation. It is likely that sample 2 had large grains (one of which was as wide as the optical aperture) but was not a single crystal. The production of a large grain sample in spite of a pressure pulse being applied to the sample is consistent with observations of Mills and Schuch[37].

Defects in the sample affect the progress of the transformation. This was most clearly seen in the transformations in sample 2 shown in fig. 3.19. The observation that the crystal defects interfere with the progress of the transformation is the most direct evidence that the transformation is martensitic. If the atomic displacements are to be highly correlated, the advance of an interface requires atoms to move from specific lattice sites of the parent crystal to specific lattice sites of the product crystal. Defects in the parent crystal will result in atoms not being at the sites on which the transformation mechanism was "designed" to operate. Civilian transformations, by contrast, do not have highly correlated atomic displacements and therefore do not require the atoms in the parent crystal to be in specific positions; *i.e.* lattice defects should not severely hinder civilian transformations.

---

[37] R.L. Mills and A.F. Schuch, J. Low Temp. Phys., 16, 305 (1974).

In the transformation illustrated in fig. 3.19, the portion of the interface that advanced did not extend to the right after advancing beyond the defect. This is difficult to understand in the context of the ISPA model. In this model, the glide plane of the partials is parallel to the advanced section of the interface. One must ask why the partials that make up the interface did not migrate entirely to the right end of the sample once the interface had passed the defect. Since the identical partials repel, there is no surface tension to hold the partials back from advancing. On the other hand, the failure for the advanced section to extend to the right can be understood if the CSPA interface model is accepted. In this model, the glide plane of the partials is not parallel to the advanced section of the interface. The defect may have blocked the migration of partials that were travelling on glide planes that intersected the defect. These glide planes would have continued to be blocked even after one section of the interface advanced beyond the defect. Alternatively, the surface tension in the interface may have kept the advanced section of the interface from extending to the right.

Figure 3.20 illustrates another transformation that was affected by a defect. The interface appeared to rotate about a pivot. This is difficult to understand in the context of the ISPA model. In this model, the interface must remain in the original orientation (the δ plane) if the partials are to remain widely separated. On the other hand, the rotation of an interface can be undestood in the context of the CSPA model. In this model, the interface tends to lie in the preferred habit plane because the energy of the interface is lowest there; however, if the interface is prevented from advancing in this orientation, the chemical driving force behind the transformation may be sufficient to force the interface out of this orientation. Outside the preferred orientation, the interface may be kept roughly planar by the surface tension in the interface. If the interface is kept roughly planar and pinned along one line, it can only advance by rotating about the pinning line.

The curved interfaces observed in sample 2 may also be consistent with the CSPA model provided that the circumstances prevented the interface from lying in the preferred orientation. Perhaps defect structures that accumulated after several transformations made it more difficult for the interface to migrate in the preferred orientation.

Light and dark bands sometimes appeared during rapid cooling or heating. Since both bands (those lighter and those darker than the shade of original grey) formed, at least two variants formed that did not have the fcc structure. Both of these variants may have been hcp variants. Alternatively, one or both variants may have been a metastable close-packed phase. These bands may have formed during twinning or during a structural phase transformation. Although the cause of these bands is not clear, the formation of the bands does not appear to be inconsistent with the CSPA model.

F. SUMMARY

Observations that the transformation was affected by defects in the solid provide the most direct evidence that the transformation is indeed martensitic. The transformation exhibited a hysteresis and athermal transformation kinetics. The hcp crystal orientation, and often the habit plane orientation, was reproduced in consecutive transformations. These features are associated with thermoelastic martensitic transformations. The transformation can occur with the migration of a single planar interface across the entire sample. This indicates that the transformation is self-accommodating and is the strongest evidence that the transformation is thermoelastic. An extraordinary observation was made of a transformation that occurred as an interface rotated about a pivot. The pivot was at the site of a defect in the crystal to which the interface was pinned. The fact that, under certain circumstances, the interface could rotate can be accounted for if the interface was modeled by an array of coupled Shockley partials, and not if the interface was modeled by an array of identical Shockley partials. Additional evidence supporting the former model (CSPA model) was found from other interactions between the interface and defects, and from the observation that the hcp orientation could be reproduced in consecutive transformations even when the interface orientation was not reproduced. All the observations on the transformation morphology were consistent with the CSPA model.

Fig. 3.1 a) (top) Thompson Tetrahedron

A,B,C,&D are the tetrahedron vertices. α,β,γ,&δ are the centroids of the tetrahedron faces. The faces represent fcc close-packed planes and the edges represent fcc close-packed lines.

b) (bottom) hcp Double-tetrahedron

a,b,c,s,&t are the vertices of the double-tetrahedron. σ is the centroid of the mid-plane. ab,bc,&cd represent the hcp close-packed directions and the mid-plane, σ, represents the hcp close-packed plane.

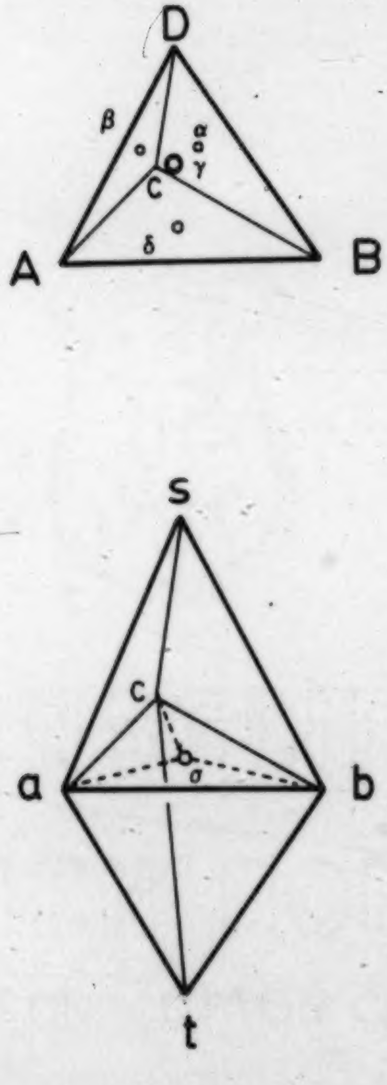
D
β
α
γ
C
δ
A
B
s
c
a
b
σ
t

Fig. 3.1 a) (top) Thompson Tetrahedron
b) (bottom) hcp Double-Tetrahedron

Table 3.1

Lattice Planes and Vectors in the Shoji-Nishiyama Relation

fcc		hcp	
Miller notation	Thompson notation	Miller notation	Thompson notation
(111)	δ	(0001)	σ
$(1\bar{1}1)$	α		
$(\bar{1}11)$	β		
$(11\bar{1})$	γ		
$\frac{1}{2}\langle\bar{1}10\rangle$	AB	$\frac{1}{3}\langle\bar{1}2\bar{1}0\rangle$	ab
$\frac{1}{2}\langle10\bar{1}\rangle$	BC	$\frac{1}{3}\langle2\bar{1}\bar{1}0\rangle$	bc
$\frac{1}{2}\langle0\bar{1}1\rangle$	CA	$\frac{1}{3}\langle\bar{1}\bar{1}20\rangle$	ca
$\frac{1}{6}\langle\bar{1}2\bar{1}\rangle$	Aδ	$\frac{1}{3}\langle01\bar{1}0\rangle$	aσ
$\frac{1}{6}\langle2\bar{1}\bar{1}\rangle$	Bδ	$\frac{1}{3}\langle1\bar{1}00\rangle$	bσ
$\frac{1}{6}\langle\bar{1}\bar{1}2\rangle$	Cδ	$\frac{1}{3}\langle\bar{1}010\rangle$	cσ
$\frac{1}{3}\langle111\rangle$	Dδ	$\frac{1}{2}\langle000\bar{1}\rangle$	sσ

Fig. 3.2 Migration of a Shockley Partial

The yellow spheres are in a close-packed planar arrangement and lie on the green spheres, which are also in a close-packed planar arrangement. Similarly, the blue spheres are in a close-packed planar arrangement and lie on the green spheres. The triangle is the δ face of the Thompson tetrahedron and serves as a coordinate system for the spheres. The gap running between the yellow spheres and the blue spheres represents a dislocation. In going from fig. 3.2a to fig. 3.2h, the dislocation line has migrated upwards and, in its course, has caused one row of spheres to be displaced by δC. This indicates that this dislocation is a δC Shockley partial. In fig. 3.2a, the partial lies along a close-packed line in the BC direction. In fig. 3.2d, the partial crosses over from one BC close-packed line to an adjacent BC close-packed line at a "kink", near the center of the figure. In figures 3.2b to fig. 3.2f, the kink migrates to the left as adjacent spheres are displaced. The result is the advance of the partial across one close-packed row of spheres.

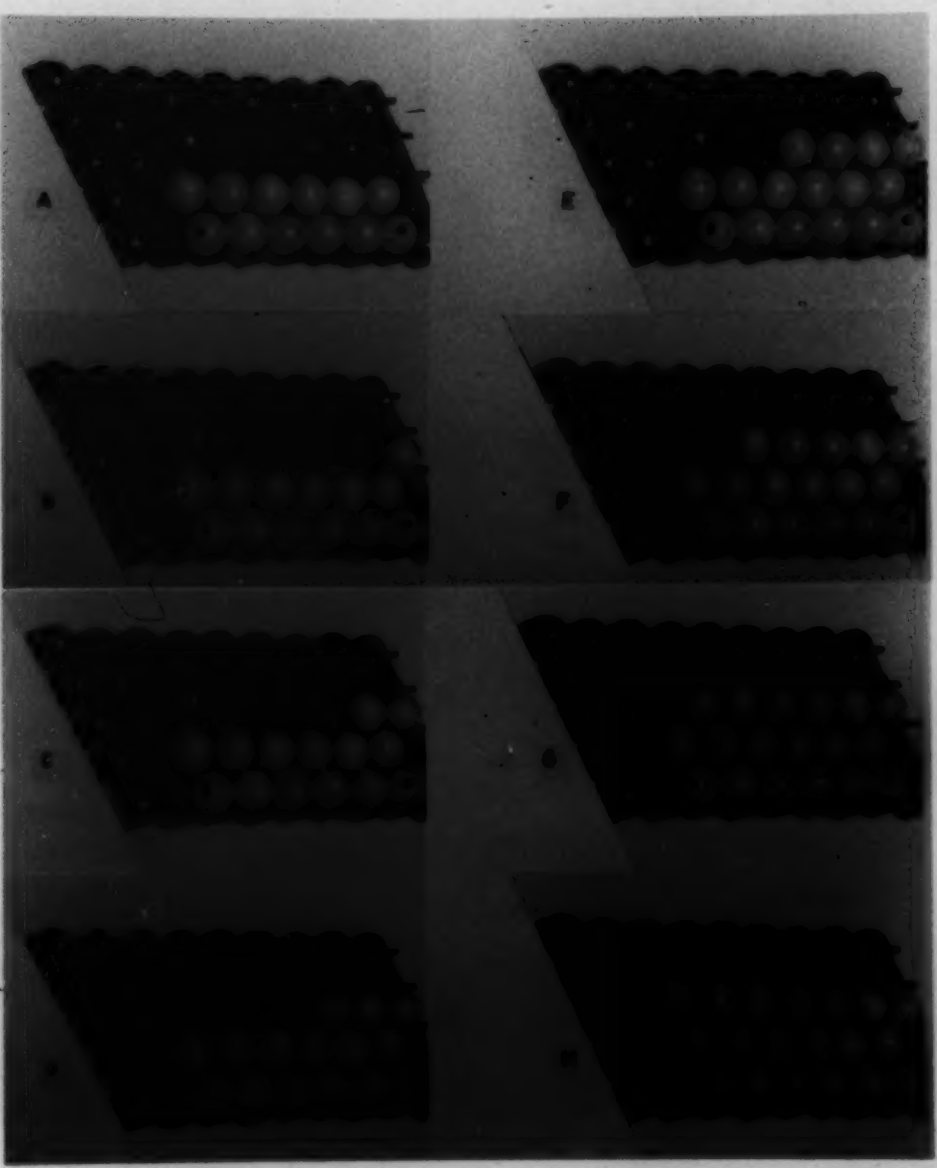
A
E

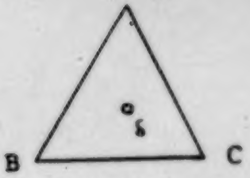
A
a
b
B
C

Fig. 3.3 Model of Identical Shockley Partials

The photographs in fig. 3.3 show four different arrangements of spheres. The photographs in the right colunm show a different perspective of the arrangement shown in the photograph to its left. The top pnotographs show spheres in the fcc structure. The Thompson tetrahedron is illustarted to serve as a reference system for the model. The color scheme of the spheres on the right half of the model draws attention to the ABCABC stacking sequence of the close-packed layers in the fcc structure. The spheres on the left half of the model are in the fcc structure even though the spheres are colored differently. The right face of the model is a {100} plane and the left face is the β close-packed plane. The second pair of photographs show a model of a partial dislocation lying along AB in the fcc structure. The partial has glided in from the left and displaced the spheres that are above the lowest layer on the left half of the model. The displacement is most easily seen in the yellow sphere marked with the arrow. Since the spheres have been displaced by Aδ, the dislocation is an Aδ partial. The partial is situated at the bottom of the gap in the model. A stacking fault lies in the δ plane to the left of the partial. The stacking fault may be thought of as a thin layer of hcp structure within a fcc lattice. In a real crystal the gap shown is closed by elastic strain that force the atoms above the partial back into a close-packed configuration. The elastic strain required to close the gap extends deep into the crystal and is responsible for most of the energy of the partial. In the third pair of photographs, a second Aδ partial has glided in from the left on a δ plane above the glide plane of the previous partial. Again, the displacement can be most easily seen in the sphere marked by the arrow. In the bottom pair of photographs, a third Aδ partial has glided in from the left and displaced the spheres in the top layer. The migration of the three partials has changed the stacking arrangement in the six layers on the left from a fcc arrangement to a hcp arrangement. The colors of the spheres on the left draw attention to the ABABAB stacking arrangement of the hcp lattice. Each partial has widened the gap and resulted in an increase of the elastic strain energy that would be necessary to close the gap in a real crystal. These partials are shown in close proximity aligned along the β plane. In reality the identical partials would repel and be more widely separated, yet the net dispacement of the spheres in the sixth layer due to the three partials would be the same. In a real crystal, the displacement of the spheres on the left half of the model relative to the displacement of the spheres on the right half of the model must approach zero as the distance from the partials increases. The strain necessary to meet the above requirement produces much strain energy in arrays of identical partials.

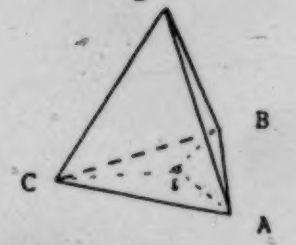
D
B
C
A

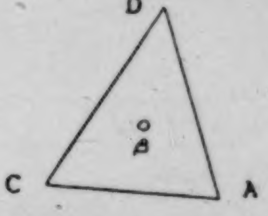
D
β
C
A

Fig. 3.4a ISPA Model of the Interface with Accommodation by Surface Relief

Each Aδ in this figure represents a partial dislocation that has a Burgers vector of Aδ and that lies along BC, the close-packed line running perpendicular to the plane of the page. The hcp c-axis is along the Dδ direction (the vertical axis in the figure). The glide plane of each partial dislocation, the δ plane, is perpendicular to the Dδ direction. Since the partials repel, they are widely separated. This results in the interface lying very close to the δ plane. As the partials glide to the right, the interface moves upward and the hcp→fcc transformation occurs. The deformation produced by the passage of the interface that transforms one crystal lattice into another is called the lattice distortive deformation. In the ISPA model, the lattice distortive deformation will rotate the plane that is perpendicular to the Burgers vectors of the partials by 19.5°. If this plane is along a free surface of the crystal, it will rotate from its original position (the position marked by the dashed line). The tilting of the free surface to accommodate the lattice distortive deformation is called surface relief.

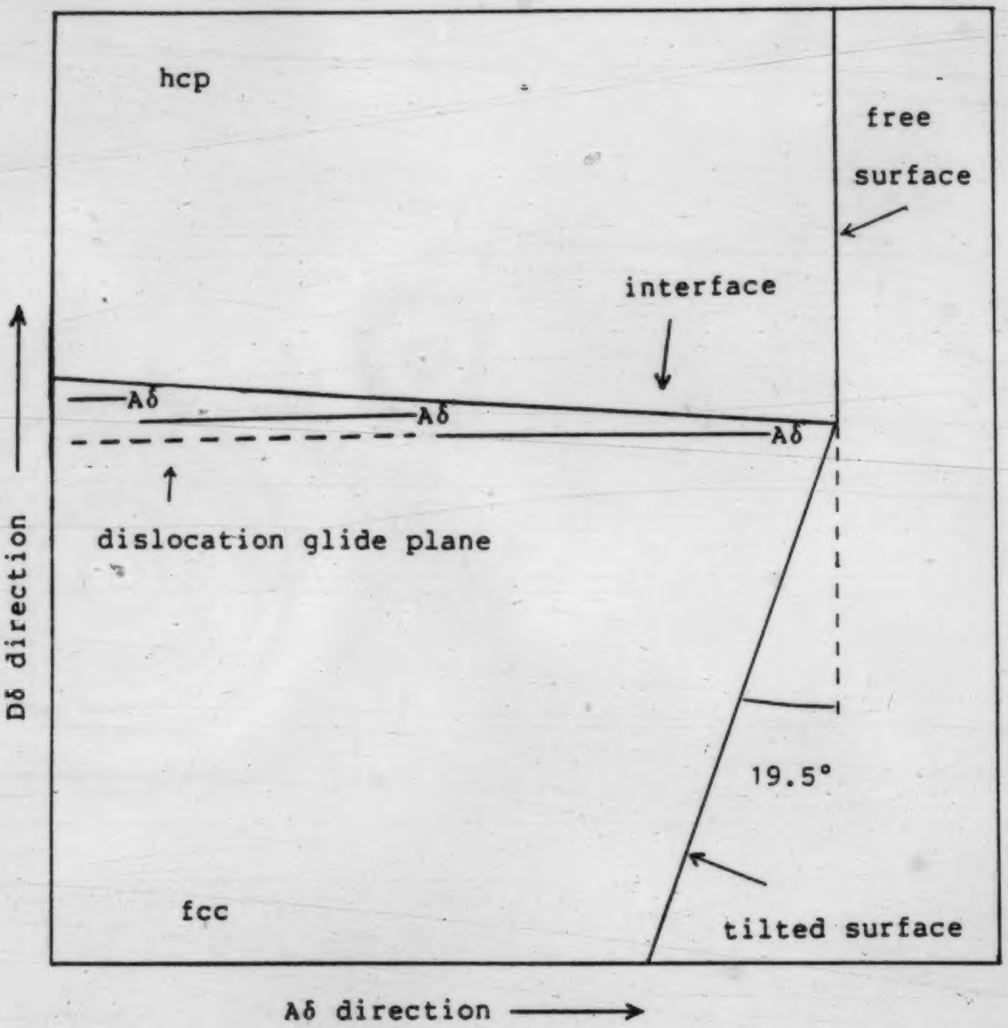
hcp
free
surface
interface
Aδ
Aδ
Aδ
Dδ direction
dislocation glide plane
19.5°
fcc
tilted surface
Aδ direction

Fig. 3.4a ISPA Model of the Interface with Accommodation by Surface Relief

Fig. 3.4b ISPA Model of the Interface
with Accommodation by Elastic Stress

In many cases, the lattice distortive deformation may not occur freely, *i.e.* retraints within the bulk may not permit planes to rotate as in fig. 3.4a. In such cases, the lattice distortive deformation is accommodated by a lattice invariant deformation. In fig. 3.4b, the lattice invariant deformation is the elastic deformation equivalent to rotating the tilted plane of fig. 3.4a back to its original orientation. In reality, the lattice distortive deformation and the lattice invariant deformation may occur simultaneously so that the "tilted plane" does not move during the course of the transformation, but simply comes under an increasing elastic stress. The elastic energy associated with this deformation increases as the transformation continues and eventually more energy may be required by the elastic deformation than is available from the transformation.

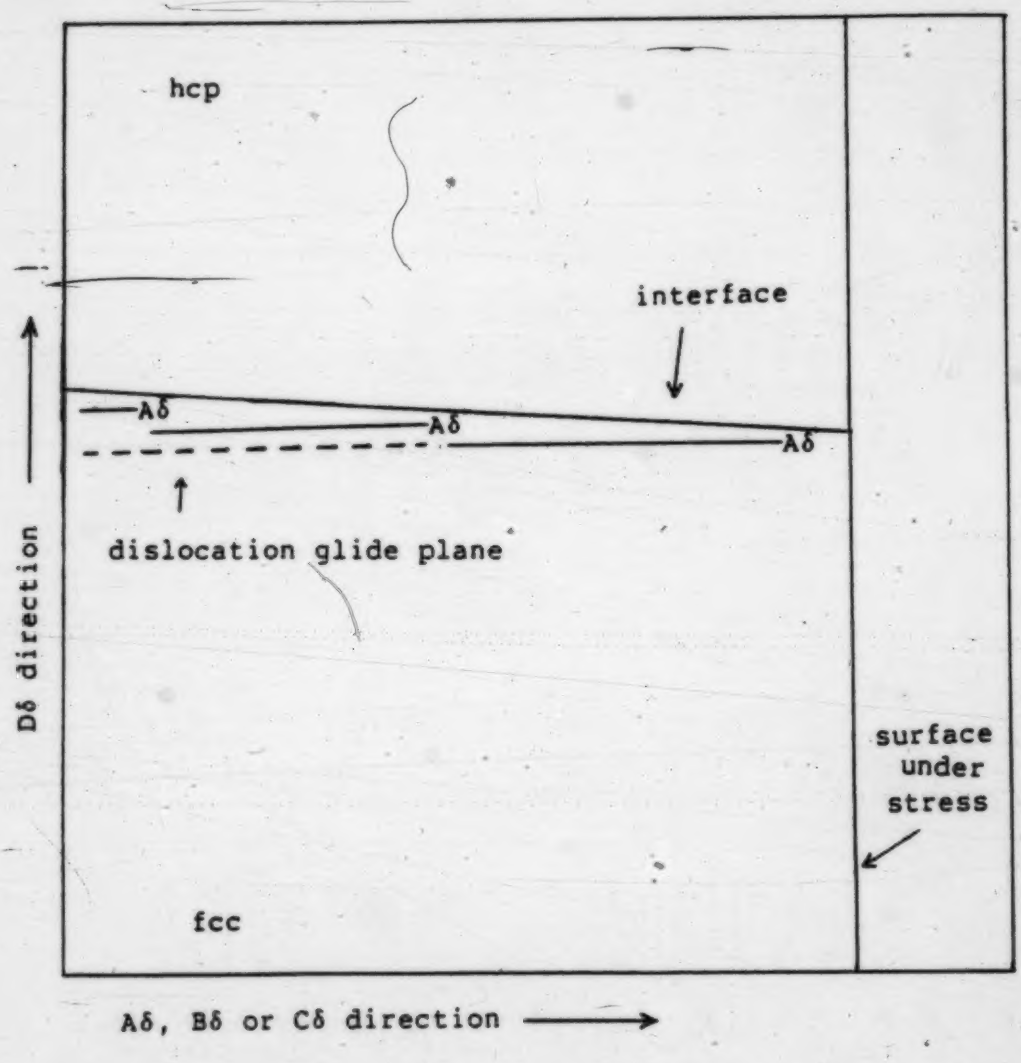
hcp
interface
Aδ
Aδ
Aδ
dislocation glide plane
surface under stress
fcc
Dδ direction
Aδ, Bδ or Cδ direction

Fig. 3.4b ISPA Model of the Interface with Accommodation by Elastic Stress

Fig. 3.4c ISPA Model of the Interface with Accommodation by Slip

The interface in this figure migrates upwards as in fig. 3.4a; however, the lattice distortive deformation is accommodated by slip. Slip is a lattice invariant deformation that may occur by perfect dislocations gliding in the δ plane. Since $3A\delta = AC + AB$, the deformation in six close-packed layers produced by three Aδ partials migrating to the right may be accommodated by an AC and an AB dislocation migrating to the left after the interface has passed.

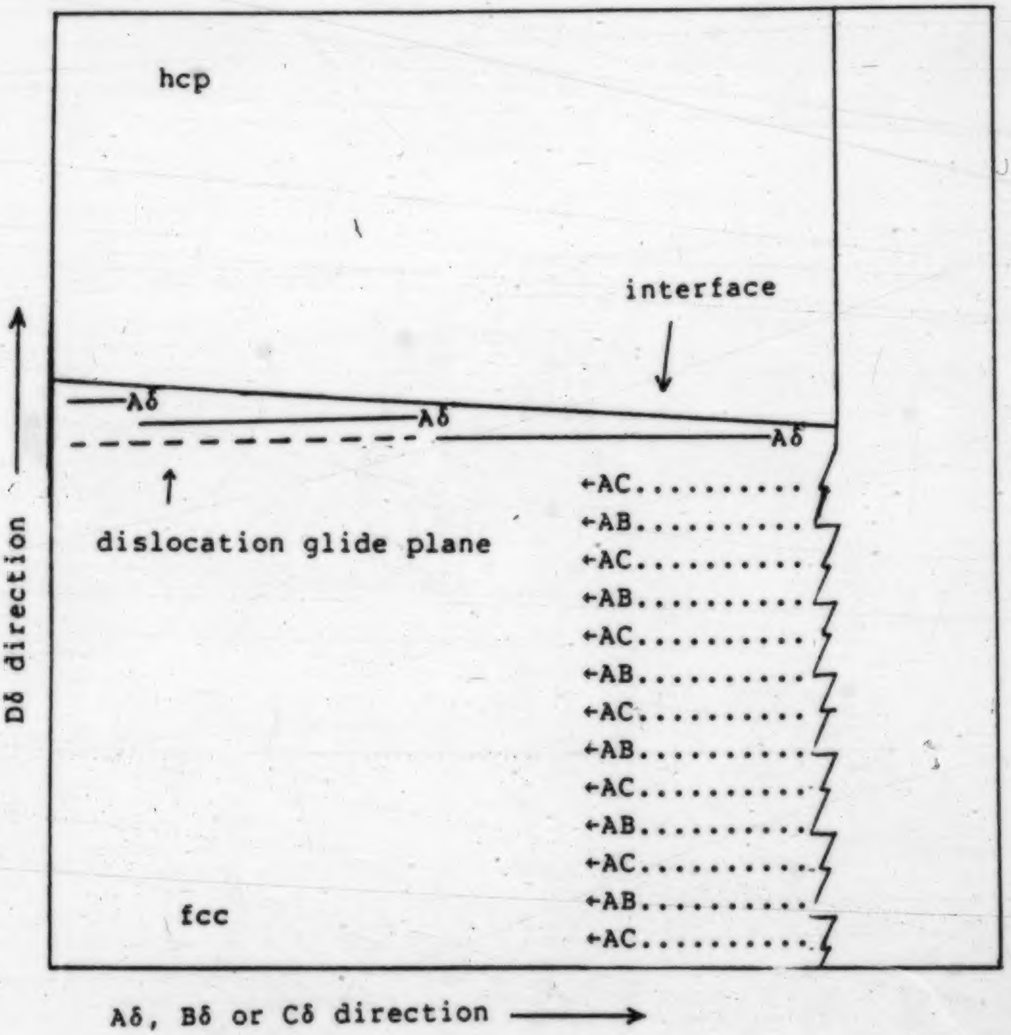
hcp
interface
Aδ
Aδ
Aδ
dislocation glide plane
←AC..........
←AB..........
←AC..........
←AB..........
←AC..........
←AB..........
←AC..........
←AB..........
←AC..........
←AB..........
←AC..........
←AB..........
←AC..........
fcc
Dδ direction
Aδ, Bδ or Cδ direction

Fig. 3.4c ISPA Model of the Interface with Accommodation by Slip

Fig. 3.4d ISPA Model of the Interface with Accommodation by Twinning

The interface in this figure migrates upwards to produce the transformation as in fig. 3.4a; however, the lattice distortive deformation is accommodated by twinning. The migration of the interface produces the "d-variant". After the migration of the interface, half of the fcc phase transforms to the "d'-variant" by twinning. The d'-variant is crystallographically equivalent to the reflection of the d-variant in the δ plane. The d'-variant may form when Aδ partials on *every* δ plane migrate to the left in the figure.

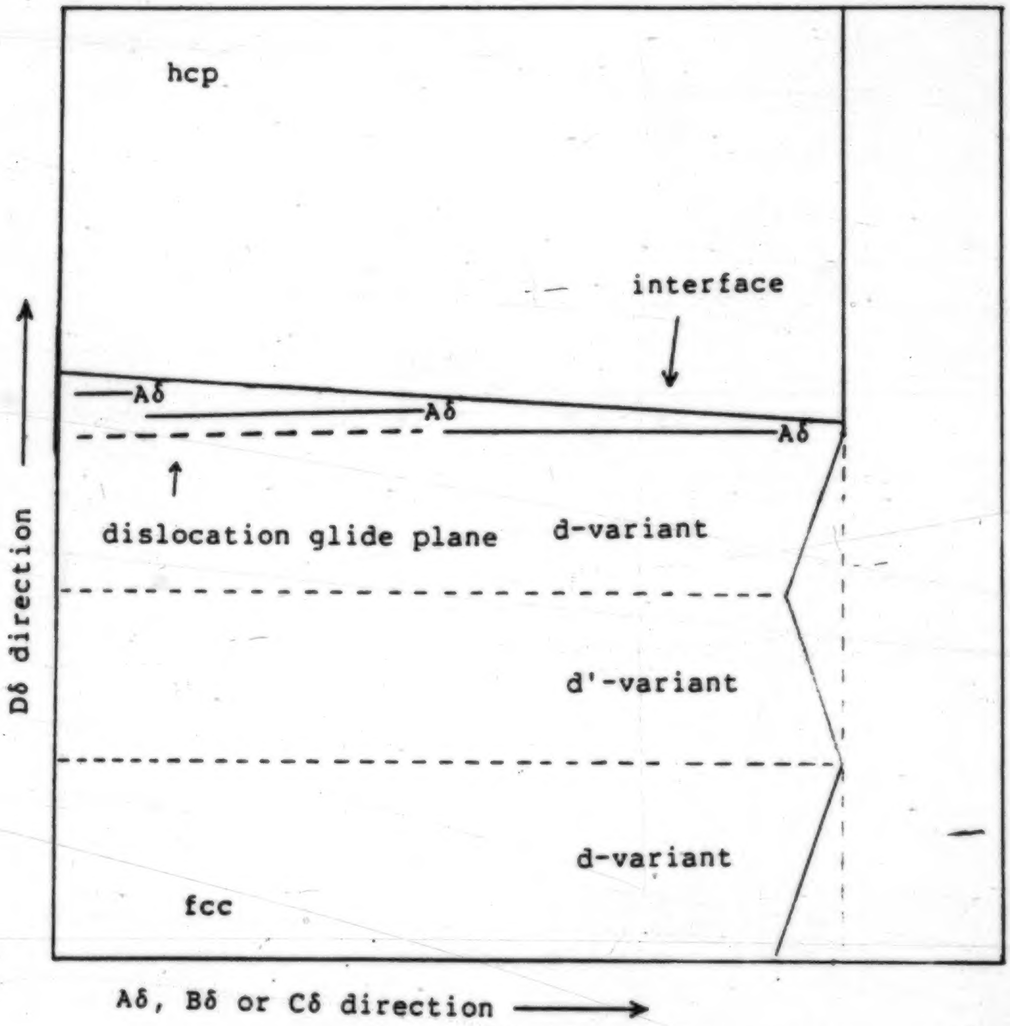
hcp
interface
Aδ
Aδ
Aδ
dislocation glide plane
d-variant
d'-variant
d-variant
fcc
Dδ direction
Aδ, Bδ or Cδ direction

Fig. 3.4d ISPA Model of the Interface with Accommodation by Twinning

Fig. 3.4e ISPA Model of the Interface
with Accommodation by Band Formation

An interface in the ISPA model may be composed entirely of Aδ partials, entirely of Bδ partials or entirely of Cδ partials. An interface of Aδ partials will retain its character if a new Aδ partial is generated on the interface for every Aδ partial that leaves the interface (at a grain boundary, for example). However, at some point, Bδ partials may replace the Aδ partials that leave the interface and the array of Aδ partials will become an array of Bδ partials. An interface may advance a particular distance while it is composed of Aδ partials, change its composition to an array of Bδ partials, advance the same distance, change its composition to an array of Cδ partials, and again advance the same distance. This process will produce bands of the same fcc variant such that the net deformation is zero. This is called a self-accommodating process and requires little lattice invariant deformation.

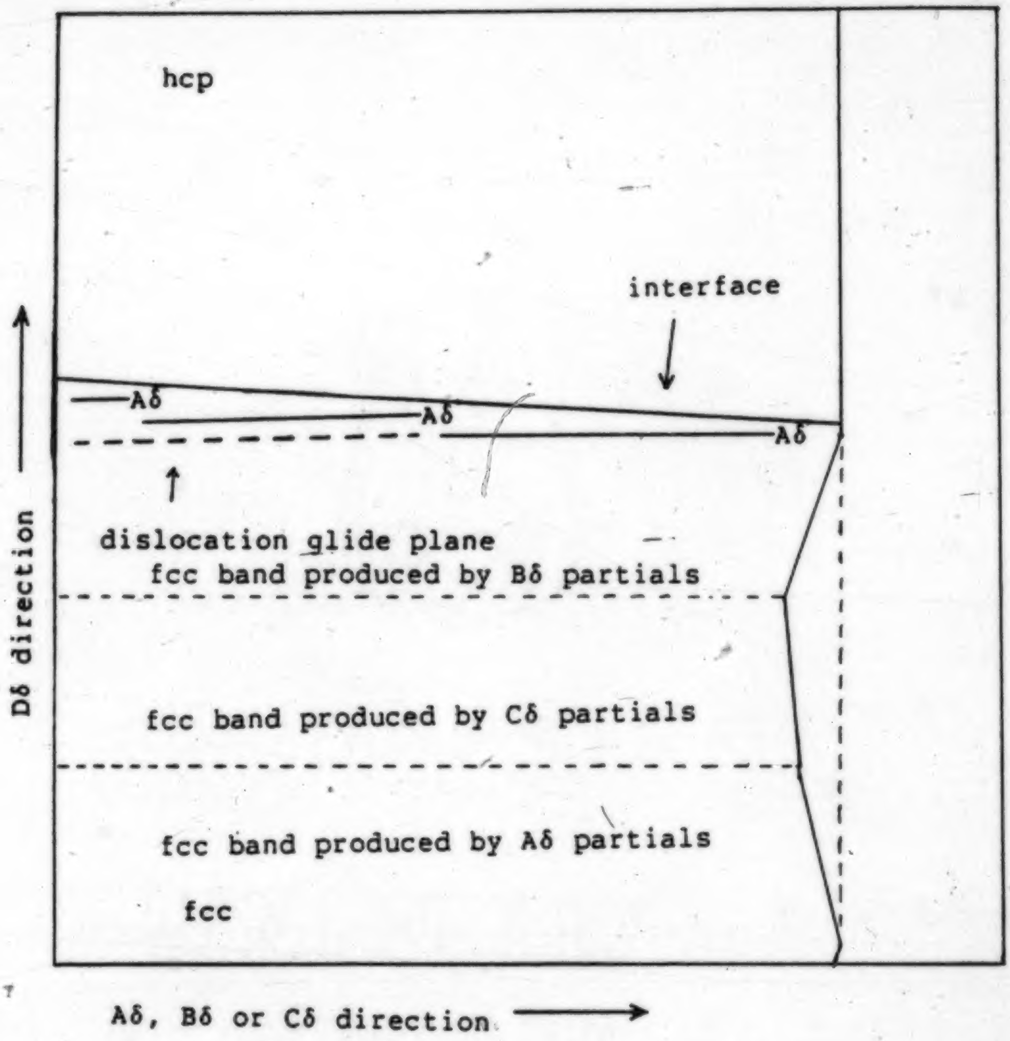
hcp
interface
Aδ
Aδ
Aδ
dislocation glide plane
fcc band produced by Bδ partials
fcc band produced by Cδ partials
fcc band produced by Aδ partials
fcc
Dδ direction
Aδ, Bδ or Cδ direction

Fig. 3.4e ISPA Model of the Interface with Accommodation by Band Formation

Fig. 3.5 Model of Coupled Shockley Partials

This figure, as does fig. 3.3, shows two perspectives of four arrangements of spheres. As in fig. 3.3, the top figures show the fcc structure and the second pair of figures show an Aδ partial along the AB direction in the fcc structure. The third pair of photographs show the addition of a second partial, this time a Bδ partial, that has glided in from the left and displaced the spheres above the third layer on the left half of the model. The displacement is most easily seen in the sphere marked by the arrow. The bottom pictures shows the addition of a third partial, this time a Cδ partial, that has glided in from the left. The gap introduced by the first two partials has been closed and the net displacement in the sixth layer is zero. As a result, no strain is required to close a gap as in the case illustrated in fig. 3.3. This means that the configuration shown here has much less strain energy associated with it. The partials shown are in close proximity and aligned along the β plane. This may occur in reality since the partials attract. The stacking arrangement on the left is the hcp ABABAB stacking arrangement. Thus, the coupled partials shown here may migrate to the left simultaneously to produce the fcc→hcp transformation. An array of coupled partials could act as as fcc-hcp interface.

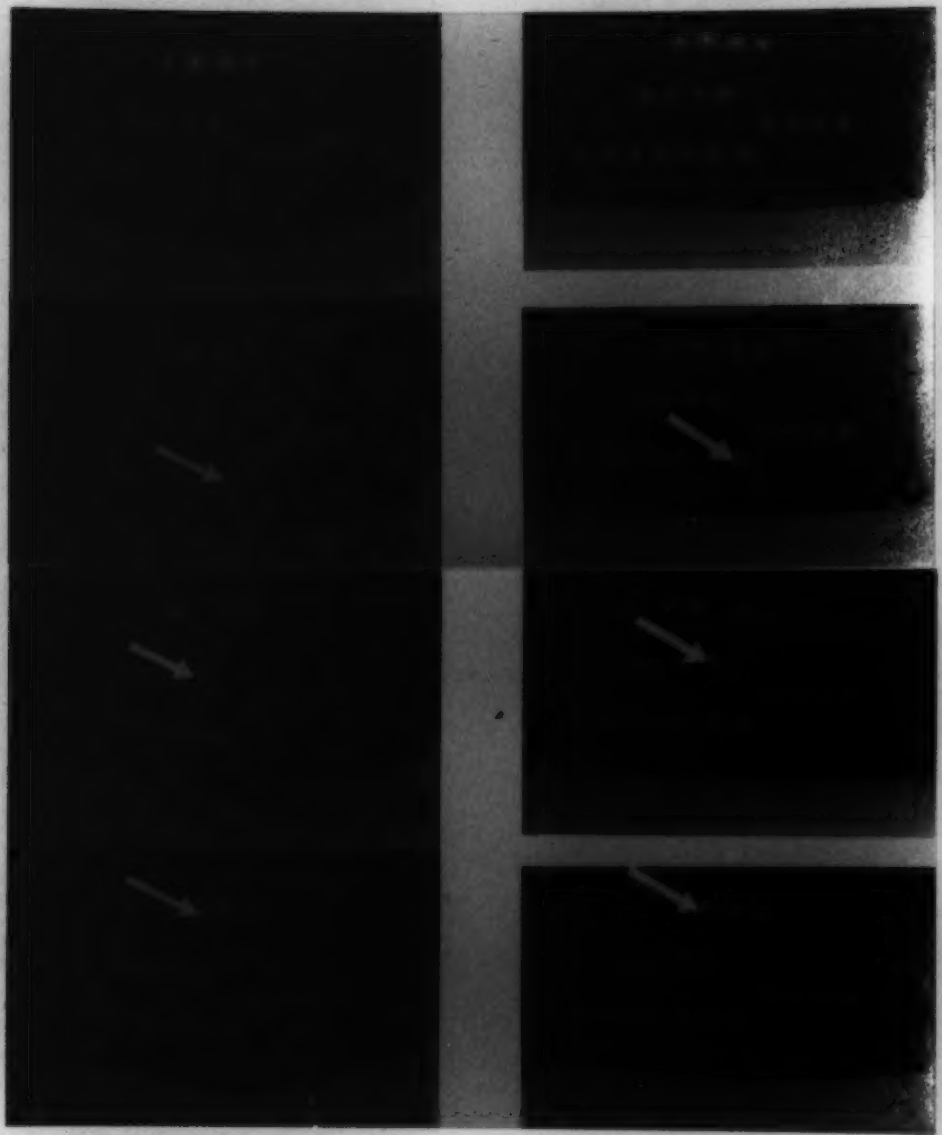

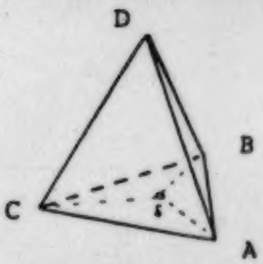
D
B
C
A
δ

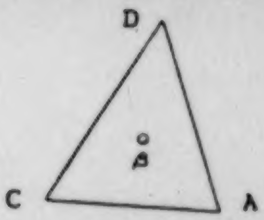
D
β
C
A

Fig. 3.6 CSPA Model of the Interface Structure

Each Aδ in this figure represents a partial dislocation that has a Burgers vector of Aδ and that lies along the close-packed line running perpendicular to the plane of the page. The hcp c-axis is along the Dδ direction (the vertical axis in the figure). The glide plane of each dislocation, the δ plane, is perpendicular to the Dδ plane. Since the partials attract, they are close together. This results in the interface being in an orientation other than the δ plane. As the partials glide to the right, the interface moves towards the upper right corner of the figure and the fcc→hcp transformation occurs. Since the sum of the Burgers vectors of the partials along the array is zero, the array produces no net displacement and no lattice invariant deformation is required to accommodate the product, *i.e.* the transformation mechanism is perfectly self-accommodating.

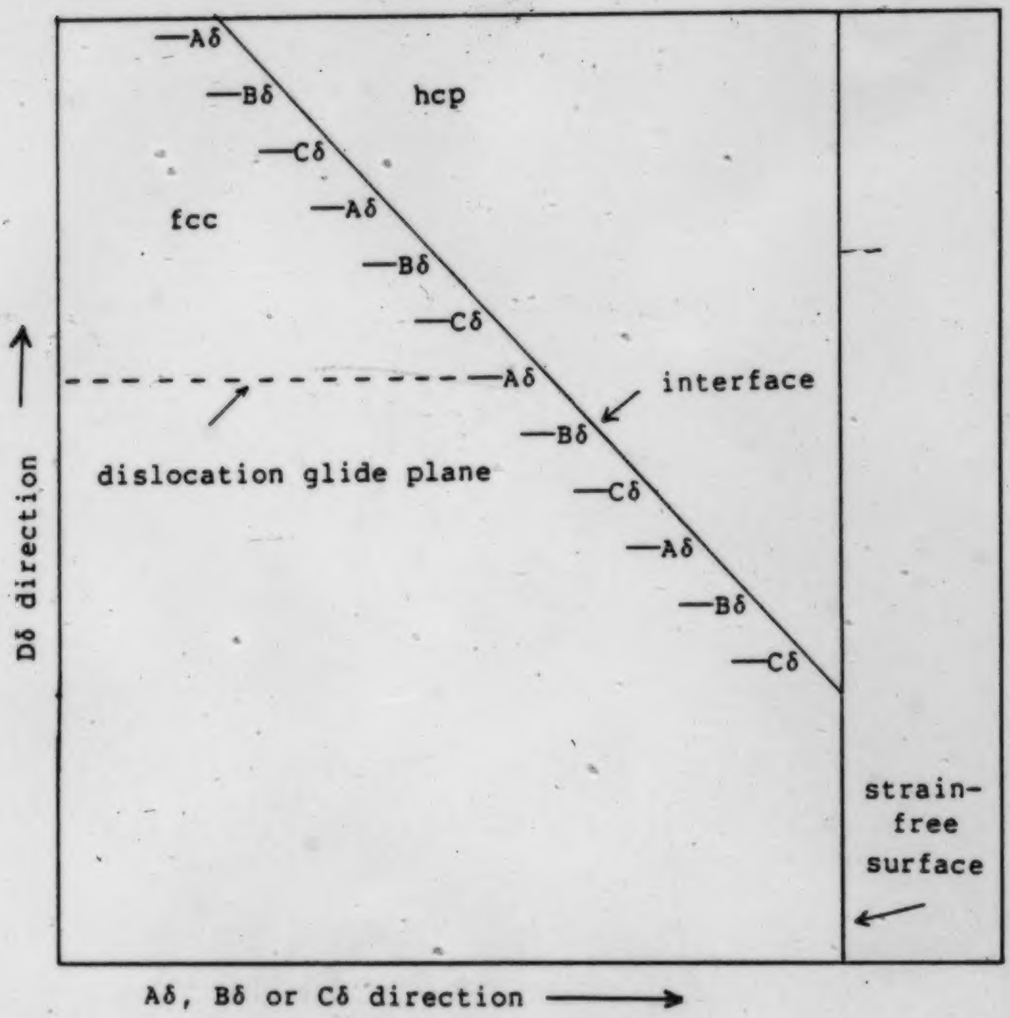
hcp
fcc
Aδ
Bδ
Cδ
Aδ
Bδ
Cδ
Aδ
Bδ
Cδ
Aδ
Bδ
Cδ
interface
dislocation glide plane
Dδ direction
strain-free surface
Aδ, Bδ or Cδ direction

Fig. 3.6 CSPA Model of the Interface Structure

Fig. 3.7 Advance of a CSPA by Kink Migration

Fig. 3.7a shows an array of coupled Shockley partial dislocations. The partials are all in the same plane except for a small piece of one partial that has advanced. On each side of the piece that has advanced, a kink joins the section that has advanced to the rest of the partial. As the kinks separate (fig. 3.7b), more of the partial advances. Kinks in adjacent partials form (fig 3.7b) so that adjacent partials advance together. Continued kink formation and migration (figures 3.7c and 3.7d) leads to the advance of the entire array.

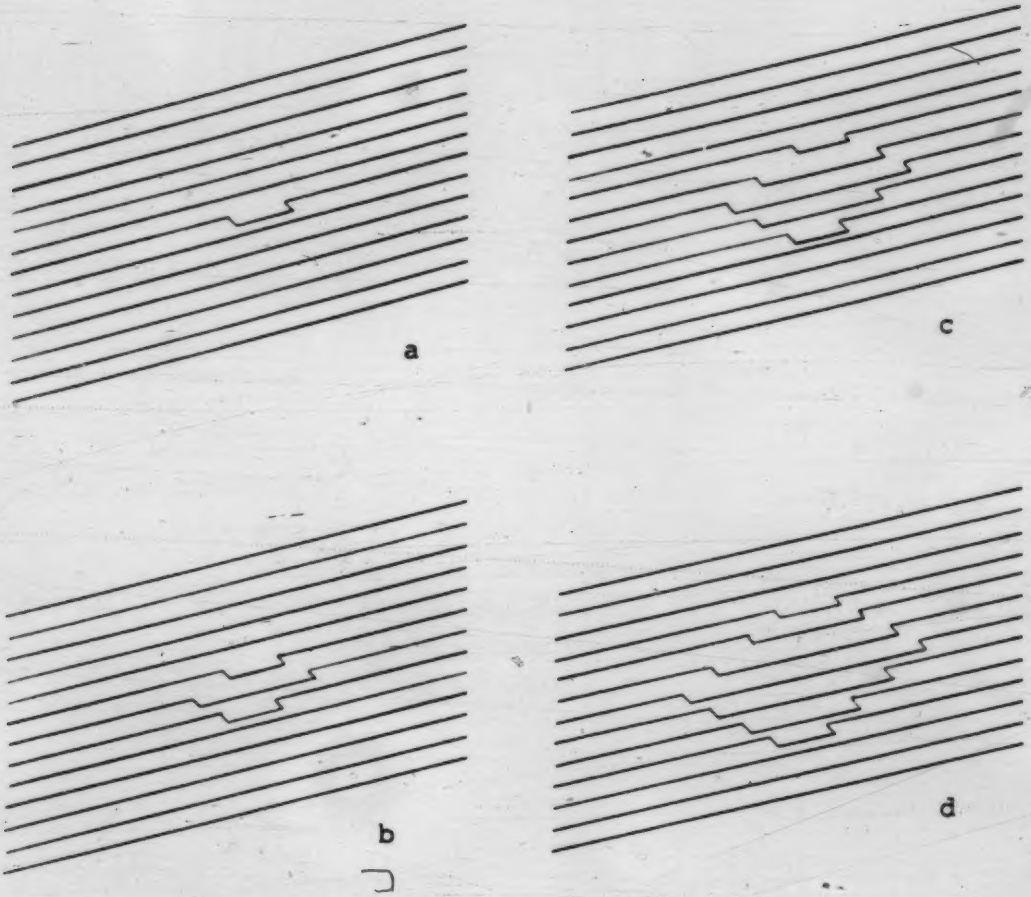

Fig. 3.7 Advance of a CSPA by Kink Migration

Table 3.2

Visually Observed Transformations: Sample 1

time	figure number	temp. K±.005K	heating rate mK/sec	athermal width mK±5mK	SB*
12:40	3.8	15.005	3.2	40	1
12:42	3.8	14.737	-3.6	15	1
12:44	3.9	14.995	4.5	10	3
12:46	3.9	14.777	-3.4	55	1
12:48	3.10	15.061	3.2	30	1
12:51	3.10	14.747	-3.4	25	5
12:53	3.11	15.076	3.2	45	1
12:59	3.12	14.853	-1.1	5	5
1:05	3.12	15.051	1.4	35	3
1:10	3.13	14.818	-1.5	35	2
1:18	3.13	14.995	.06	20	2
1:29	3.14	14.833	-1.3	10	4
1:31	3.14	15.025	2.7	40	2
1:32	3.15	14.894	-3.4	25	3
1:33	3.15	15.030	5.4	20	5
1:42	3.15	14.823	-3.9	55	2
1:45	3.16	15.056	4.1	30	5
1:47	3.16	14.894	-3.4	60	3

* Sharpness of the boundary:
"1"=very sharp, "5"=very diffuse.

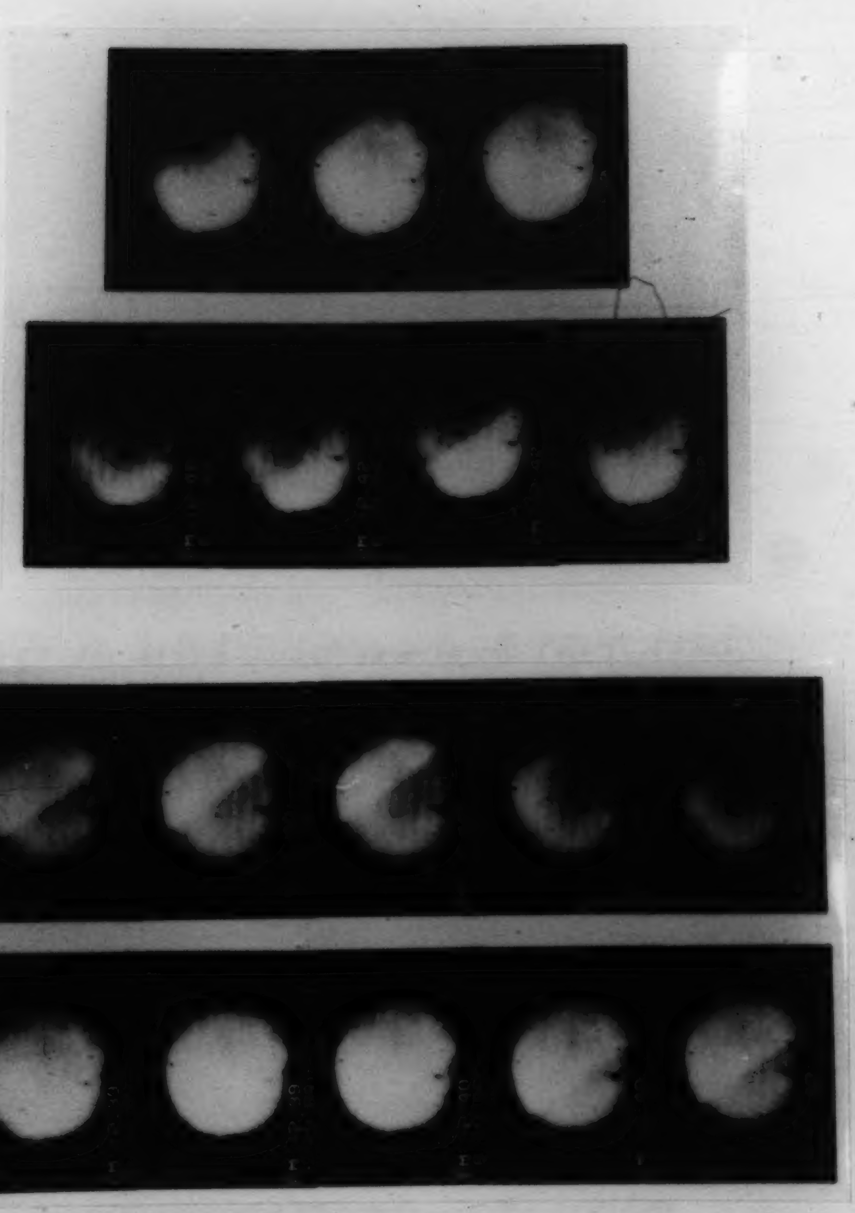

Fig. 3.8 Transformations Occurring at 12:40 & 12:42

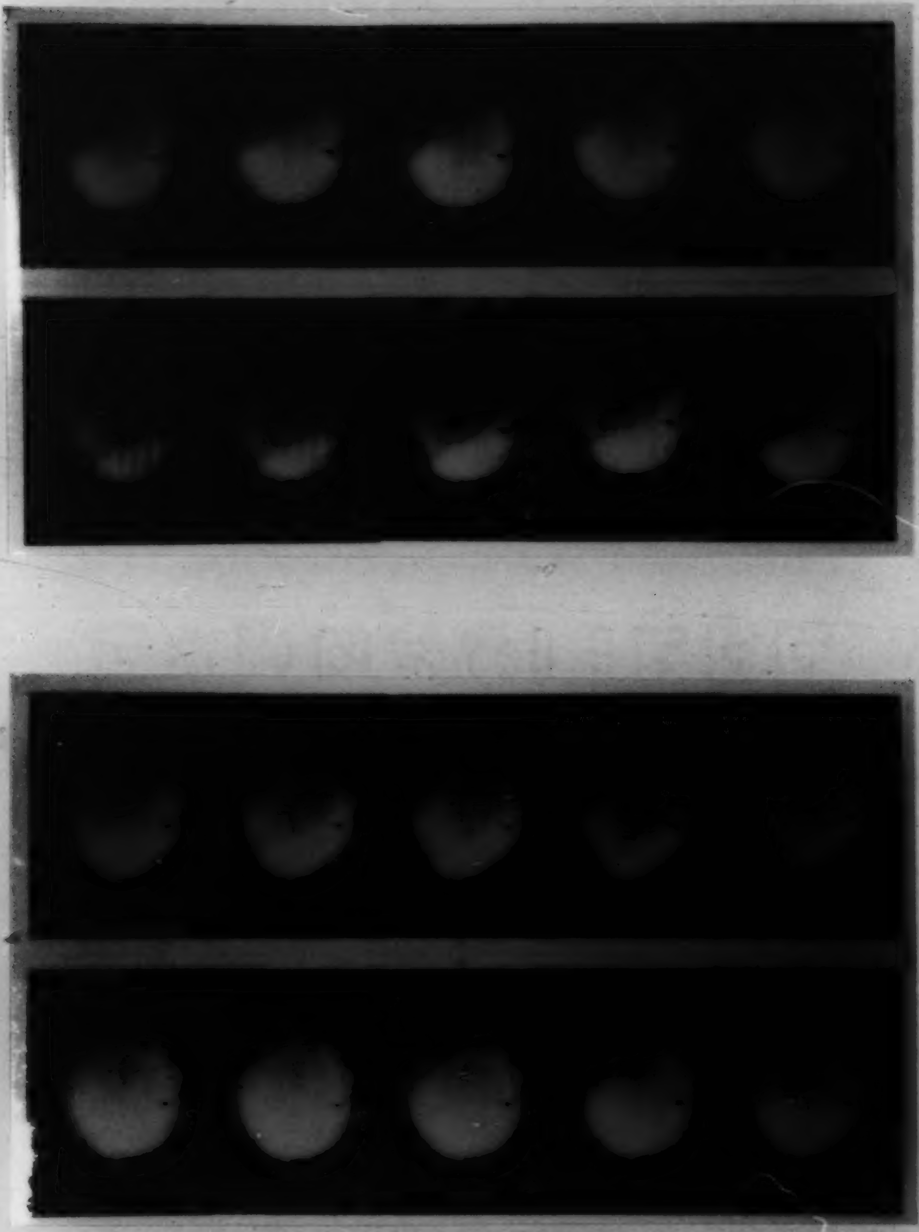

Fig. 3.9 Transformations Occurring at 12:44 & 12:46

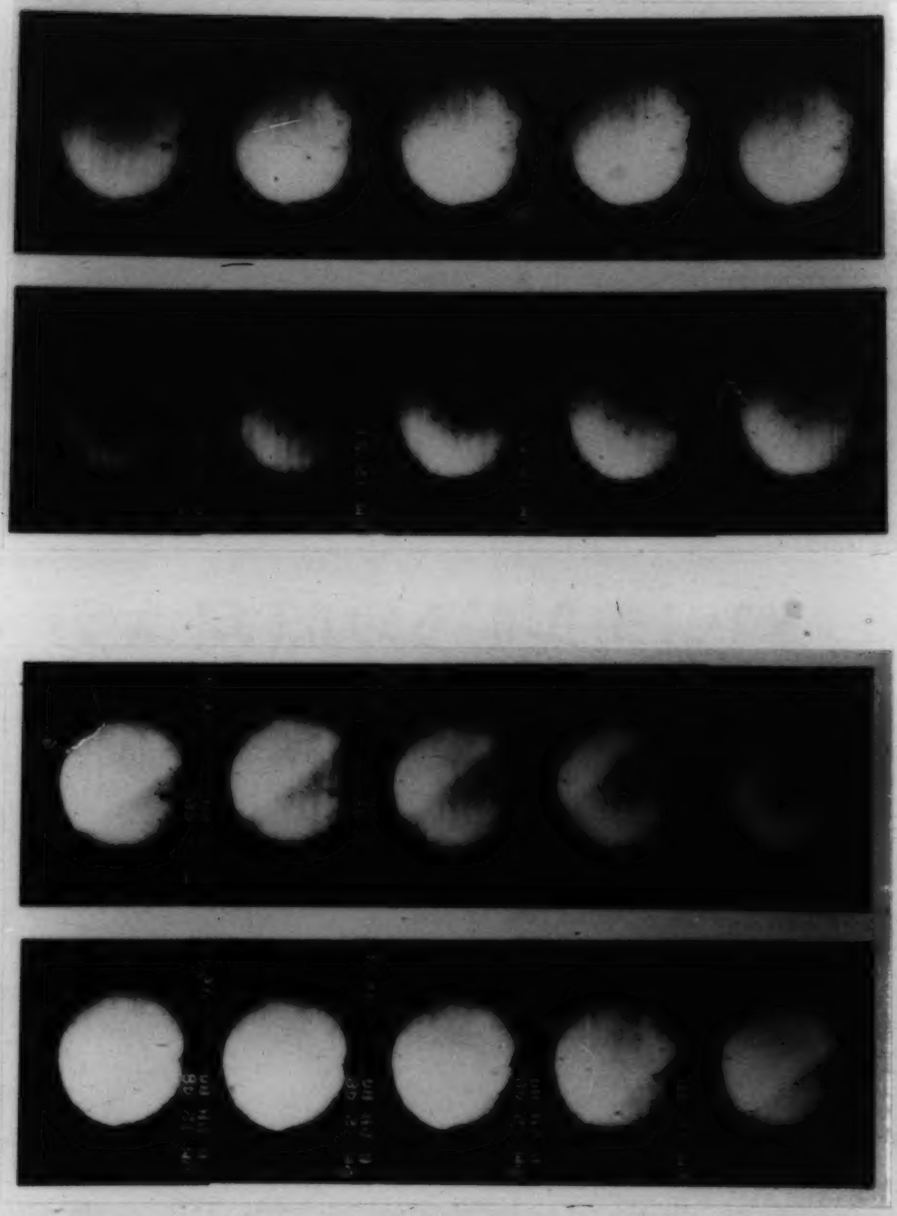

Fig. 3.10 Transformations Occurring at 12:48 & 12:51

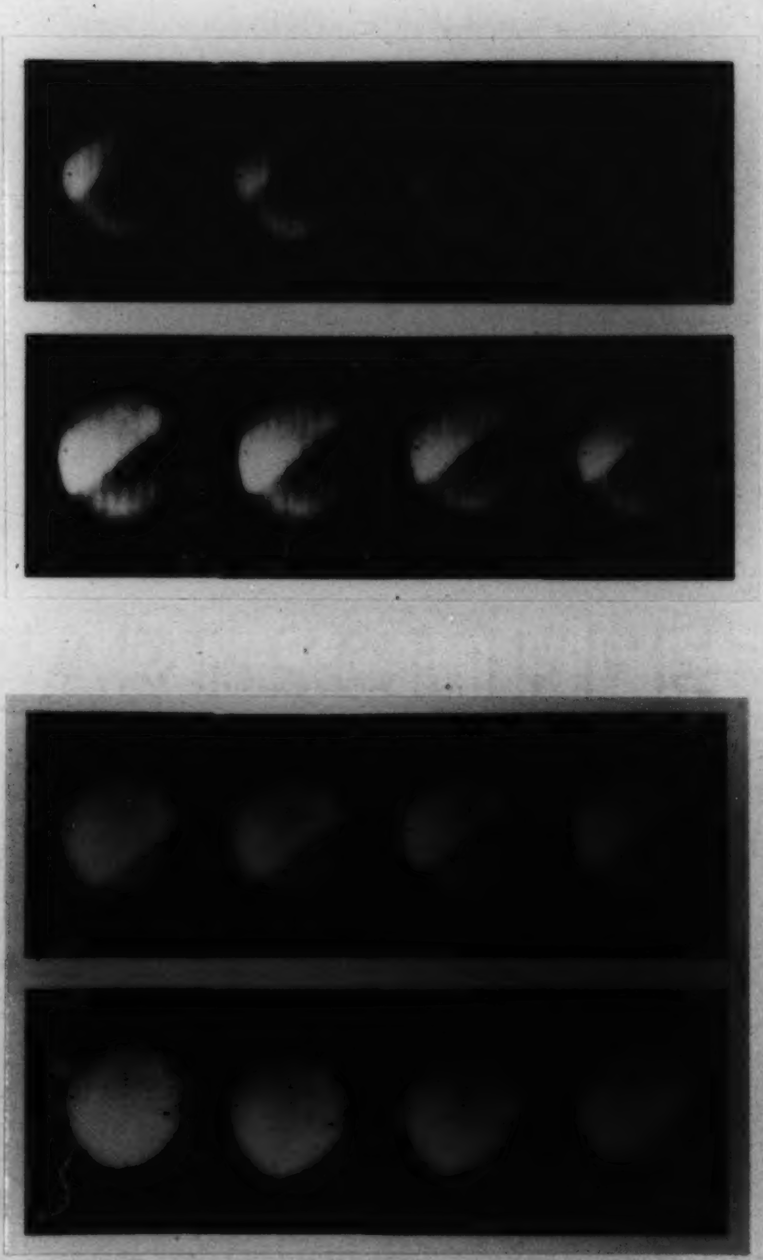

Fig. 3.11 Transformation Occurring at 12:53

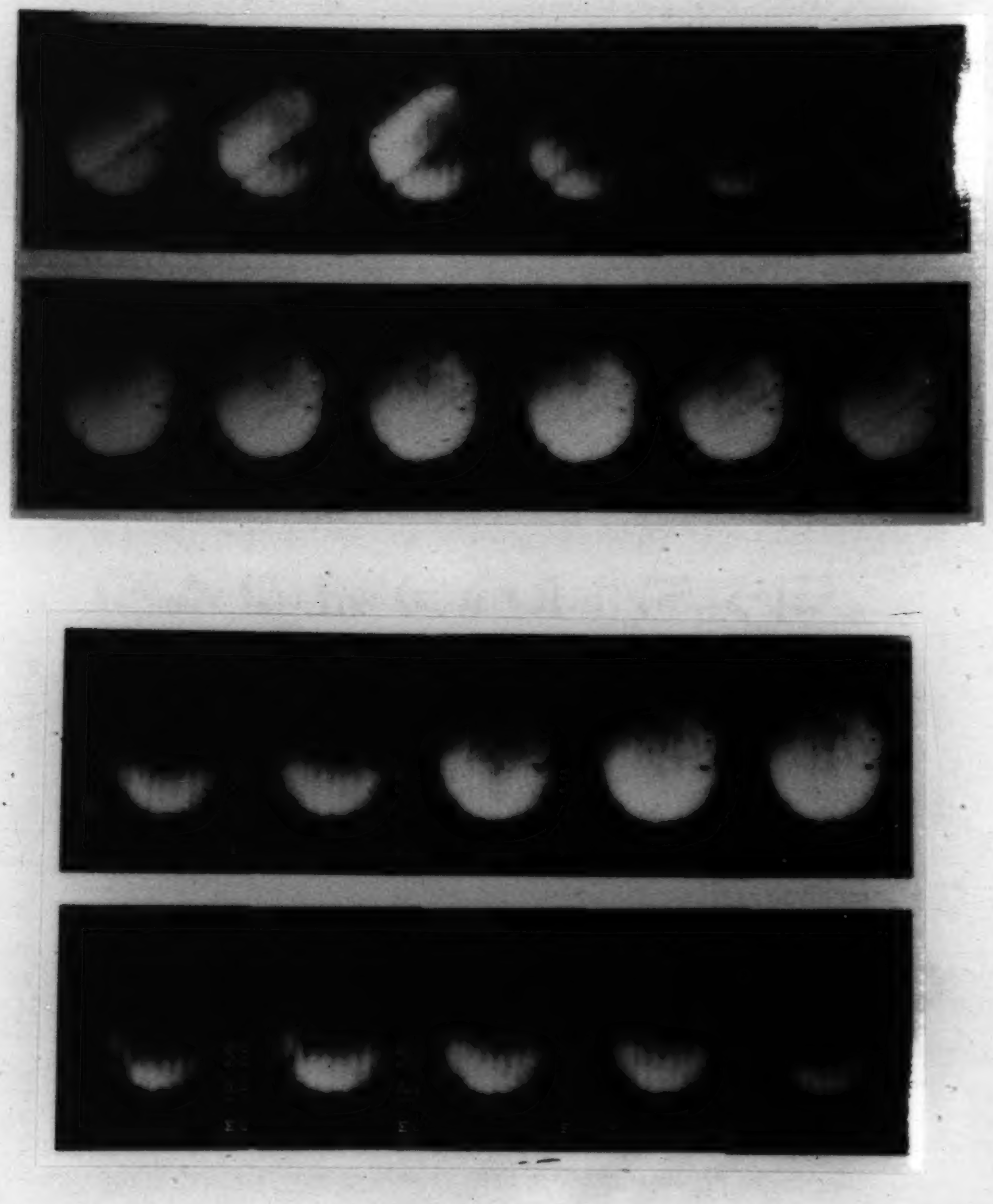

Fig. 3.12 Transformations Occurring at 12:59 & 1:05

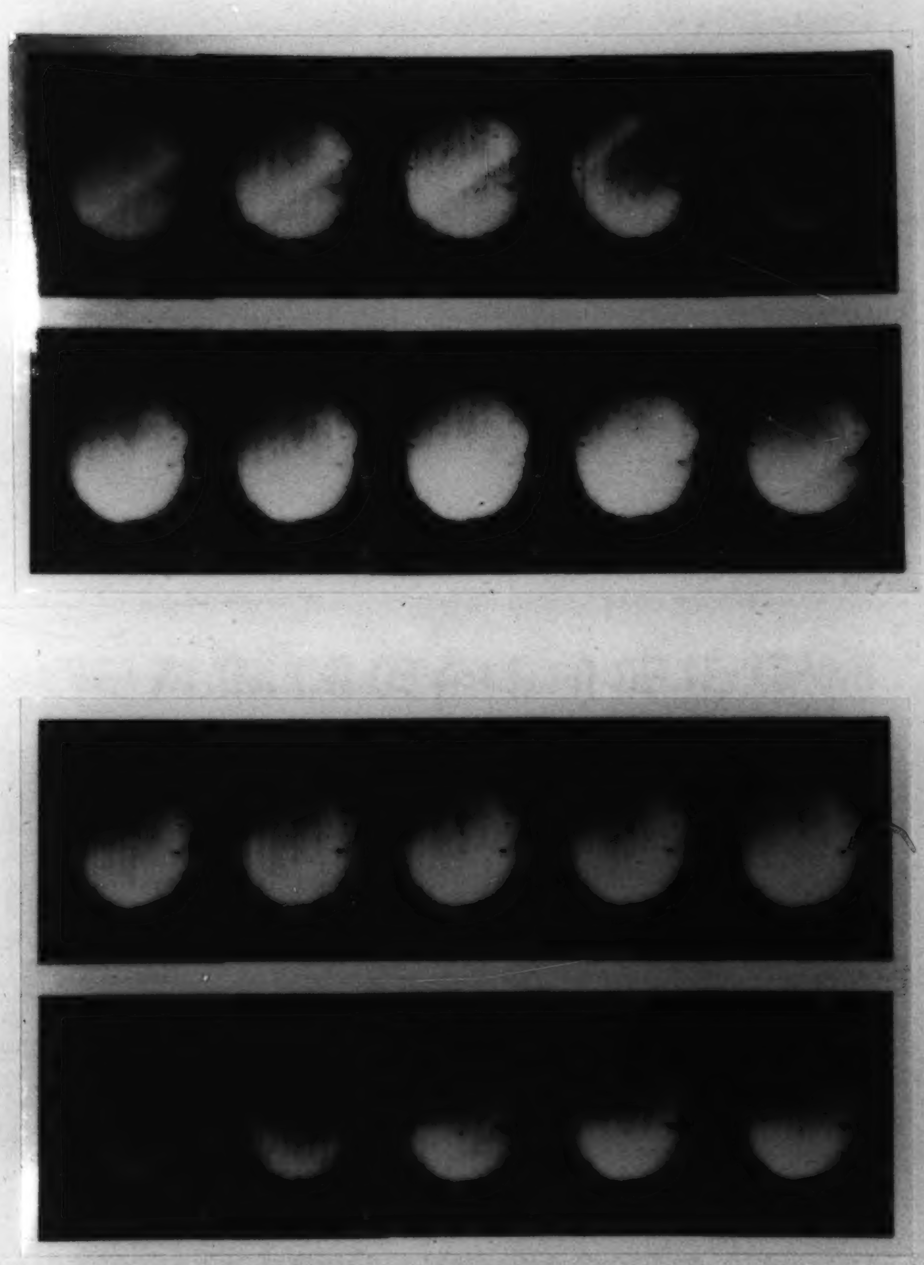

Fig. 3.13 Transformations Occurring at 1:10 & 1:18

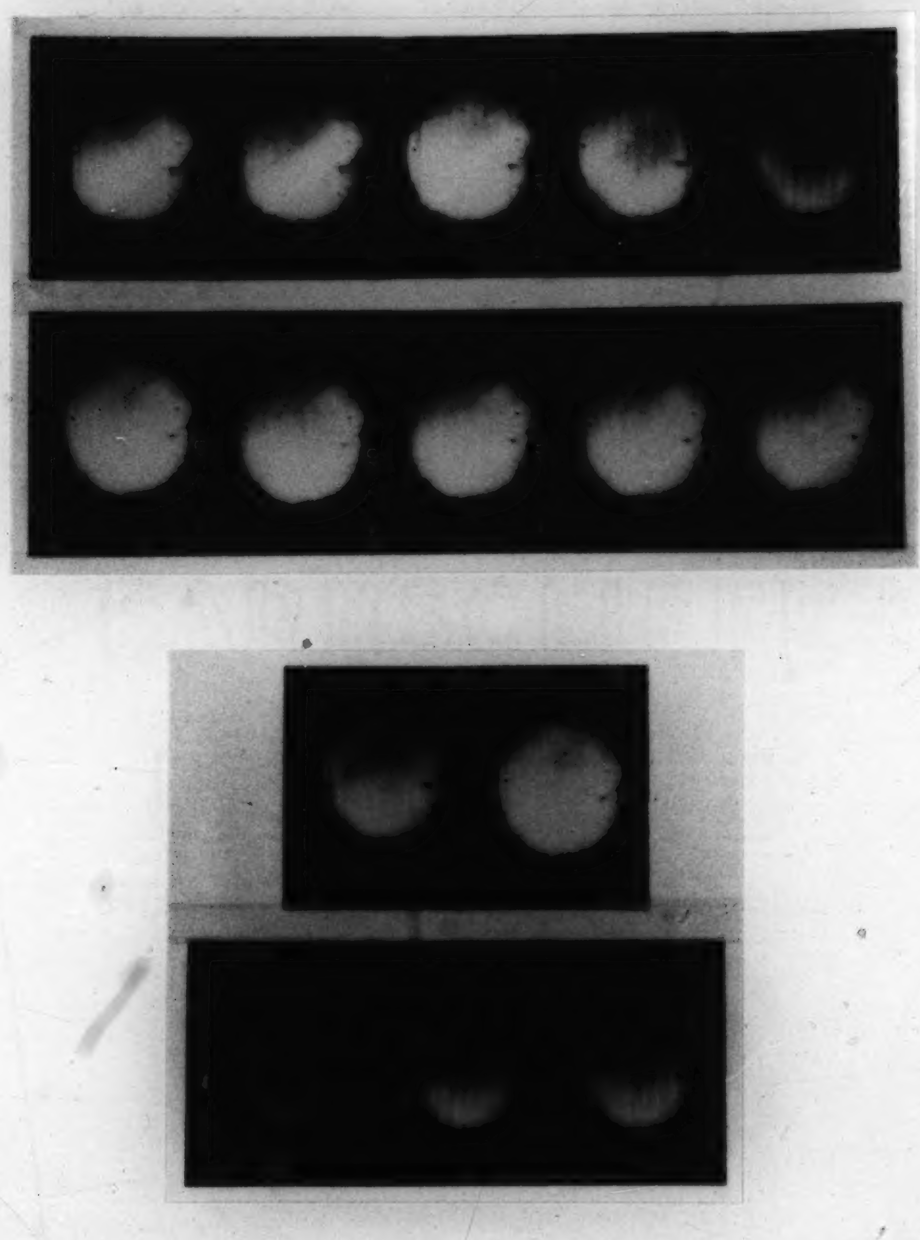

Fig. 3.14 Transformations Occurring at 1:29 & 1:31

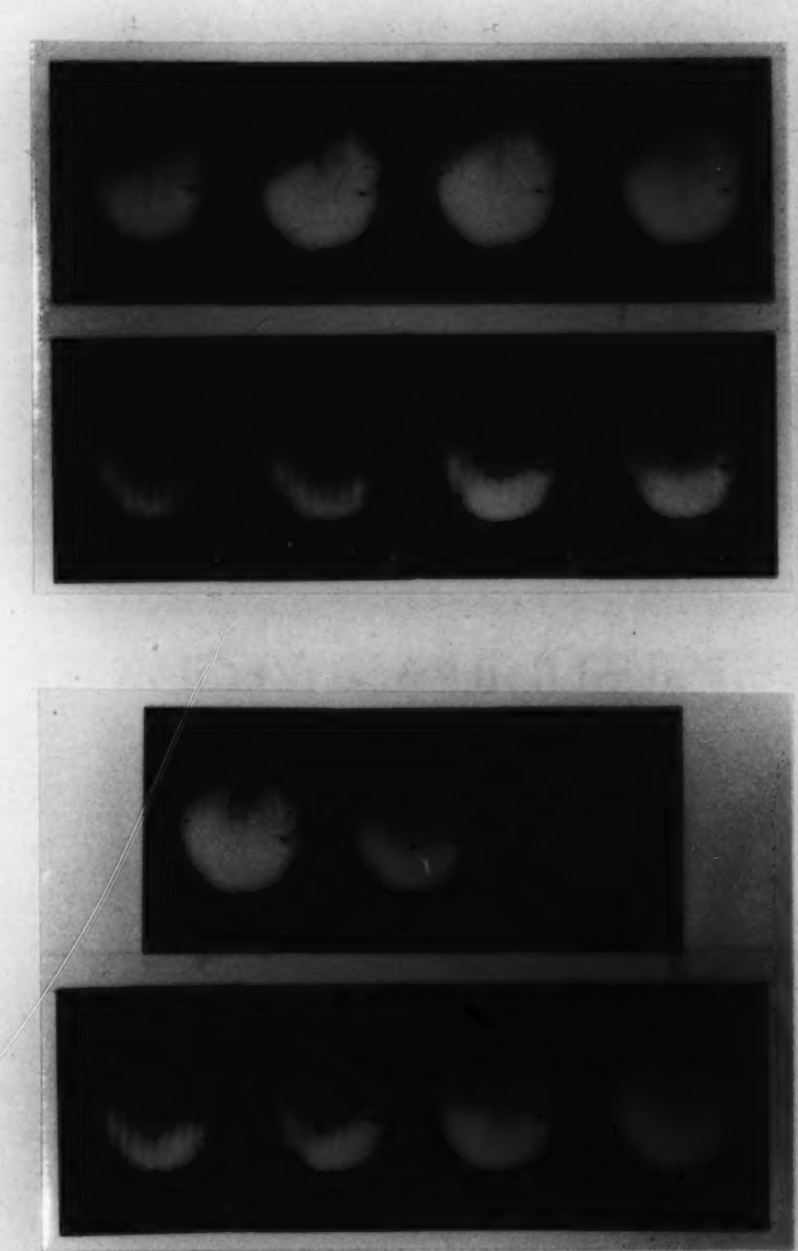

Fig. 3.15 Transformations Occurring at 1:32, 1:33 & 1:42

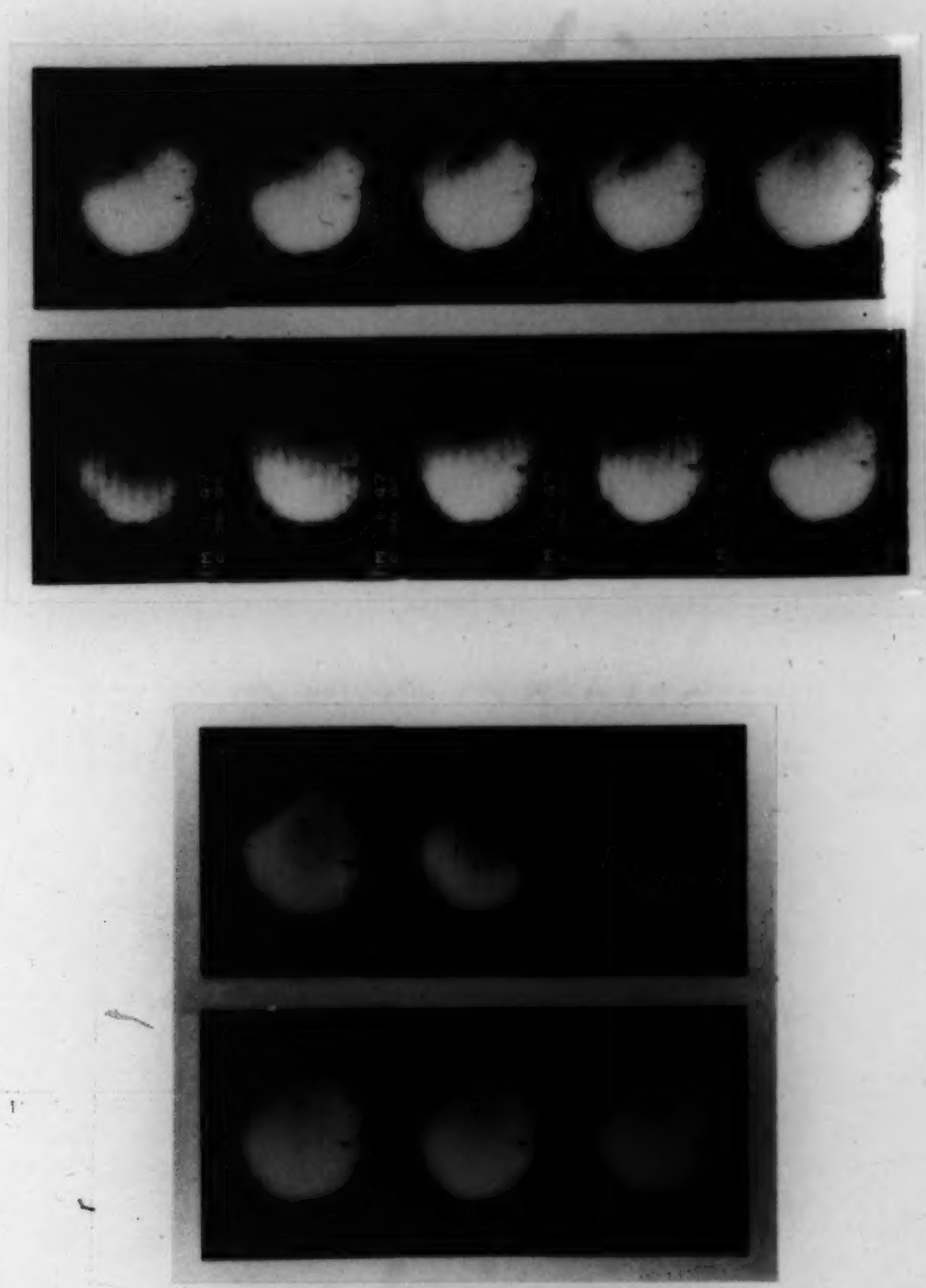

Fig. 3.16 Transformations Occurring at 1:45 & 1:47

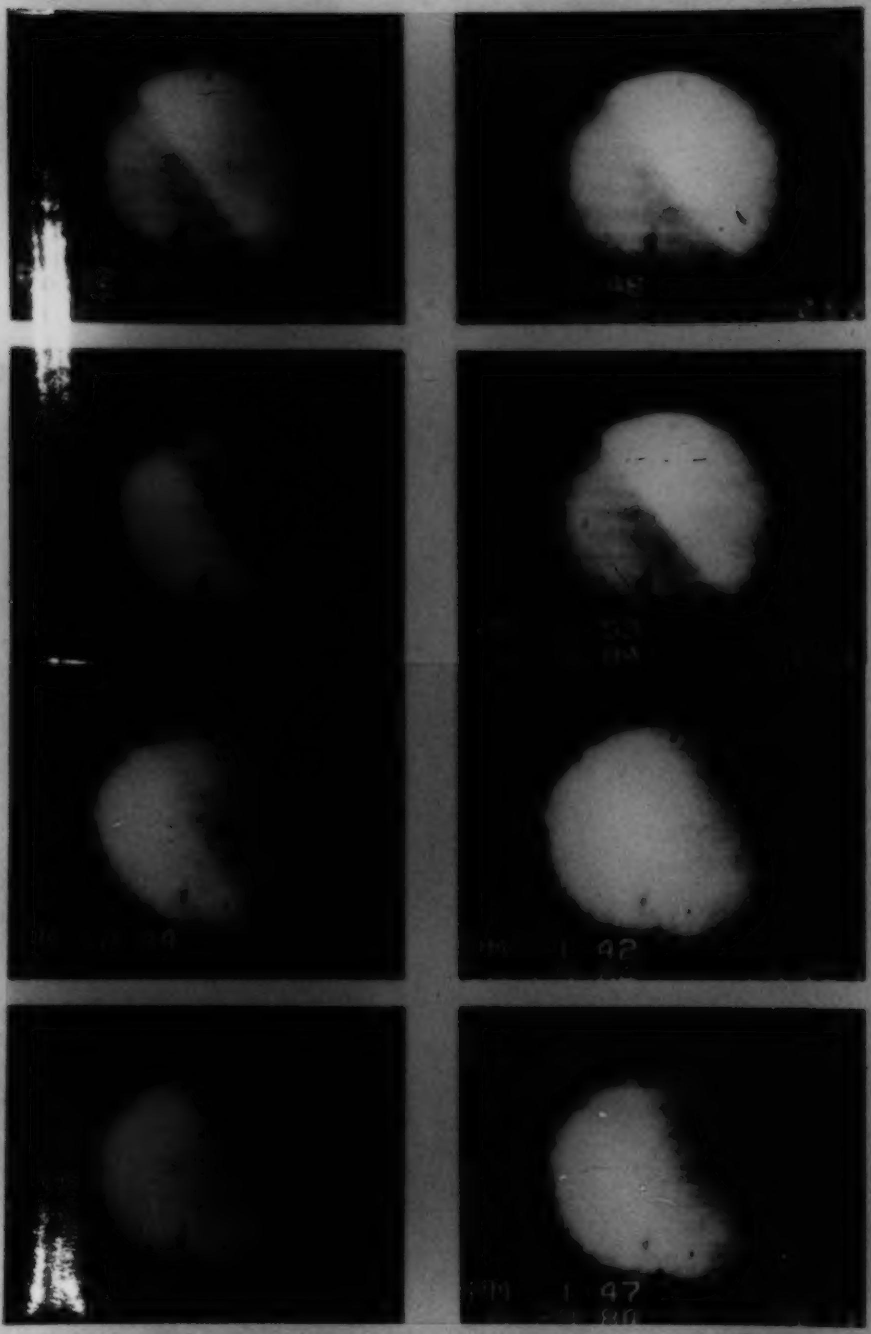

Fig. 3.17 Eight Interfaces in the Preferred Orientation

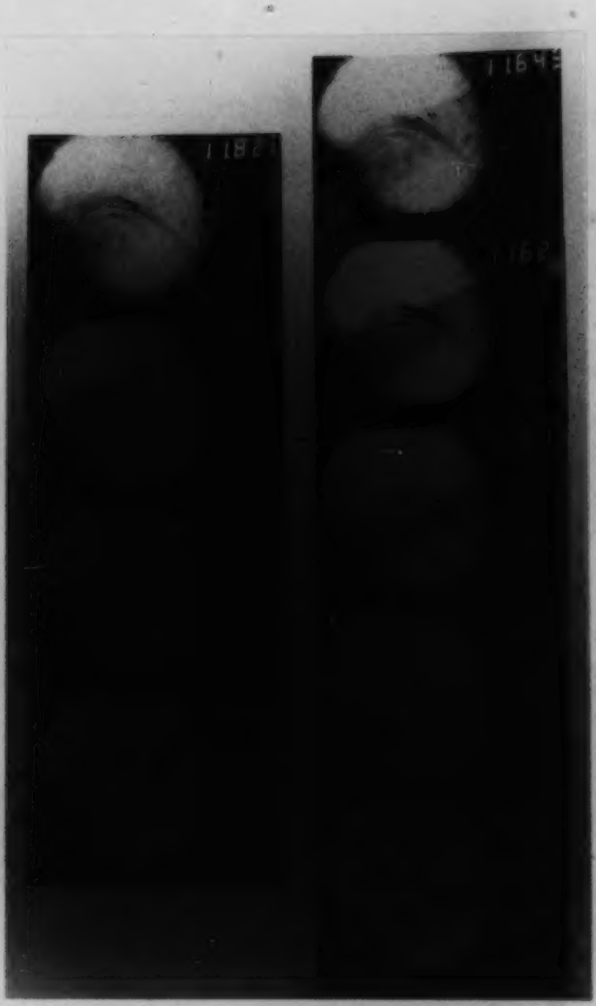

Fig. 3.18 Planar Interface in Sample 2

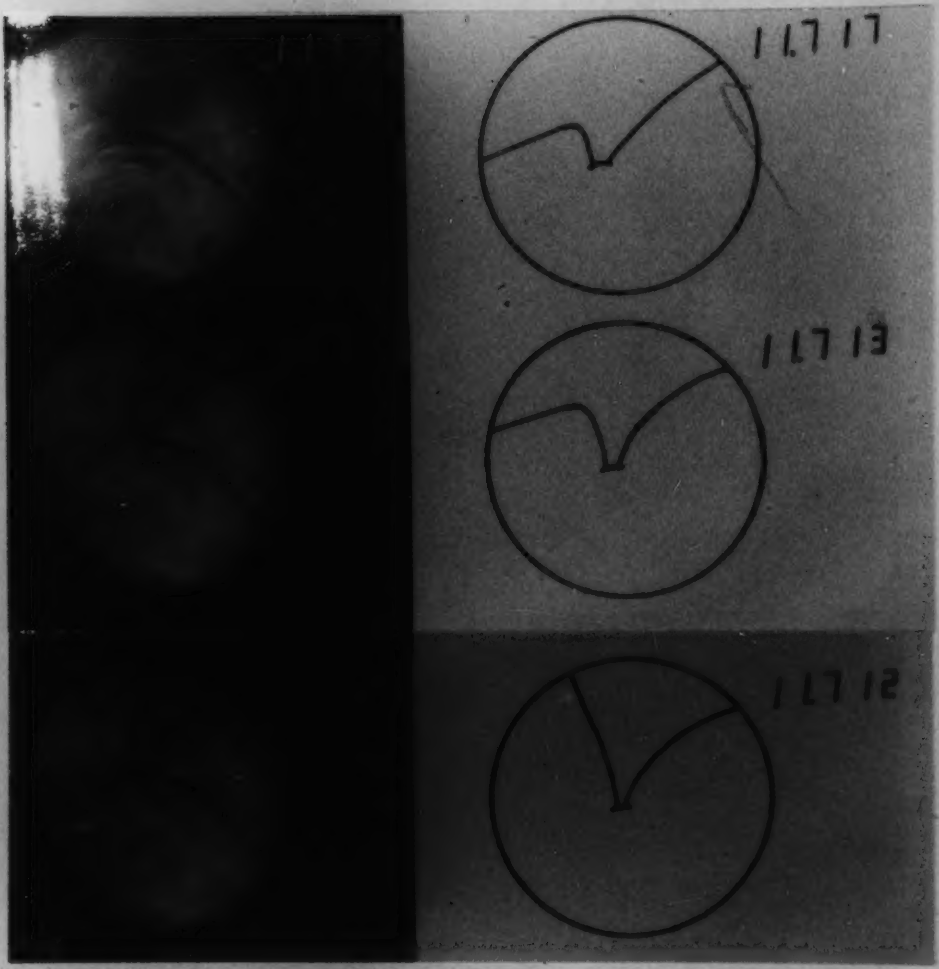
1 1.7 17
1 1.7 13
1 1.7 12

Fig. 3.19 Defect Pinning of the Interface

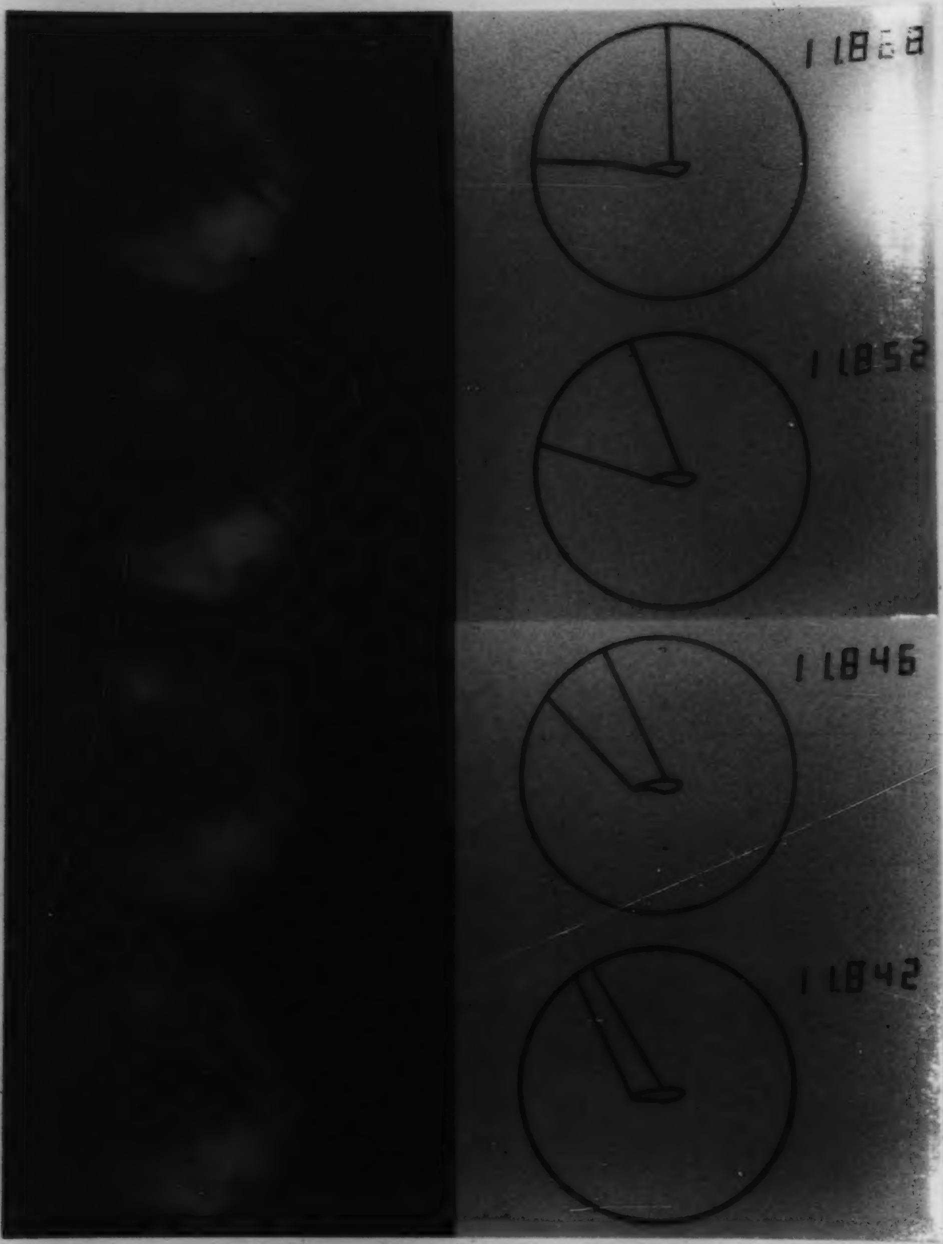
11858
11852
11846
11842

Fig. 3.20 Rotating Interface

Fig. 3.21 Partial Transformation Preceding the Formation of Bands

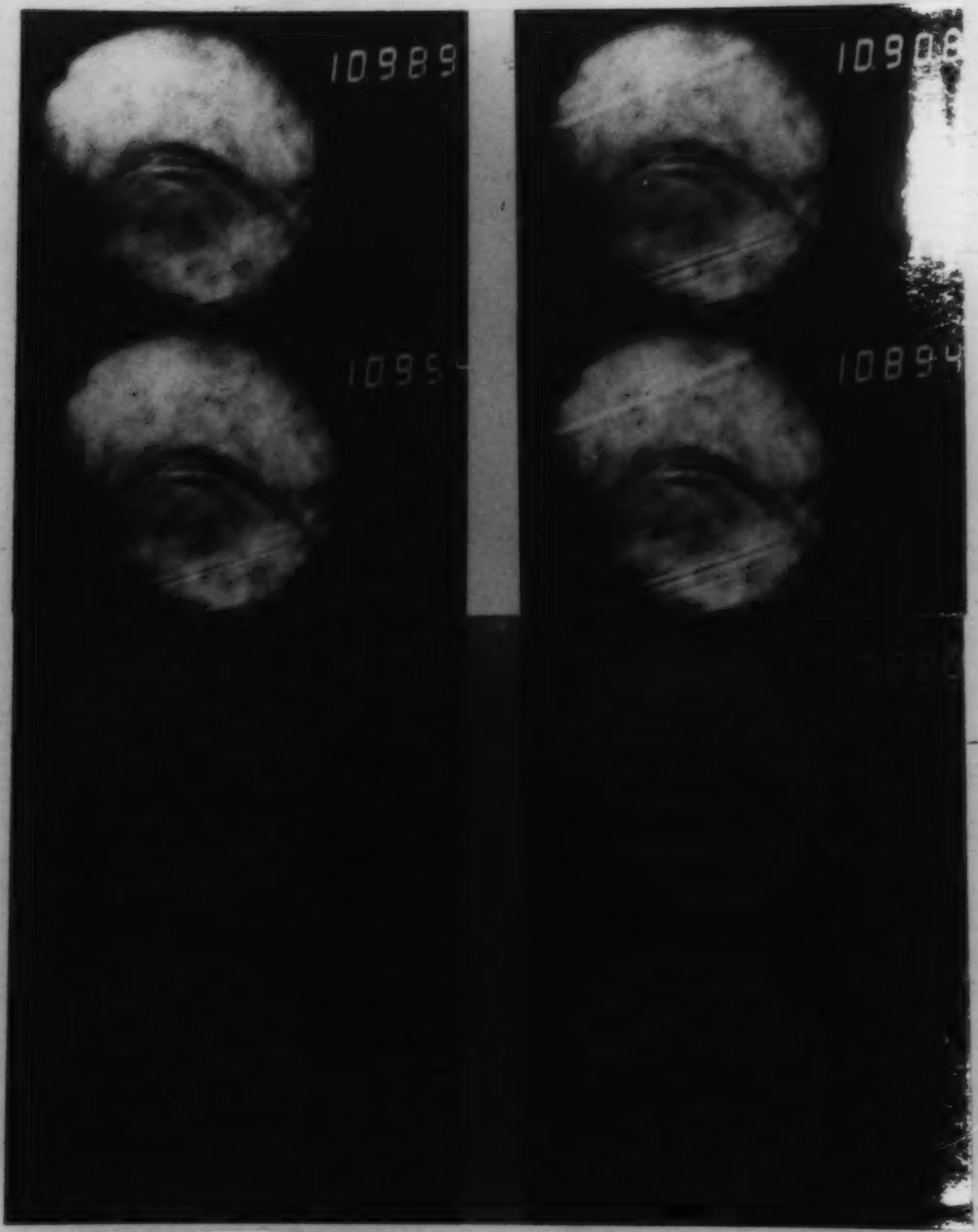
10989
10954
10908
10894

Fig. 3.22 Formation of Bands

Fig. 3.23 Continued Formation of Bands

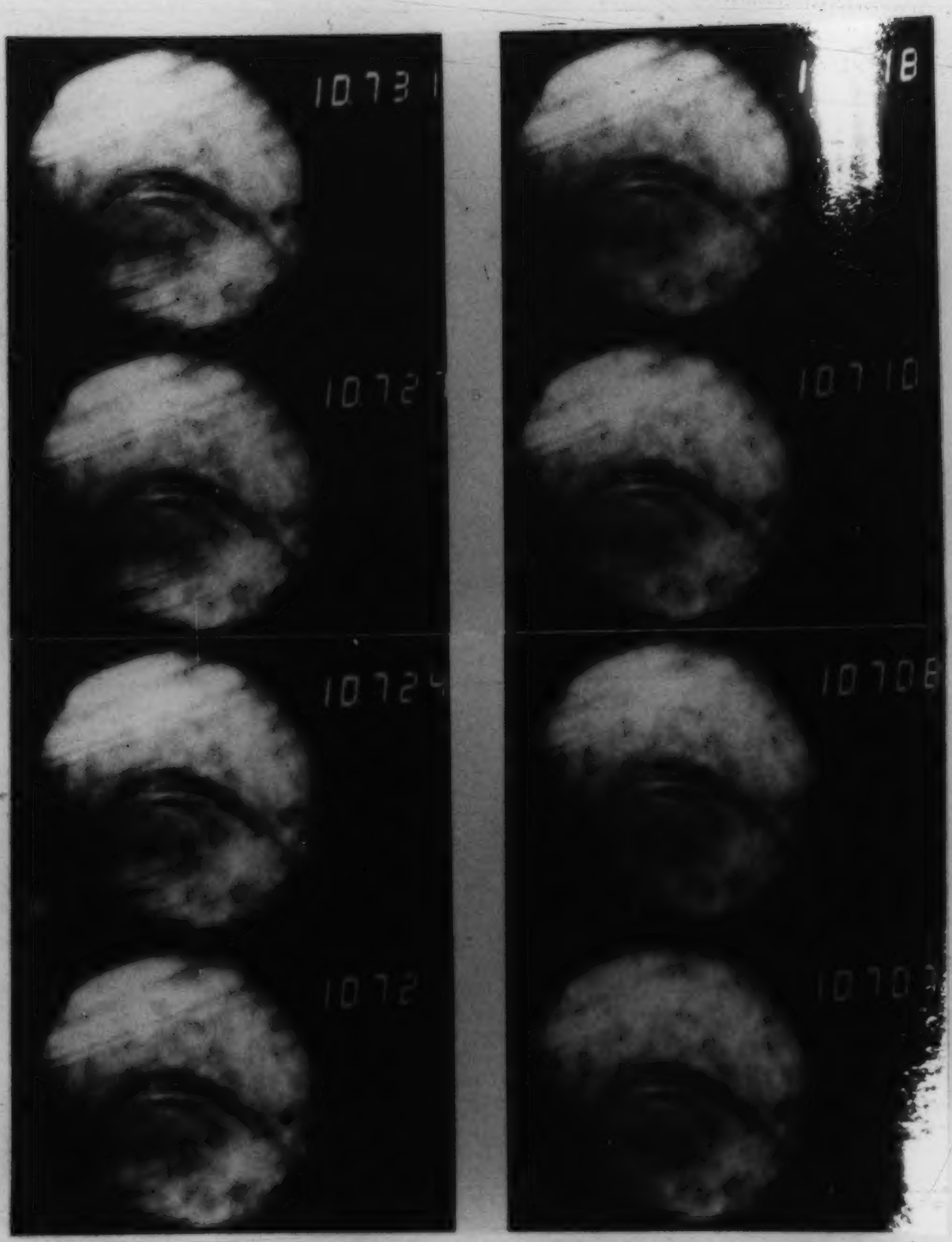
10731
10727
10724
1072
18
10710
10708
1070

Fig. 3.24 Fading of Bands

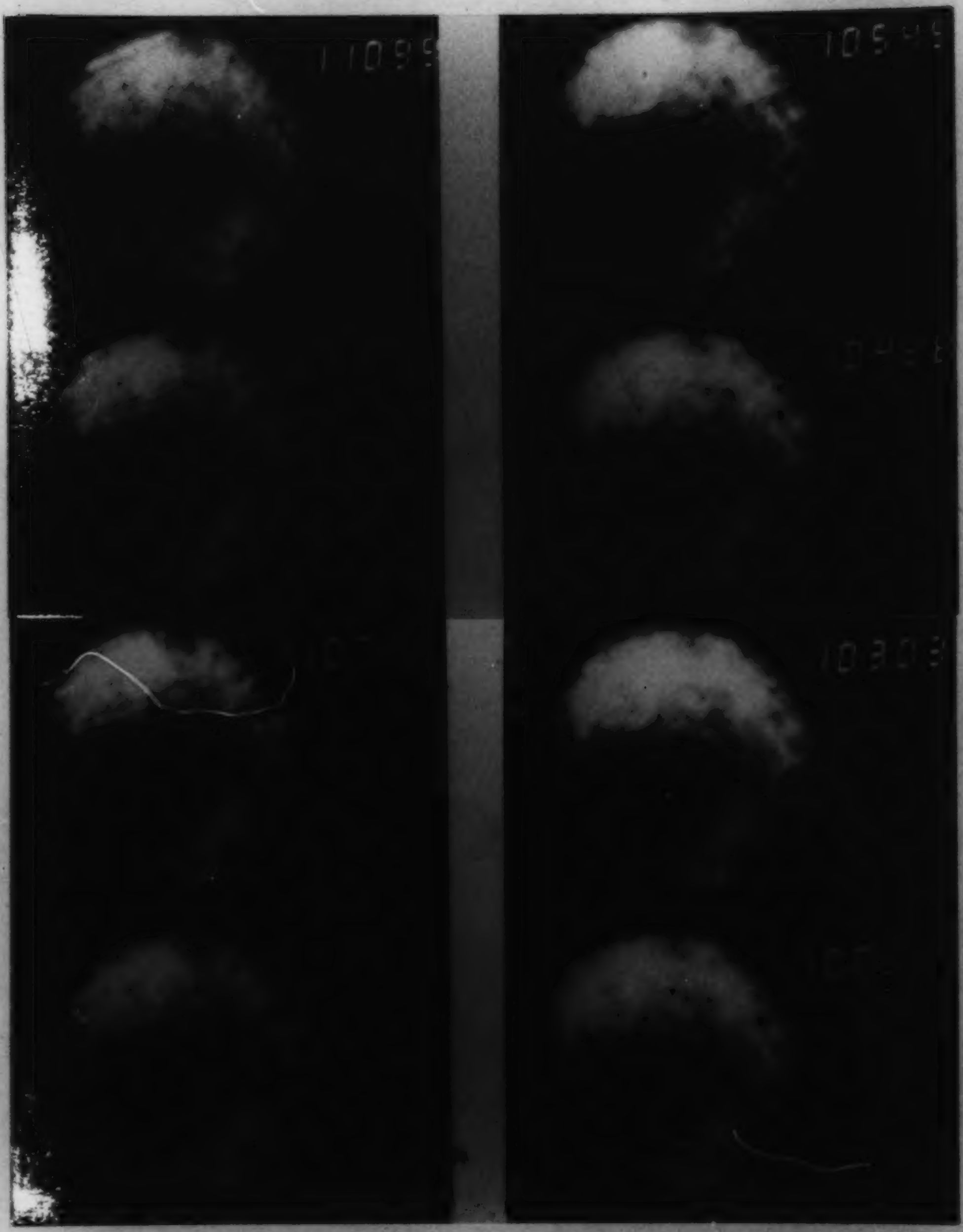

Fig. 3.25 Bands in Two Orientations

G. BIBLIOGRAPHY

Basinski, Z.S., and Christian, J.W., Acta Met., 2, 148 (1954).

A. Berghezan, A. Fourdeux, and S. Amelinckx, Acta. Met., 9, 464 (1961).

Bergmann, L. and Schaefer, C., Optik, (Walter de Gruyter, Berlin, 1966).

Bibring, H., Sebilleau, F. and Buckle, C., J. Inst. Met., 87, 71 (1958-59).

Burkart, M.W., and Read, T.A., Trans. AIME, 196, 1516 (1953).

Chang, L.C., and Read, T.A., Trans. AIME, 191, 47 (1951).

Christian, J.W., The Theory of Transformations in Metals and Alloys, (Pergamon Press, New York, 1965).

Christian, J.W., Proc. Roy. Soc. A, 206, 51 (1951).

Dash, J., and Otte, H.M., Acta Met., 11, 1169 (1963).

Fujita, H., and Ueda, S., Acta Met., 20, 759 (1972)..

Kuhlmann-Wilsdorf, D., "Dislocations", in Physical Metallurgy, R.W. Cahn ed, (John-Wiley & Sons, New York, 1965).

Longhurst, R.S., Geometric and Physical Optics, (Longman, London, 1973).

Mahajan, S., Green, M.L., Brasen, D., Metall. Trans. A, 8, 283 (1977).

Nishiyama, Z., Metal Physics, 7, 107 (1961).

Mills, R.L., and Schuch, A.F., J. Low Temp. Phys., 16, 305 (1974).

Olson, G.B., and Cohen, M., Met. Trans, 79, (1981): Part I, 1897; Part II, 1905; Part III, 1915.

Otsuka, K., Takahashi, M., and Shimizu, K., Metall. Trans., 4, 2003 (1973).

Takeuchi, S. and Honma, T., Sci. Rep. RITU, 9A, 492 (1957).

Thompson, N., Proc. Roy. Soc. B, 66, 481 (1953).

Venables, J.A., Phil. Mag., 7, 35 (1962).

Voltava, E., Acta Met., 8, 901 (1960).

Wayman, C.M., "Martensitic Transformations: An Overview" in Proc. Intl. Conf. Solid→Solid Phase Transformations, H.I. Aaronson, D.E. Laughlin, R.F. Sekerka, C.M. Wayman eds., (The Metallurgical Society of AIME, 1981), P. 1119.

IV. STUDY OF PRETRANSITION ACOUSTIC EFFECTS NEAR THE fcc-hcp ^{4}He TRANSFORMATION

A. INTRODUCTION

There are many reports of acoustic anomalies that occur in martensitic materials as the transformation temperature is approached.[1] Both increases in attenuation and acoustic mode softening (decreases in the velocity of particular transverse sound modes) have been observed. Acoustic mode softening is thought to play an important role in the dynamics of several thermoelastic martensitic transformations.

Previous ultrasonic measurements of the temperature dependence of the sound velocity in hcp ^{4}He have been limited to pressures that were too low to approach the hcp→fcc transformation and limited primarily to longitudinal modes. To investigate the possibility of the role of acoustic mode softening in the dynamics of the hcp→fcc martensitic transformation, the temperature dependence of the transverse sound velocity was measured in several samples of hcp ^{4}He at pressures of 1.1 kbar and 1.5 kbar. The observed thermoelastic nature of this martensitic transformation heightened the motivation for looking for acoustic mode softening.

---

[1] N. Nakanishi, Progress in Materials Science, 24, 143 (1979).

B. THEORY

Acoustic Mode Softening and Homogeneous Nucleation

Acoustic mode softening can be described in terms of the temperature dependence of the elastic constants. In this thesis, a particular model for mode softening, the quasi-harmonic approximation of the anharmonic theory of lattice vibrations according to Leibfried and Ludwig[2], is described and compared with experimental results. Elastic constants were determined from measured sound velocities. Since solid helium is under pressure, care must be taken to introduce the effect of pressure on the relation between sound velocity and elastic constants.

The following introduction to elastic constants, including the discussion of the relationship between sound velocities and elastic constants in materials under pressure, follows a careful discussion by Wallace[3]. Suppose a point in a material moves from point $\underline{X}$ to $\underline{x}$, due to a deformation. The displacement is given by:

$$u_i=x_i-X_i \tag{4.1}$$

The displacement gradient is given by:

---

[2] G. Leibfried and W. Ludwig, in Solid State Physics, eds. F. Seitz & D. Turnbull, (Academic Press, New York, 1961), vol. 12, P. 275.

[3] D.C. Wallace, Thermodymanics of Crystals, (John Wiley & Sons, New York, 1972.)

$$u_{ij}=(\partial u_i/\partial X_j) \tag{4.2}$$

Define the Lagrangian strain tensor as:

$$\eta_{ij}=\tfrac{1}{2}(u_{ij}+u_{ji}+u_{ki}u_{kj}) \tag{4.3}$$

(Here, and throughout this thesis, implicit summation notation will be used.) The last term in the Lagrangian strain tensor does not appear in the infinitesimal strain tensor but is required to investigate deformed solids. Define the stress tensor as:

$$\tau_{ij}=V^{-1}(\partial U/\partial\eta_{ij})_{S,\eta'}\ \big|_{\eta=0} \tag{4.4}$$

Where U is the internal energy and V is the volume. The subscript S indicates the derivative is at constant entropy (adiabatic conditions). The η' index indicates that all the strain tensor elements (except η_{ij}) are held constant during the derivative with respect to η_{ij}. The adiabatic stress-strain derivatives are defined as:

$$B_{ijkl}=(\partial\tau_{ij}/\partial\eta_{kl})_{S,\eta'}\ \big|_{\eta=0} \tag{4.5}$$

The thermodynamic adiabatic elastic constants are defined as:

$$C_{ijkl}=V^{-1}(\partial^2U/\partial\eta_{ij}\partial\eta_{kl})_{S,\eta'}\ \big|_{\eta=0} \tag{4.6}$$

The dynamic adiabatic elastic constants, $\hat{C}_{ijkl}$, (or the "wave propagation coefficients") are defined by the equations of motion for adiabatic propagation of elastic strain waves:

$$\rho\ddot{x}_i=\hat{C}_{ijkl}(\partial^2 x_k/\partial X_j\partial X_l) \tag{4.7}$$

The sound velocity, v, can be calculated from the dynamic adiabatic elastic constants as the solutions to the secular equation:

$$\det[\rho v^2\delta_{ik}-\hat{C}_{ijkl}\hat{k}_j\hat{k}_l]=0 \tag{4.8}$$

where $\hat{k}_i$ are the components of a unit vector in the direction of the wave vector, $\underline{k}$. $\hat{C}_{ijkl}$ is related to C_{ijkl} through:

$$\hat{C}_{ijkl}= C_{ijkl} + \tau_{jl}\delta_{ik} \tag{4.9}$$

Distinguishing amoung $\hat{C}_{ijkl}$, B_{ijkl}, and C_{ijkl} is only necessary for solids under external stress. If the solid is deformed by isotropic pressure only, then the following relations hold:

$$\tau_{jl}=-P\delta_{jl} \tag{4.10a}$$

$$B_{ijkl}=C_{ijkl} - P(\delta_{jl}\delta_{ik}+\delta_{il}\delta_{jk}-\delta_{ij}\delta_{kl}) \tag{4.10b}$$

$$\hat{C}_{ijkl}=C_{ijkl} - P\delta_{jl}\delta_{ik} \tag{4.10c}$$

For solids under pressure the secular equation becomes:

$$\det[(\rho v^2+P)\delta_{ik}-C_{ijkl}\hat{k}_j\hat{k}_l]=0 \tag{4.11}$$

This equation is simpler than eq. 4.8 because the C_{ijkl} have Voigt symmetry whereas the $\hat{C}_{ijkl}$ do not.

For crystals of hexagonal symmetry (and with c-axis along the x_3-axis), the pure-transverse (pt), quasi-transverse (qt), and the quasi-longitudinal (ql) velocities can be calculated from eq. 4.11. The velocities have been calculated for zero pressure[4] [5] and can easily be corrected for nonzero pressure as:

$$\text{(pt)}\ \rho v^2+P = C_{44}\hat{k}_3{}^2+C_{66}(1-\hat{k}_3{}^2) \tag{4.12a}$$

$$\text{(qt)}\ \rho v^2+P= \tfrac{1}{2}[(C_{11}+C_{44})\hat{k}_3{}^2+ (C_{33}+C_{44})(1-\hat{k}_3{}^2)- \psi(\hat{k})] \tag{4.12b}$$

$$\text{(ql)}\ \rho v^2+P= \tfrac{1}{2}[(C_{11}+C_{44})\hat{k}_3{}^2+ (C_{33}+C_{44})(1-\hat{k}_3{}^2)+ \psi(\hat{k})] \tag{4.12c}$$

---

[4] C. Zener, Phys. Rev., 49, 122 (1936).

[5] Musgrave, M.J.P., Crystal Acoustics, (Holden-Day, San Francisco, 1970).

with:

$$\psi^2(\hat{k}) = (C_{11}-C_{44})^2\hat{k}_3^4 + (C_{33}-C_{44})^2(1-\hat{k}_3^2)^2 \qquad (4.12d)$$
$$+ [2(C_{13}+C_{44})^2-(C_{11}-C_{44})(C_{33}-C_{44})]2\hat{k}_3^2(1-\hat{k}_3^2)$$

Here, Voigt notation has replaced tensor index notation.

Leibfried and Ludwig[4], derived an expression for the temperature dependence of the stess-strain derivatives that follows the quasi-harmonic theory. These expressions may easily be converted to expressions for the thermodynamic elastic constants through the use of eq. 4.10b and eq. 4.10c. The thermodynamic elastic constants at constant volume in the quasi-harmonic theory can be given by:

$$C_{ijkl}(T)=C_{ijkl}(0)-\Gamma_{ijkl}\ u_s(T) \qquad (4.13)$$

where:

$$C_{ijkl}(0)=V^{-1}(\partial^2\phi/\partial\eta_{ij}\partial\eta_{kl}) \qquad (4.14a)$$

$$\Gamma_{ijkl}=-½(\partial^2\ln\overline{\omega^2}/\partial\eta_{ij}\partial\eta_{kl}) - \gamma_{ij}\gamma_{kl} \qquad (4.14b)$$

$$\gamma_{ij} =-½(\partial\ln\overline{\omega^2}/\partial\eta_{ij}) \qquad (4.14c)$$

---

[4] G. Leidfried and W. Ludwig, in Solid State Physics, eds. F. Seitz & D. Turnbull, (Academic Press, New York, 1961), vol. 12, P. 275.

$$u_s(T) = u(T)-u(0) = (U(T)-U(0))/V \tag{4.14d}$$

where V is volume, ϕ is crystal potential energy, u is the internal energy per unit volume, u_s is the thermal contribution of the internal energy, $\overline{\omega^2}$ is the spectral averaged squared phonon frequency, and γ_{ij} is the generalized Grüneisen parameter. In addition, at constant volume:

$$P(T) = P_0 + \gamma\ u_s(T) \tag{4.15}$$

where γ is the Grüneisen constant and P_0 is the pressure at absolute zero.

An expression for the temperature dependence of the sound velocity at constant volume can be obtained in the quasi-harmonic theory by inserting the expressions for the elastic constants in eq. 4.13 and the pressure in eq. 4.15 into the expressions for velocity in eqs. 4.12. The result to first order in u_s is:

$$\rho v^2 \equiv \hat{C}_r(\hat{k}) \simeq \hat{C}_{r,0}(\hat{k}) - [\Gamma_r(\hat{k})]\ u_s(T) \tag{4.16}$$

where $\hat{C}_r(\hat{k})$ is the dynamic elastic constant for the branch r with the wave direction $\hat{k}$ and $\hat{C}_{r,0}(\hat{k})$ is the value of $\hat{C}_r(\hat{k})$ at absolute zero. For hexagonal crystals:

$$\hat{C}_{pt,0}(\hat{k}) = C_{44,0}\hat{k}_3^2 + C_{66,0}(1-\hat{k}_3^2) - P_0 \tag{4.17a}$$

$$\hat{C}_{qt,0}(\hat{k}) = \tfrac{1}{2}[(C_{11,0}+C_{44,0})\hat{k}_3^2+(C_{33,0}+C_{44,0})(1-\hat{k}_3^2)-\psi_0(\hat{k})]-P_0 \tag{4.17b}$$

$$\hat{C}_{ql,0}(\hat{k}) = \tfrac{1}{2}[(C_{11,0}+C_{44,0})\hat{k}_3^2+(C_{33,0}+C_{44,0})(1-\hat{k}_3^2)+\psi_0(\hat{k})]-P_0 \tag{4.17c}$$

and:

$$\Gamma_{pt}(\hat{k}) = \Gamma_{44}\hat{k}_3^2+\Gamma_{66}(1-\hat{k}_3^2) + \gamma \tag{4.18a}$$

$$\Gamma_{qt}(\hat{k}) = -\tfrac{1}{2}[(\Gamma_{11}+\Gamma_{44})\hat{k}_3^2+(\Gamma_{33}+\Gamma_{44})(1-\hat{k}_3^2)-\psi_1(\hat{k})]+\gamma \tag{4.18b}$$

$$\Gamma_{ql}(\hat{k}) = -\tfrac{1}{2}[(\Gamma_{11}+\Gamma_{44})\hat{k}_3^2+(\Gamma_{33}+\Gamma_{44})(1-\hat{k}_3^2)+\psi_1(\hat{k})]+\gamma \tag{4.18c}$$

where:

$$C_{\alpha\beta,0} = C_{\alpha\beta}(T=0) \tag{4.19a}$$

$$\psi_0(\hat{k}) = \psi(\hat{k},T=0) \tag{4.19b}$$

$$\begin{aligned}\psi_0(\hat{k})\cdot\psi_1(\hat{k}) = &\\ -[(C_{11,0}-C_{44,0})&(\Gamma_{11}-\Gamma_{44})\hat{k}_3^4 +(C_{33,0}-C_{44,0})(\Gamma_{33}-\Gamma_{44})(1-\hat{k}_3^2)^2] +\\ &[(C_{11,0}-C_{44,0})(\Gamma_{33}-\Gamma_{44})+(C_{33,0}-C_{44,0})(\Gamma_{11}-\Gamma_{44})\\ &\quad -4(C_{13,0}+C_{44,0})(\Gamma_{13}+\Gamma_{44})] \times\hat{k}_3^2(1-\hat{k}_3^2)\end{aligned} \tag{4.19c}$$

The solutions for the quasi-transverse and quasi-longitudinal branches have higher than first order terms of u_S; the pure-transverse branch does not. According to Ludwig and Leibfried[7], Γ_{ijkl} and γ are independent of temperature; therefore,the temperature of the sound velocity comes entirely from the temperature dependence of $u_S(T)$.

Lattice stability requires that ρv^2 be positive definite for every sound mode and wave vector direction. This can be interpreted mechanically as the requirement of a positive definite restoring force per unit volume (f) against a displacemant (w). The restoring force is given by:

$$f_i = \rho\omega^2 w_i = \hat{C}_{ijkl} k_j k_l w_k \tag{4.20}$$

where w is the displacement vector. There is also a quantum mechanical interpretation. If the velocity (and therefore the energy) of a particular mode drops to zero, the phonon condensation into that mode will cause the amplitude of the mode to increase to levels that cannot be supported by the crystal.

Soft mode theories of martensitic nucleation rely on the loss of crystal stability correlated with ρv^2 approaching zero for a particular branch and wave vector direction.[8] These theories require a normal mode with displacement vector in the direction of the lattice distortive shear required by the martensitic transformation.

---

[7] G. Leidfried and W. Ludwig, in Solid State Physics, eds. F. Seitz & D. Turnbull, (Academic Press, New York, 1961), vol. 12, P. 275.
[8] F. Faulk, J. de Physique, sup. 12, C4-3 (1982).

As the transformation temperature is approached, the restoring force against this deformation drops to zero and consequently the velocity of this mode (called the "soft mode") decreases to zero. Phonon condensation into this mode occurs and the vibrational amplitude increases until, at a particular site, its magnitude is sufficient to transform the lattice, forming a nucleus of the product phase. This type of homogeneous nucleation has been coined "phonon nucleation" by Perkins[9]. I will refer to this process as "critical mode softening". The adjective "critical" is used to distinguish it from mode softening that occurs to an extent that is insufficient for homogeneous nucleation. The extent to which a particular shear mode softens as the transformation temperature is approached is a measure of the tendency towards homogeneous nucleation of the new phase. Nakinishi[10] has reviewed observations of pretransition mode softening in martensitic transformation. Several martensitic transformations show acoustic mode softening that is consistent with the phonon nucleation process (*i.e.* they show critical mode softening). The $(\hat{k}\|[110],\hat{w}\|[1\bar{1}0])$ mode, for example, is thought to be responsible for the nucleation of the fct phase from the fcc phase in In-Tl alloys.[11] Since the polarization vector, $[1\bar{1}0]$, is in the direction of the required shear for the fcc→hcp transformation, this mode is a candidate for a soft mode in the ^{4}He fcc→hcp transformation. Similarly, the $(\hat{k}\|[0001],\hat{w}\perp[0001])$ mode is a candidate for a soft mode for the ^{4}He hcp→fcc transformation. This is effectively a displacement gradient in which u_{13} is the only nonzero u_{ij}. The velocity of this mode is given by: $\rho v^2=C_{44}-P$. If there is critical mode softening, C_{44} will decrease to P (the pressure) as the transformation temperature is approached. If the quasi-harmonic theory holds, then this mode will critically soften if Γ_{44} is large enough to make $(\Gamma_{44}+\gamma)u_S$ approach $C_{44,0}-P_0$ as the equilibrium temperature is approached.

---

[9] A.J. Perkins, Scr. Metall., 8, 31, (1974).

[10] N. Nakanishi, Progress in Materials Science, 24, 143 (1979).

[11] D.J. Gunton and G.A. Saunders, Solid St. Commun., 14, 865 (1974).

Anomalous Dispersion and Heterogeneous Nucleation

Heterogeneous nucleation, unlike homogeneous nucleation, does not require a soft mode. A lattice defect, acting as a nucleation site, will distort the interatomic potential so that the atoms can be sufficiently displaced without requiring a decrease in the lattice restoring force and associated soft mode. After nucleation, the interface will distort the interatomic potential and again no soft mode is required. Heterogeneous nucleation may, however, produce acoustic effects that are different than those for homogeneous nucleation.

One site that has been proposed as a heterogeneous nucleation site for the hcp→fcc transformation is a collection of perfect dislocations of the type ab. If the ab dislocations in fact generate the partials required for the transformation, then they must exist in the crystal prior to the transformation. It has been shown that these dislocations become extended according to the reaction: $ab \rightarrow a\sigma + \sigma b$. To examine the effect of this type of nucleation, it is instructive to examine first the acoustic effect of a single extended dislocation.

Granato *et al.*[12] considered the acoustic effects of an extended dislocation. The two Shockley partials of an extended dislocation are attracted to each other by the surface tension of the stacking fault between them and repelled by the interaction of their strain fields. An external elastic strain will cause a perturbation in the force with which the partials repel; therefore, an oscillating external strain field will cause oscillations in the separation between the partials. To first order, the motion can be modeled as that of a damped harmonic oscillator. This theory is similar to the theory of damped harmonic oscillations of perfect dislocations[13] that has been successfully applied to account for acoustic anomalies in ^{4}He at lower pressures[14] [15] [16]. The partials will interact with the propagating strain field and cause anomalous dispersion, which will decrease the elastic shear modulus by ΔG according to:

---

[12] A.V. Granato, R.R. Schwarz, and G.A. Kneezel, J. de Physique, 42, sup. 10, C5-1055 (1981).

[13] A.V. Granato and J. Lucke, J. Appl. Phys., 27, 583 (1956).

[14] Wanner, R., Iwasa, I. and Wales, S., Solid State Commun, 18, 853 (1976).

[15] Iwasa, I. and Suzuki, H., J. Phys. Soc. Jpn., 49, 1722 (1980).

[16] J.R. Beamish and J.P. Franck, Phys. Rev. Lett., 47, 1736 (1981).

$$\frac{\Delta G}{G} = \frac{G}{\rho} \frac{\Lambda\,(\omega_0{}^2-\omega^2)}{(\omega_0{}^2-\omega^2)^2 + (\omega b/m)^2} \qquad (4.21)$$

where G is the shear modulus, Λ is the dislocation density, ω is the frequency of the sound being measured, ω_0 is the extended dislocation resonant frequency, b is the dampening coefficient, and m is the effective mass per unit length of a Shockley partial. In the theory of Granato *et al.*, the stacking fault energy decreases as the difference in free energy between the fcc and hcp phases decreases and approaches zero monotonically as the transformation temperature is approached. The resonant frequency decreases monotonically with the stacking fault energy and, as it approaches the frequency of the sound field, a decrease in shear modulus occurs. Observations of an anomalous velocity decrease of .01% by Granato *et al.*[17] preceding the fcc→hcp phase transformation in a Co-Ni alloy are consistent with this explanation.

If the extended dislocations form part of an fcc-hcp interface they will not act as independent harmonic oscillators as described by Granato *et al.*. Nevertheless, it appears likely that the interacting extended dislocations could produce an effect that is qualitatively similar.

---

[17] A.V. Granato and G.A. Kneezel, J. de Physique, 42, sup. 10, C5-1061 (1981).

C. EXPERIMENT

Introduction

The ultrasonic experiments on solid helium were done in the temperature range from 8 K to 16 K and at pressures of 1.1 and 1.5 kbar. As with the optical experiments, low temperatures were maintained in an optical cryostat (International Cryogenics). The cryostat was modified to have a heater on the experimental stage for temperature control. The pressure system was the same as for the optical experiments (see chapter II).

The Acoustic High Pressure Cell

A high pressure ultrasonic cell, as shown in fig. 4.1, was constructed of high nickel steel. Two lithium niobate piezoelectric ultrasonic shear transducers with a diameter of 1.27 cm and a first harmonic of 3 MHz were spaced .45 cm apart with a spacing ring that was carefully ground and polished to ensure parallel alignment of the transducer surfaces. Helium was solidified between the transducers. Except for a small circular indentation at the center, a backing piece lay flat against each transducer. The side of each backing piece away from the transducer had a hemi-spherical shape to scatter the sound that was transmitted backwards into the backing piece. The backing pieces and the transducers were pressed against the spacer by a stiff support spring. Electrical contact between the backing piece and the electrical feedthrough was provided by soft stainless steel spring. The electrical feedthrough was in the shape of a cone with some unsupported area at the tip. A .010" thick Vespel (a high strength plastic from Dupont) jacket provided electrical insulation between the electrical feedthrough and the feedthrough housing. The seal between the cone and the housing was self-sealing because the unsupported area caused the pressure in the Vespel to be greater than the pressure inside the cell. The electrical wire soldered to the cone was a steel wire so that extrusion of the Vespel would not pinch off the wire. The capacitance of the feedthrough was measured to be approximately 15 pF, an acceptable load. The feedthrough body had sealing rings with an unsupported area for self-sealing. A steel ring with one side against the unsupported area provided the strength to hold the ring assembly in place against the pressure. A Vespel ring against the steel ring extruded outwards towards the cell wall and the feedthrough housing to provide the pressure seal. A brass ring provided the initial pressure on the Vespel ring for sealing at low pressures. A nut pressed the feedthrough body into place. Threads for a coax connector were machined onto the nut. Sapphire windows on the cell permitted visual observations of the transformation during the ultrasonic experiments. The windows were cylinders .375" in diameter and .280" thick. The c-axis of the sapphires were within 5 minutes of arc off the optical path to prevent birefringence in the sapphire. A Vespel washer was placed between the window and the cell wall to prevent stress concentration on the window that might crack the window when the cell was pressurized. The windows were held in place with a push piece backed by a nut. Between the window and the push piece was another Vespel washer. This washer, like the one on the other side, cushioned the window from stress concentration points. It also acted as an unsupported area seal between the window and the push piece. A germanium resistance thermometer (Cryocal) was coated with "Apiezon N" thermally conducting grease and inserted into a snuggly fitting hole in the cell. The leads of the thermometer were thermally anchored to the cell. The current leads were twisted together and the voltage leads were twisted together to prevent cross-talk. A resistor, serving as a capillary heater, was attached to the capillary near the cell.

Ultrasonic Method

The absolute sound velocity was measured with a basic pulse echo technique[18] and the relative velocity was measured with the pulse echo overlap technique[19] [20]. In both techniques, short 3 MHz RF pulses from an RF pulse generator (Matec 6600 with Matec 755 insert) were applied to one of the transducers in the high pressure cell. This generated a pulse of ~3 MHz transverse sound that reflected between the transducers. The width of each RF pulse was controlled by the RF generator driver (HP 8013A) to ~2μsec, a sufficiently short time for the transmitting transducer to finish vibrating (*i.e.* the pulse to complete) well before the leading edge of the ultrasonic pulse returned (after reflecting off the opposite transducer) to the transmitting transducer. The repetition rate of the RF pulses was sufficiently slow (~1/msec) so that the ultrasonic pulse reflecting between the transducers died away before the next pulse was produced. A sync signal sent to the RF generator driver controlled the RF pulse repetition rate. The sync/strobe generator (Matec 122B decade divider/dual delay generator), locked onto a sine wave and produced the sync signal at .01 times the frequency of the locking sine wave. A digitally controlled oscillator (Rockland 5100) produced a sine wave at a frequency near 100 KHz onto which the sync/strobe generator locked. A microcomputer (Apple IIe) controlled the oscillator through a custom made interface. The decaying ultrasonic pulse (reflecting between the transducers) produced an exponentially decaying sequence of signals in the receiving transducer. The sequence of signals is referred to as the echo train. The echo train was amplified by the RF receiver (Matec 6600). The signals were sufficiently strong so as not to require impedance matching or preamplification. Passive impedance matching networks (Matec 60) were not used because they introduced resonances into the tranmission line that distorted the signal without providing much signal enhancement. The signal-to-noise ratio in the amplified signal was improved by an order of magnitude by filtering the amplified signal with a passband filter (custom made) with a center frequency of ~3 MHz and Q~2. All or part of the echo train was displayed on an oscilloscope (HP 182C).

---

[18] E.A. Hiedemann and K.H. Hoesch, Z. Phys., 90, 322 (1934).
[19] J.E. May Jr., IRE Nat. Conv. Rec., 6, Pt. 2, 134 (1958).
[20] M.A. Breazeale, J.H. Cantrell Jr. and J.S. Heyman, in *Methods of Experimental Physics* ed. Edmonds, P.D., (Academic Press, New York, 1981) vol. 19, P. 67.

The arrangement for measuring absolute sound velocity is shown in fig. 4.2. The oscilloscope was triggered simultaneously with the RF generator driver and the entire echo train was displayed on the oscilloscope. The sine wave from the oscillator was in sync with the echo trains (because the oscillator was locked to the sync/strobe generator) and displayed on the oscilloscope. The frequency of the oscillator was adjusted through the computer until it had the same frequency as the leading edges of the echoes in the displayed train. The frequencies were equal when the sine wave crossed the baseline of the echo train (which was not necessarily the baseline of the sine wave) at precisely the points where the leading edges of the echoes occur. The velocity of sound was calculated from the return transit time which was simply the period of the sine wave. The accuracy of this method was limited by the accuracy of the visual determination of the position of the leading edge of the echoes, which usually had rather irregular shapes. The accuracy of this method varied widely from sample to sample but was about 1% in crystals with a reasonably clear echo train.

The arrangement for measuring relative velocity is shown in fig. 4.3. Once the absolute velocity was measured, the oscillator frequency was approximately the frequency with which the echoes occur in the echo train. The oscillator was used to trigger the oscilloscope through a trigger generator (PAR 222A pulse generator) so that the trace of each echo within a train was placed in the same position on the oscilloscope screen. The oscilloscope time base generator was adjusted so that a single echo or fraction of an echo filled the entire oscilloscope screen. When only a fraction of the echo was displayed, the portion displayed was set by adjusting the delay time in the trigger generator. Two echoes in the train were singled out for viewing by applying a strobe signal to the oscilloscope remote intensity control. The strobe signal consisted of two pulses having the same width and delay times (the length of time between the event and the sync signal) as the selected echoes. The strobe controlled the oscilloscope intensity so that only the selected echoes where visible. The selected echoes could be made to appear in phase on the oscilloscope by making fine adjustments to the oscillator frequency. If the leading edges of the echoes were aligned so that each cycle from one echo lay over its matching cycle from the other echo, then this method would produce an accurate absolute measure of the sound velocity. Typically there was potential for an error in the measured return transit time of an integral number of RF periods. In practice, the RF cycles of the echoes were adjusted to appear 180° out of phase on the screen because this condition could be maintained more precisely than the in phase condition. Thus, the relation between the velocity, v, and oscillator frequency, f, was:

$$2d/v = 1/f + (n+\tfrac{1}{2})/f_{RF} \qquad (4.22)$$

where d is the separation of the transducers, n is a small integer, and f_{RF} is the RF frequency (about 3 MHz). The term involving f_{RF} did not affect the relative measure of the velocity so long as the integer, n, was not changed. A change of the integer by one would cause an apparent change in velocity of about 3% and an apparent change in elastic constant of about 6%. The pulse echo overlap technique was selected over pulse superposition techniques because it was less demanding on the quality of the echo train; the high apparent attenuation made pulse superposition techniques impossible for most samples.

Data Acquisition

The temperature and ultrasonic data were acquired by a microcomputer (Apple IIe) and stored on floppy disk for off-line analysis. The computer accepted keyboard input to adjust the oscillator frequency. When the frequency was properly adjusted, the computer accepted keyboard inputs to record a data point. Recording a data point consisted of the following: reading the thermometer conductance via a 4-point bridge (SHE Potentiometric Conductance Bridge) with an interface, storing the conductance of the thermometer and the oscillator frequency into memory, and (if desired) producing a hard copy. The computer also controlled a chart recorder through a DAC to produce a temperature record for on line inspection. This was useful since the temperature was being controlled manually by adjusting the flow of liquid through the Svenson cooler of the cryostat. To expedite data acquisition, data were transferred to disk only after many data points were collected. The interface was designed and constructed and the software was written by this author.

Video recordings of the solid helium were made during the experiment. The intensity contrast visual method (described in chapter III) was used. The light intensity received by the video camera was monitored on a chart recorder.

The pressure of the helium was recorded from a Heise gauge immediately after the helium was solidified.

Sample Preparation

Samples were generally solidified into the fcc phase over the course of five minutes. During solidification, the capillary was kept unblocked through the use of a heater. Some samples where annealed within .5 K of the melting temperature for over 12 hours. After solidifying (and annealing in some cases) samples where cooled continuously until the fcc→hcp transformation occurred. Approximately half the samples were rejected because the attenuation was too high to permit velocity measurements. There was no indication that annealing improved ultrasonic transmission in the sample. Occasional visual observations of planar interfaces traversing the entire width of the sample suggested that the samples were single crystals.

Calculation of Internal Energy

In order to compare the experimental temperature dependence of the sound velocity with the quasi-harmonic theory, a calculation of the thermal component of the internal energy per unit volume, $u_S(T)$, was required. To calculate the internal energy, the Debye approximation was used. For simplisity, the "S" subscript can now be dropped from "$u_S(T)$" and u will refer to the thermal component of the internal energy. According to Leibfried and Ludwig[31] the Debye approximation is sufficiently accurate to investigate the first order corrections to the harmonic approximation. The internal energy calculation required the Debye temperature and the molar volume of the solid. These values were obtained by using tables of volume and Debye temperature of solid ^{4}He tabulated against pressure on the melting curve published by Driessen *et al.*[22]. A linear interpolation of Driessen's data was used to find the volume and Debye temperature of the samples in this study. The internal energy in the Debye approximation is given by:

---

[31] G. Leibfried and W. Ludwig, in Solid State Physics, eds. F. Seitz & D. Turnbull, (Academic Press, New York, 1961), vol. 12, P. 275.

$$u(T) = u(x) = \frac{9nk}{x^4\Theta} \int_0^x \frac{y^3}{(e^y-1)}\, dy \tag{4.23}$$

where n is the number of atoms per unit volume, k is Boltzman's constant, Θ is the Debye temperature, and $x=\Theta/T$. Application of Simpson's rule to the evaluation of the above integral is not straightforward due to the fact that the denominator of the integrand vanishes at one of the limits of integration. To avoid problems associated with this, the value of u/3nk at x=.2 was obtained from tables published by Beattie[23] and other values of u/3nk were calculated from the equation:

$$u(x) - u(.2) = \frac{9nk}{x^4\Theta} \int_{.2}^x \frac{y^3}{(e^y-1)}\, dy \tag{4.24}$$

The integral was evaluated using Simpson's rule. Several values of u(T) were compared with those in the tables of Beattie and found to be consistent within .001%. Figure 4.4 shows the internal energy as a function of temperature for ^{4}He at two different volumes.

---

[22] A. Driessen, E. van der Poll, & I.F. Silvera, Phys. Rev. B, 33, 3269 (1986).
[23] J.A. Beattie, J. Math. and Phys., 6, 1, (1926-1927).

D. RESULTS

The velocity of transverse sound showed a strong dependence on temperature in hcp ^{4}He at the pressures of 1.1 kbar and 1.5 kbar. Temperature changes caused velocity changes of up to 7%. The sound velocity dependence on temperature is primarily reported in terms of the elastic constant[24] dependence on internal energy[25]. Internal energy changes (due to temperature changes) caused elastic constant changes of up to 14%. The dependence of the elastic constant on the internal energy appeared to be very nearly linear for most of the samples studied. The slope and intercept of the line fitting the data varied from sample to sample, but there was no indication that any elastic constant approached zero as the transformation temperature was approached.

Twenty-one samples of hcp ^{4}He were studied. Samples were labeled with a number and a letter. Samples with the same number but different letter were produced from the same solid but from different fcc→hcp transformations. For example, sample 1A was heated until it transformed to an fcc sample and was immediately cooled until the ensuing fcc→hcp transformation produced sample 1B. Samples 10A, 10B, and 10C were solidified at 1.1 kbar; all other samples were solidified at 1.5 kbar. The data were fit to the straight line:

---

[24] Hereafter, "elastic constant" refers to the dynamic elastic constant, $\hat{C}$, for the mode of sound being observed. This is equal to ρv^2 (see eq. 4.16). Since the crystal orientation is undetermined, the branch and wave vector arguements are dropped from the symbol "$\hat{C}_r(\hat{k}_s)$" used previously in this thesis.

[25] Hereafter, "internal energy" refers to the thermal component of internal energy per unit volume in the Debye approximation, u. (See eq. 4.24 for the calculation of u).

$$\hat{C}=\hat{C}_0-\Gamma u \qquad (4.25)$$

with a least squares fit. Only points marked with dots were included in the fitting procedure; points marked with crosses were assumed to have excessive experimental error or to be anomalous deviations from the nearly linear relation. The values of $\hat{C}_0$ and Γ obtained from the fitting procedure, as well as the pressure at the melting point (P), are inset into each figure.

Sample 1A showed the typical features of the temperature dependence of the sound velocity. Figure 4.5 shows the velocity dependence on temperature for the first experimental run on sample 1A. The pressure on the melting curve for this sample was 1.50 kbar. The volume was 11.40 cm^3/mole and the Debye temperature was 95.57 K. The data (1307 points) were collected for this run as the range of temperatures was traversed four times (twice in cooling and twice in heating). The heating or cooling rates used were about 50 mK/min. Occasional interruptions to heating or cooling allowed the thermal gradients to decrease. The derivative of the velocity with respect to temperature approached zero as the temperature approached zero. Over the range of temperatures measured for this run (8 K to 15 K), the change in velocity was 7%. Figure 4.6 shows the same data plotted in terms of elastic constant versus internal energy. The elastic constant appeared to be very nearly a linear function of internal energy for this sample. A linear least squares fit to this data yielded a value for Γ of 13.4 and a $\hat{C}_0$ of 2.249 kbar. Over the range of temperatures measured for this run, the change in elastic constant was 14%. Figure 4.7 shows a second run for the same sample. This data set was separated from the data set of the first run because less care was taken to keep the heating/cooling rate at a minimum. The data agreed well with that of the first run and showed that the linear dependence of the elastic constant on internal energy was maintained up to the transformation temperature.

Most other samples showed qualitatively similar results. The elastic constant is plotted for the other samples in figures 4.8 to 4.31. The values of $\hat{C}_0$ and Γ obtained from a least squares fit are tabulated in table 4.1. The distribution of the values of $\hat{C}_0$ and Γ are shown in figures 4.32 and 4.33 respectively.

As the transformation temperature was reached, the ultrasonic signal diminished to the point where it was impossible to measure the sound velocity. Usually the elastic constant remained linear with the internal energy until the ultrasonic signal was lost. Sample 1A(run 2) (fig. 4.7) nicely demonstrated this phenomenon. In contrast, sample 10C(run 2) (fig. 4.31) clearly did not, since the elastic constant started to rise prior to the loss of the ultrasonic signal caused by the hcp→fcc transition. The elastic constant anomaly also occurred during cooling in the preceding run on the same sample (fig. 4.30). The anomaly occurred to a lesser extent in sample 5A (fig. 4.13). Samples 10A and 10B also showed a nonlinear dependence of the elastic constant on internal energy near the transition temperature. Figure 4.28 shows sample 10A during heating and fig. 4.29 shows sample 10B during cooling. During heating of sample 10A there was an anomalous rise in the elastic constant before the signal was lost. The signal intensity began to fluctuate and was lost before the transition was expected to occur. During cooling of sample 10B, the next sample, a very nonlinear dependence of the elastic constant on internal energy was observed until the signal was lost.

Often when an hcp sample transformed to an fcc sample, the fcc sample was cooled to produce another hcp sample from the same solid. In some cases, the values of $\hat{C}_0$ and Γ were reproduced in the second sample. This clearly occurred when sample 1B was produced from sample 1A and when sample 5B was produced from sample 5A. This also appears to have occurred in the production of samples 5E and 6B; however, the larger uncertainties in the values of $\hat{C}_0$ and Γ make these cases less convincing. Conversely, in some cases the measured values of $\hat{C}_0$ and Γ were different in the second sample. Such cases are shown in the production of samples 5C, 7B, 9B(run1), and 10C(run1). The values of $\hat{C}_0$ and Γ were reproduced in consecutive hcp samples of the same solid for approximately half the cases.

Occasionally, the intensity of the received ultrasonic signal changed when the fcc→hcp transformation was not expected. These changes usually started with a sudden decrease in the received signal, progressed with the signal fluctuating for approximately one minute, and ended with the signal intensity different (sometimes higher, sometimes lower) from that present before the fluctuations started. It was sometimes noticed that the light intensity received in the video camera fluctuated simultaneously with the acoustic signal fluctuations. During the course of these fluctuations it was not possible to measure the sound velocity. After such a fluctuation, it was necessary to realign two of the received echoes on the oscilloscope (as required by the pulse echo overlap technique). Often two different echoes were selected to accommodate for the change in signal strength. A markedly different value of the oscillator frequency was required to realign the echoes. This usually indicated that there was an abrupt change in the sound velocity during these fluctuations. In these samples, the values of $\hat{C}_0$ and Γ were different before and after the fluctuations. Such a fluctuation occurred in sample 7A. A change in elastic constant during the fluctuation of 1.5% is marked by the arrow in fig. 4.22; the value of Γ was 10.5 before the fluctuation and 16.0 after the fluctuation. The same effect occurred in samples 9B and 10C. In these samples, the data set taken before the signal fluctuation is labeled run 1 and the data set after the fluctuation is labeled run 2. During heating of sample 9B there was a 12% change in the elastic constant that occurred when the internal energy reached 17.0 x 10^4 erg/cm^3. The value for Γ changed from 14.4 to 11.2. Data for sample 10C were collected during cooling and reheating until the internal energy reached 12.8 x 10^4 erg/cm^3, at which point the elastic constant changed by 2%. The value for Γ changed from 12.3 to 11.8. It appeared that the sound mode observed changed at the time these fluctuations occurred. The process occurring during these fluctuations could be an annealing process or a rotation of the crystal inside the cell.

Sample 5D had a fluctuation in signal intensity. After the signal fluctuation the measured elastic constant in sample 5D was 5% higher than the measured elastic constant before the fluctuation. The value of Γ, however, was unchanged. A possible explanation for this sample is that different cycles were aligned (that is, the value for n in eq 4.22 had changed) and no real change in elastic constant occurred. This explanation can not apply to the samples dicussed in the previous paragraph since the change in the oscillator period required to align the echoes was not close to one RF period.

E. DISCUSSION

The elastic constants measured in this work are consistent with the values measured in ^{4}He at other pressures. An appropriate method for comparing elastic constants at different pressures is to plot the elastic constant against the bulk modulus. If the generalized Grüneisen parameters are equal to the Grüneisen constant (a condition that frequently is a good approximation), then the bulk modulus and the elastic constants should have an identical dependence on the pressure and a graph of an elastic constant against the bulk modulus should yield a straight line through the origin. The values of the zero temperature, transverse mode elastic constants obtained from this work, and the values of C_{44} [26] obtained from the literature[27] [28] are plotted in fig. 4.34. The line is an interpolation of the values from the literature. The interpolated value for C_{44} lies within the range of values of transverse mode elastic constants measured in this work. A more detailed comparison is prohibited because crystal orientation was not determined in this work. To the extent that comparison is possible, the values of elastic constant measured in this work are consistent with the values in the literature.

---

[26] The elastic constants from the literature are interpreted to be the dynamic elastic constants from the context.
[27] J. Eckert, W. Thomlinson, and G. Shirane, Phys. Rev. B, 18, 3074 (1978).
[28] D. Greywall, Phys. Rev. A, 3, 2106 (1970).

The quasi-harmonic approximation appears to hold for hcp ^{4}He between 1.1 and 1.5 kbar. This is shown by the linearity of the curves of $\hat{C}$ versus u. Slight nonlinearities in the curves may be attributed to terms that are higher than first order in internal energy that are required for the quasi-transverse branch. The fact that the derivative of the velocity with respect to temperature appeared to be approach zero as the temperature approached zero is consistent with the quasi-harmonic approximation. This is because the temperature derivative of internal energy approaches zero as the temperature approaches zero.

Anomalous deviations from the quasi-harmonic approximation near the transformation temperature were observed in some samples. In the anomalous region, the elastic constants were higher than predicted from the quasi-harmonic approximation. While the theory of Granato *et al.*[29] predicts an anomalous decrease in elastic constant near the hcp-fcc transition temperature, there appears to be no theory to explain anomalous increases in the elastic constant. The anomalies appeared primarily in the samples at 1.1 kbar. At this pressure, the anomalies may be associated with the approach to the melting curve, which is very close to the fcc→hcp phase line at 1.1 kbar. Alternatively, the anomalies may be due the start of the fcc→hcp transformation. In the latter case, it is interesting that the start of the transformation did not immediately cause the ultrasonic signal to be lost as in the other cases. While the anomalies appear interesting, it is not clear what they indicate.

---

[29] A.V. Granato, R.R Schwarz, and G.A. Kneezel, J. de Physique, 42, sup. 10, C5-1055 (1981).

There appears to be a large mode dependence on the values of Γ. This is shown by the large spread (covering a range from -2 to 16) of values measured for Γ. The values for Γ measured at 1.5 kbar are shown in the histogram in fig. 4.33. The temperature dependence of elastic constants for hcp ^{4}He[30] and hcp ^{3}He[31] are fit to a functional form[32] that permits a mode dependence without explaining its theoretical basis. The quasi-harmonic approximation provides a theoretical basis for the observed mode dependence.

The negative values of Γ are very unusual. Perhaps these samples were not single crystals and grain boundaries caused internal reflections that invalidated the pulse echo overlap method of velocity measurement.

Even though the acoustic modes did soften by various amounts, it appears that there is no acoustic mode that softens completely as the transformation temperature is approached. The value of Γ required for complete mode softening in hcp ^{4}He at 1.5 kbar would be about 100 (the value depends on the value of $\hat{C}_0$). The histogram of measured values of Γ (fig. 4.33) suggests no mode is likely to have a value of Γ greater than 20. No mode appears to critically soften.

---

[30] For example: I. Iwasa and H. Suzuki, J. Phys. Soc. Jpn., 49, 1722 (1980).

[31] J.R. Beamish and J.P. Franck, Phys. Rev. Lett., 47, 1736 (1981).

[32] R. Wanner, K.H. Mueller, and H.A. Fairbank, J. Low Temp. Phys., 13, 153 (1973).

The reproduction of the exact elastic constant versus internal energy curve in successive hcp crystals indicates that the hcp crystal orientation is reproduced. This result supports the visual evidence of crystal orientation reproduction that was presented in the preceding chapter. The orientation was not always reproduced, but it was reproduced more frequently than can be accounted for by random orientation of the hcp phase. The hcp crystal has a preference for its original orientation.

There is no indication of a simple correlation between the measured values of Γ and $\hat{C}_0$. The two measured values are plotted against each other in fig 4.35.

The values of Γ measured for this thesis can be compared with those calculated from the velocity versus temperature data in solid helium at lower pressures reported by other experimenters. At low temperatures:

$$u=\frac{\pi^4}{5}\,\frac{3RT^4}{\upsilon\Theta^3} \tag{4.26}$$

where υ is the molar volume, R is the gas constant, and Θ is the Debye temperature. For small velocity changes:

$$v \simeq v_0 + \frac{dv}{d\hat{C}}\Delta\hat{C} = v_0 + \frac{1}{2\rho v_0}\,(-\Gamma u) \tag{4.27}$$

which gives:

$$\frac{v-v_0}{v_0} = -\Gamma \frac{3\pi^4}{10} \frac{R}{mv_0{}^2\Theta^3} T^4 \qquad (4.28)$$

where m is the molar mass of ^{4}He and v_0 is the velocity at absolute zero. Some experimenters have reported their data in terms of the T^4 coefficient. In this thesis, Γ was calculated from these coefficients. The calculated values of Γ covered a wide range. This was expected from the dependence of Γ on the wave vector direction. The value of Γ_{11} was assumed to lie within the values of Γ calculated from longitudinal sound measurements, and the values of Γ_{44} and Γ_{66} were assumed to lie within the values of Γ calculated from transverse sound measurements. This allowed rough estimates of Γ_{11}, Γ_{44}, and Γ_{66}. These estimates are tabulated in table 4.2. The estimates of $\Gamma_{\alpha\beta}$ from this work and the work of Iwasa *et al.*[33] [34] are imprecise because the crystal orientation was not determined. Calder[35] measured the c-axis orientation of the samples used in his ultrasonic studies, but nevertheless only an imprecise value for Γ_{11} could be estimated from his work.

The values of Γ measured for solid helium can also be compared with those measured for various other materials. Leibfried and Ludwig[36] used

---

[33] I. Iwasa, H. Suzuki and K. Araki, J. Phys. Soc. Jpn., 46, 1119 (1979).
[34] I. Iwasa and H. Suzuki, J. Phys. Soc. Jpn., 49, 1722 (1980).
[35] I.D. Calder, Ph.D. Thesis, University of Alberta, Edmonton Canada, (1977, unpublished).
[36] G. Leibfried and W. Ludwig, in Solid State Physics, eds. F. Seitz & D. Turnbull, (Academic Press, New York, 1961),

$C_{\alpha\beta}$ and $kD_{\alpha\beta}$ as fitting parameters in their theory. They calculated the values of these parameters for hcp metals from results published in the literature. For this thesis, the values of $\Gamma_{\alpha\beta}$ were calculated from these parameters with the following equation:

$$\Gamma_{\alpha\beta} = \tilde{C}_{\alpha\beta}(kD_{\alpha\beta}) \frac{\upsilon}{3R} \tag{4.29}$$

The values of $\Gamma_{\alpha\beta}$ can also be estimated for H_2 and D_2 from the work of Wanner and Meyer[37]. The values of $\Gamma_{\alpha\beta}$ for several hcp materials are tabulated in table 4.2. All values of $\Gamma_{\alpha\beta}$, including the values for helium, are within a factor of three (and most are within a factor of two) of the median values (24 for Γ_{11} and 11 for Γ_{44} and Γ_{66}) for the hcp metals tabulated. This is remarkable since the C_{11} elastic constant ranged from 4470 kbar (in Be) to .5 kbar (in ^{4}He at low pressure).

In the hcp metals, the values of Γ_{11} are approximately twice the values of Γ_{44}. This is also true of the results in ^{4}He in spite of the fact that the measurements were done at different pressures. The values of Γ in helium appear to be independent of pressure over a range of pressures from .04 to 1.5 kbar. This is true in spite of the fact that solid helium was expected to have greater anharmonic properties at lower pressures.

---

[36] (cont'd) vol. 12, P. 275.
[37] R. Wanner and H. Meyer, J. Low Temp. Phys., 11, 715 (1972).

The reason that the observed changes in elastic constants were an order of magnitude larger in this study than in the studies at lower pressures is that much higher values of internal energy were achieved at 1.1 kbar and 1.5 kbar than the pressures used in previous studies. As illustrated in fig 4.4, the highest internal energy achievable before melting in helium at .04 kbar is 1×10^4 erg/cm^3 whereas at 1.5 kbar, an internal energy of 28×10^4 erg/cm^3 is attainable.

F. SUMMARY

The quasi-harmonic approximation predicts that the elastic constants have a nearly linear dependence on the internal energy. This appears to hold very well in hcp ^{4}He at pressures of 1.1 and 1.5 kbar. Γ, the derivative of the elastic constant with respect to internal energy, is typically 12, but ranges between -2 and 16 at these pressures. The values of Γ are the same order of magnitude as those measured in hcp metals. Comparing the values of Γ calculated from the results of this work and from the results of studies on ^{4}He at other pressures indicate that the values of Γ are insensitive to pressure. There does not appear to be critical mode softening associated with the hcp→fcc transformation.

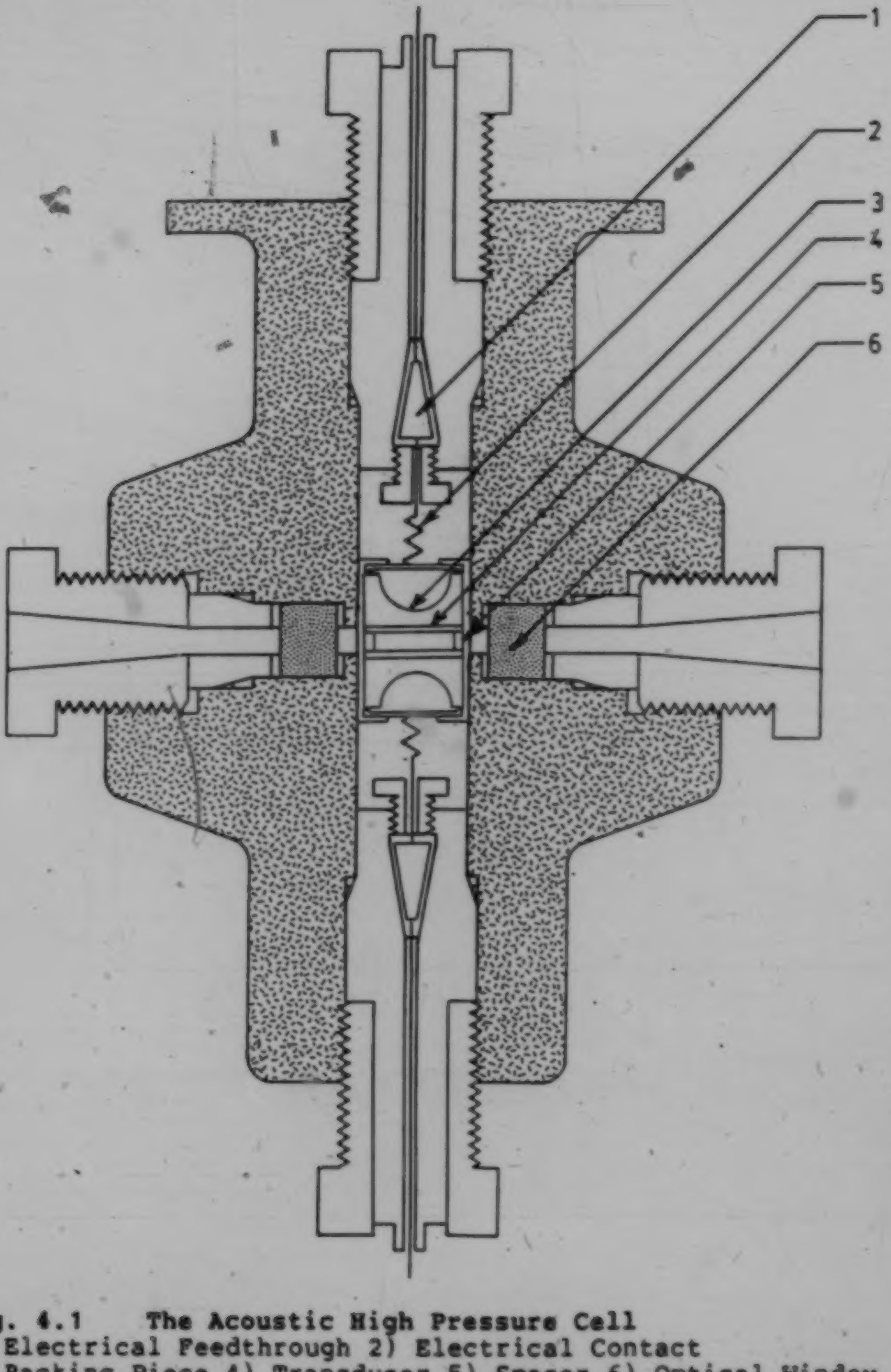

Fig. 4.1 The Acoustic High Pressure Cell
1) Electrical Feedthrough 2) Electrical Contact
3) Backing Piece 4) Transducer 5) Spacer 6) Optical Window

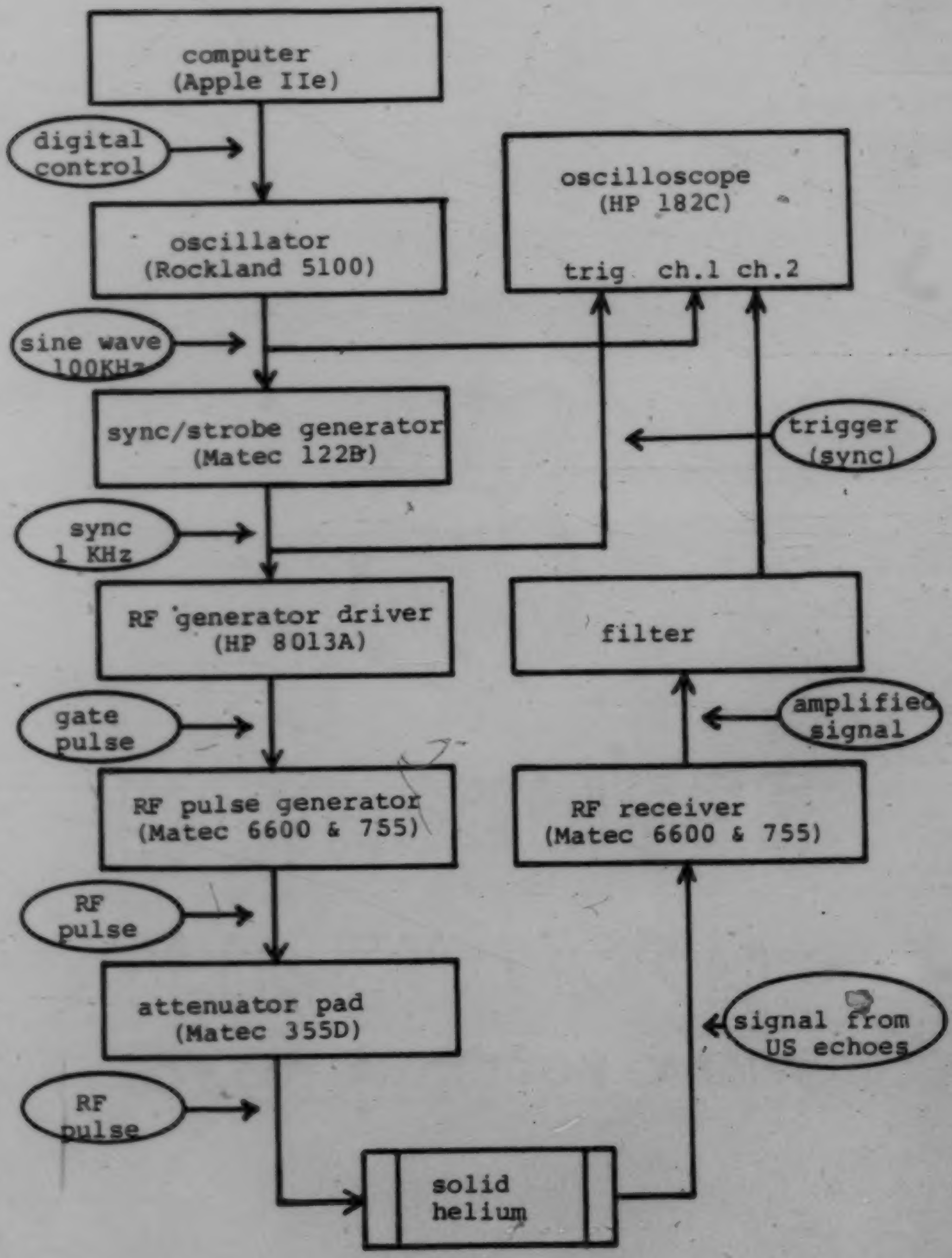
computer
(Apple IIe)
digital control
oscillator
(Rockland 5100)
sine wave 100KHz
sync/strobe generator
(Matec 122B)
sync 1 KHz
RF generator driver
(HP 8013A)
gate pulse
RF pulse generator
(Matec 6600 & 755)
RF pulse
attenuator pad
(Matec 355D)
RF pulse
solid helium
oscilloscope
(HP 182C)
trig ch.1 ch.2
trigger (sync)
filter
amplified signal
RF receiver
(Matec 6600 & 755)
signal from US echoes

Fig. 4.2 Electronics for Absolute Velocity Measurement

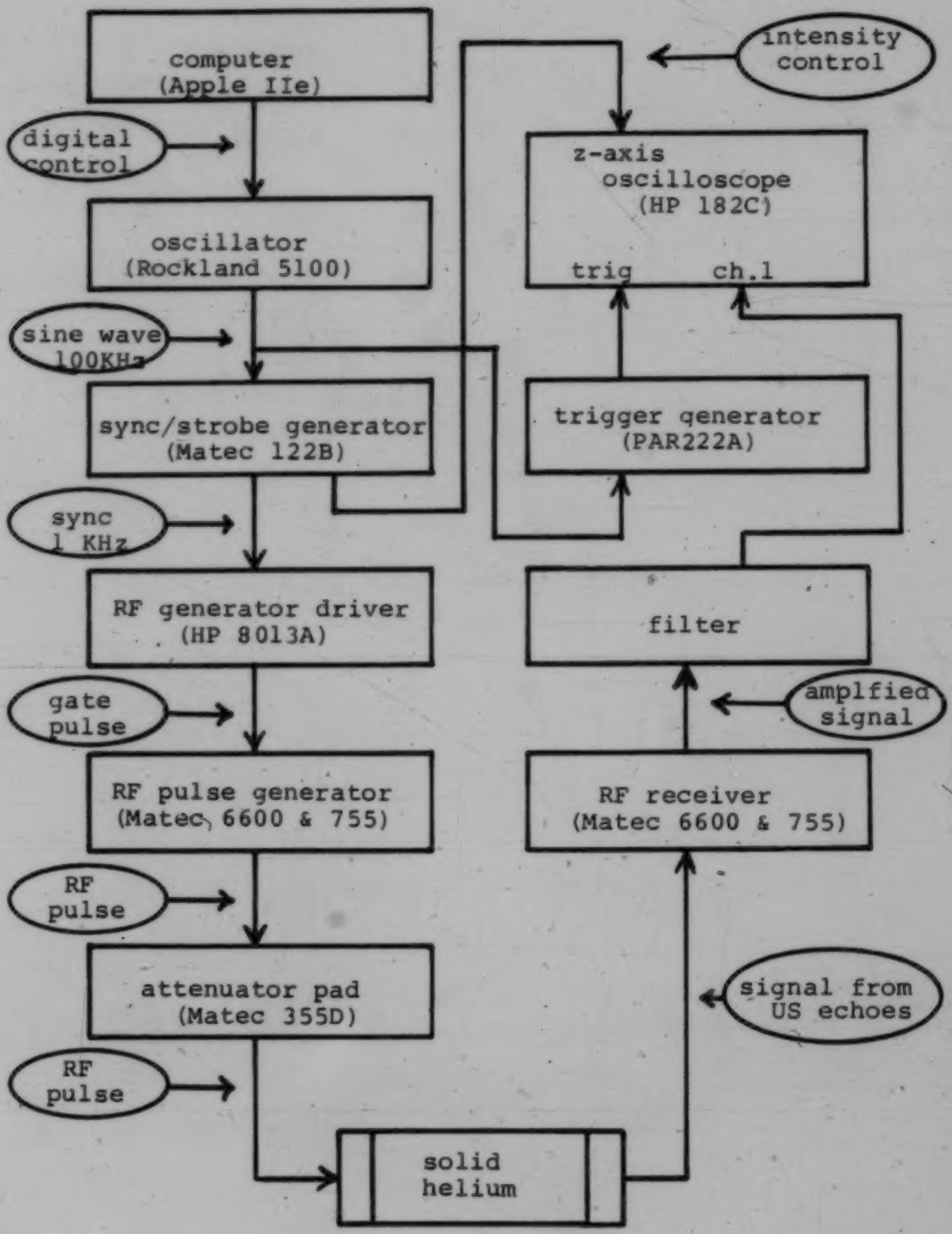
computer
(Apple IIe)
digital control
oscillator
(Rockland 5100)
sine wave 100KHz
sync/strobe generator
(Matec 122B)
sync 1 KHz
RF generator driver
(HP 8013A)
gate pulse
RF pulse generator
(Matec 6600 & 755)
RF pulse
attenuator pad
(Matec 355D)
RF pulse
solid helium
intensity control
z-axis
oscilloscope
(HP 182C)
trig
ch.1
trigger generator
(PAR222A)
filter
amplfied signal
RF receiver
(Matec 6600 & 755)
signal from US echoes

Fig. 4.3 Electronics for Relative Velocity Measurement

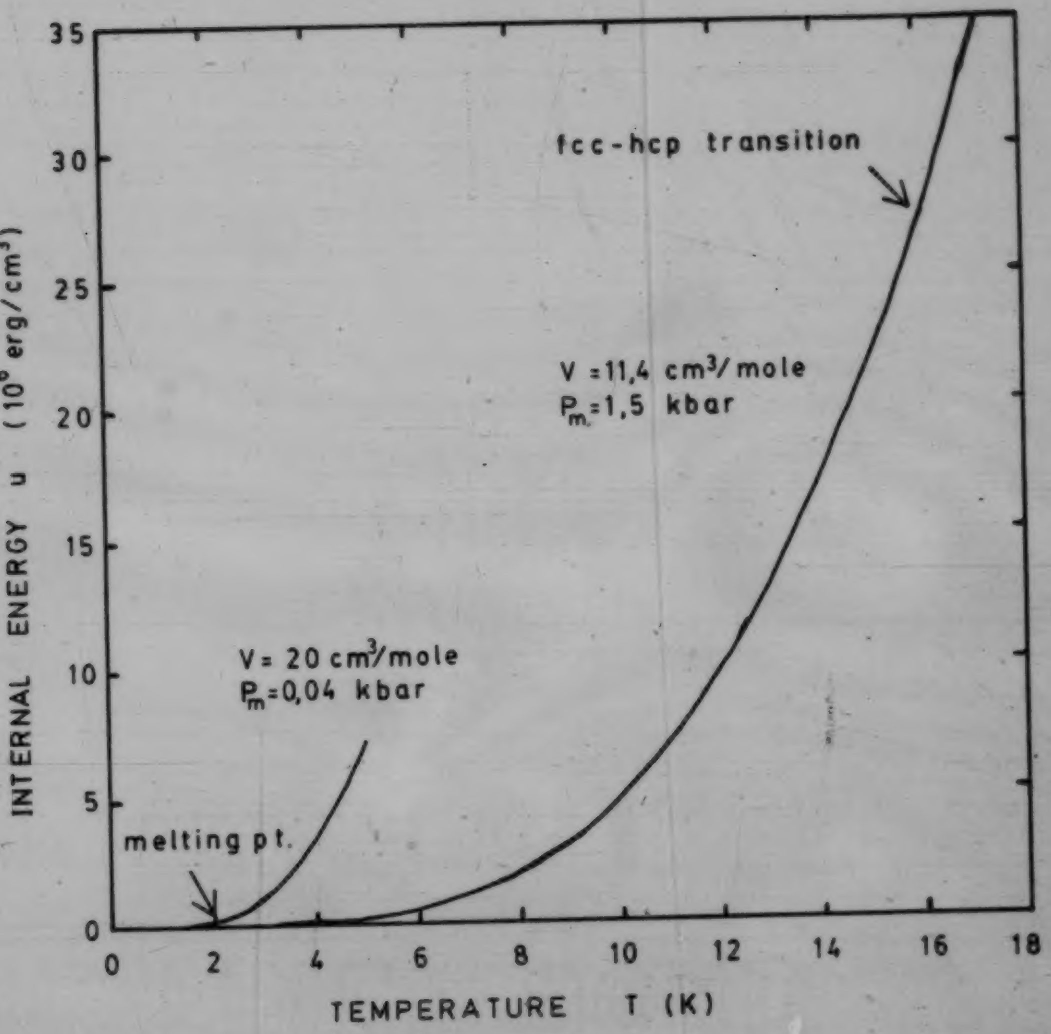

Fig. 4.4 Internal Energy Dependence on Temperature

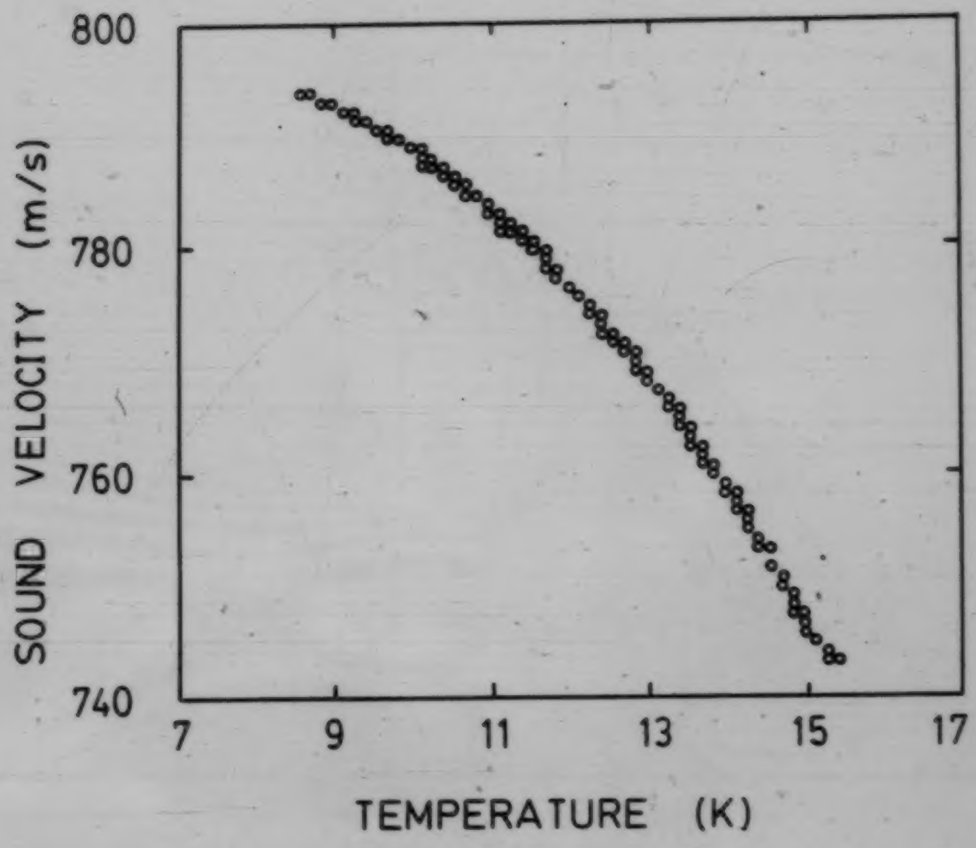

Fig. 4.5 Velocity Dependence on Temperature in Sample 1A run1

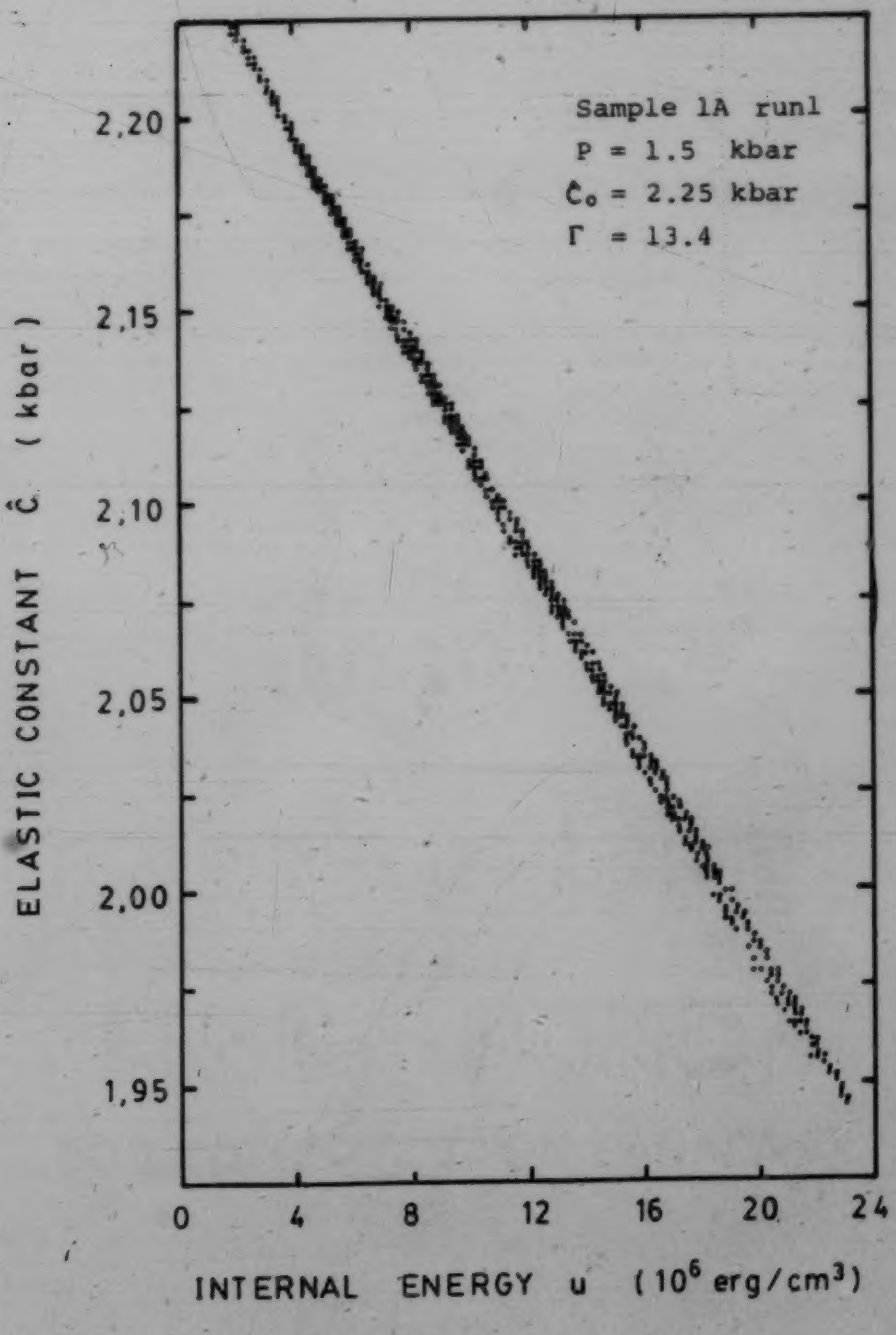

Fig. 4.6 Ĉ Dependence on u(T) in Sample 1A run1

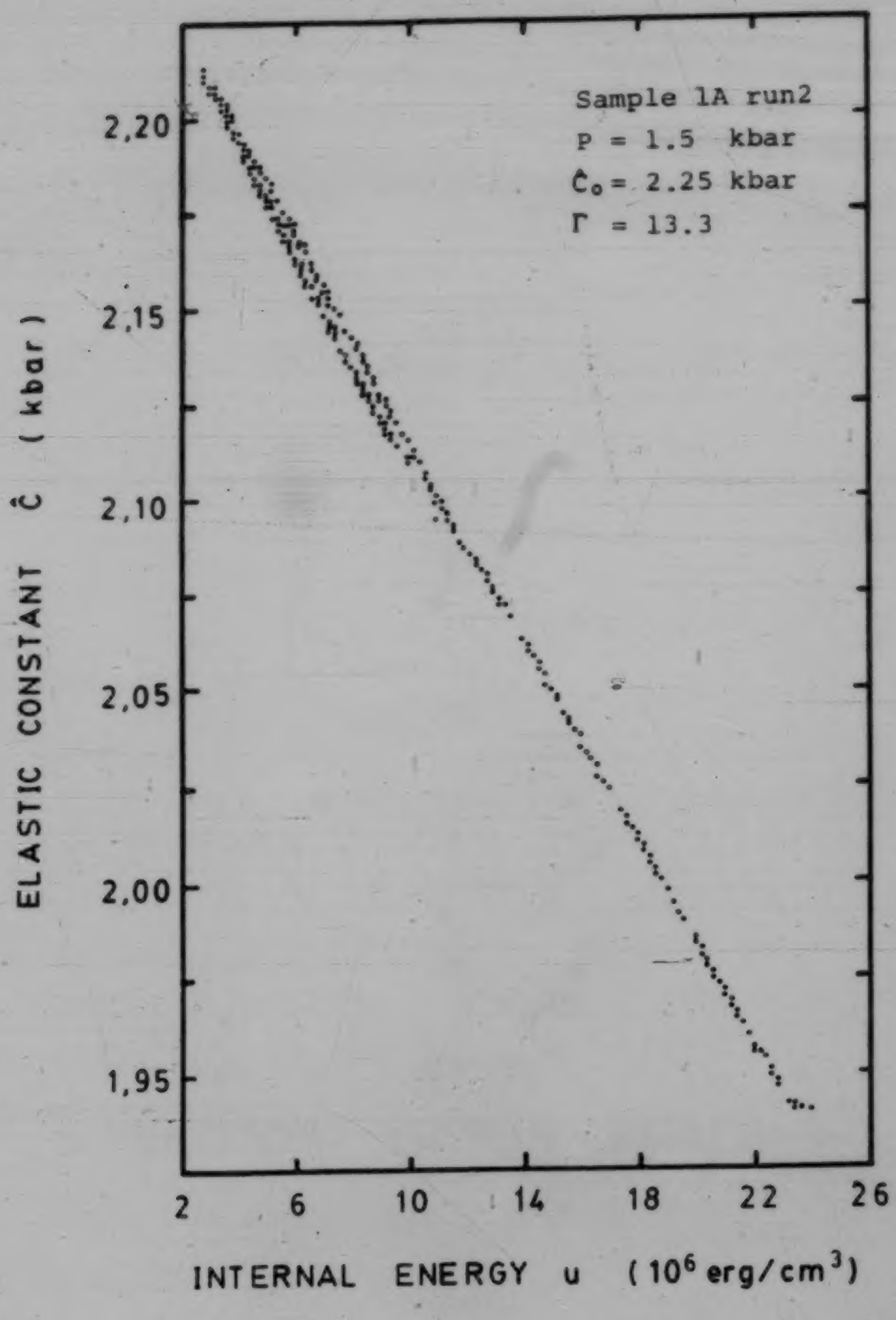

Fig. 4.7 Ĉ Dependence on u(T) in Sample 1A run2

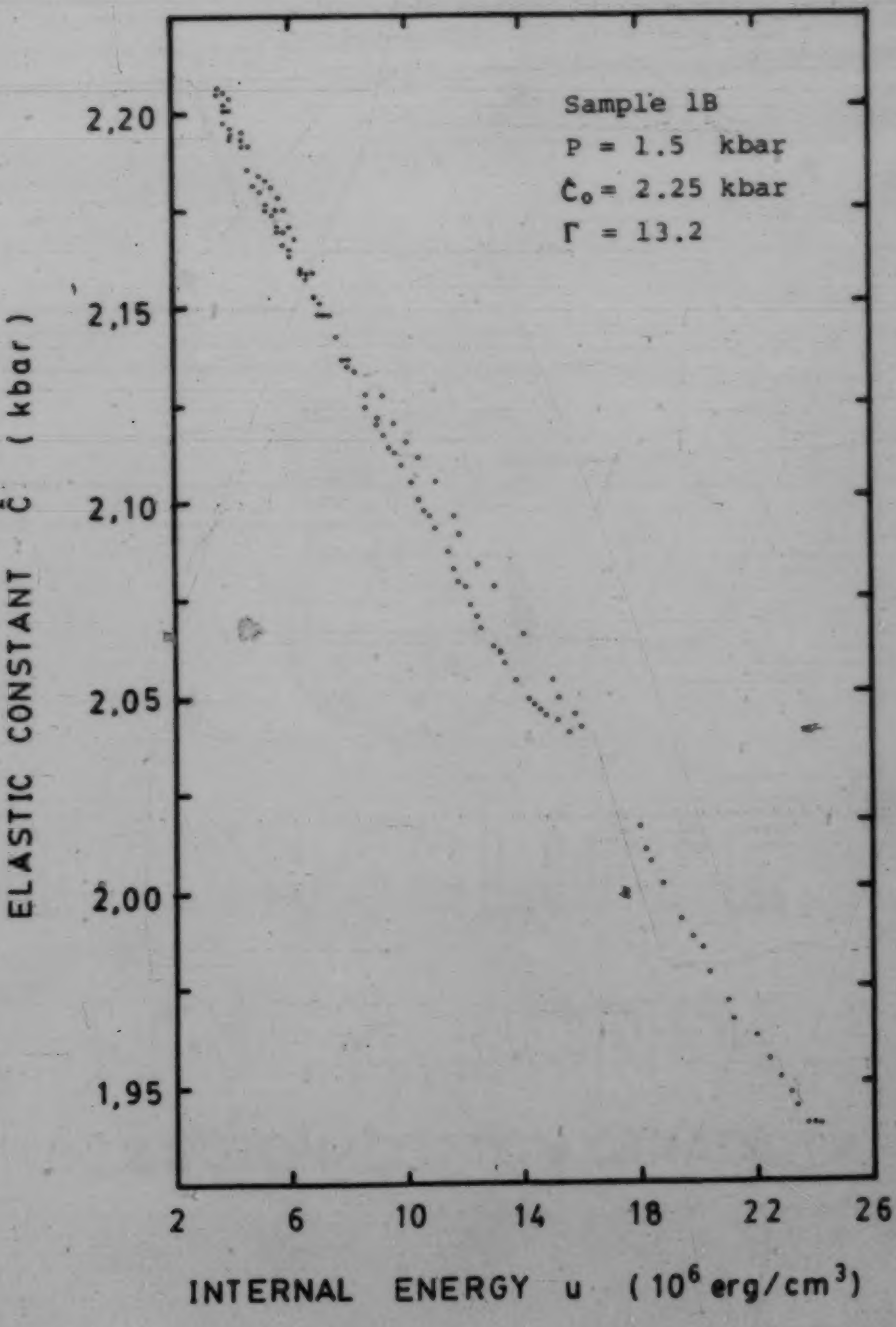

Fig. 4.8 $\hat{C}$ Dependence on u(T) in Sample 1B

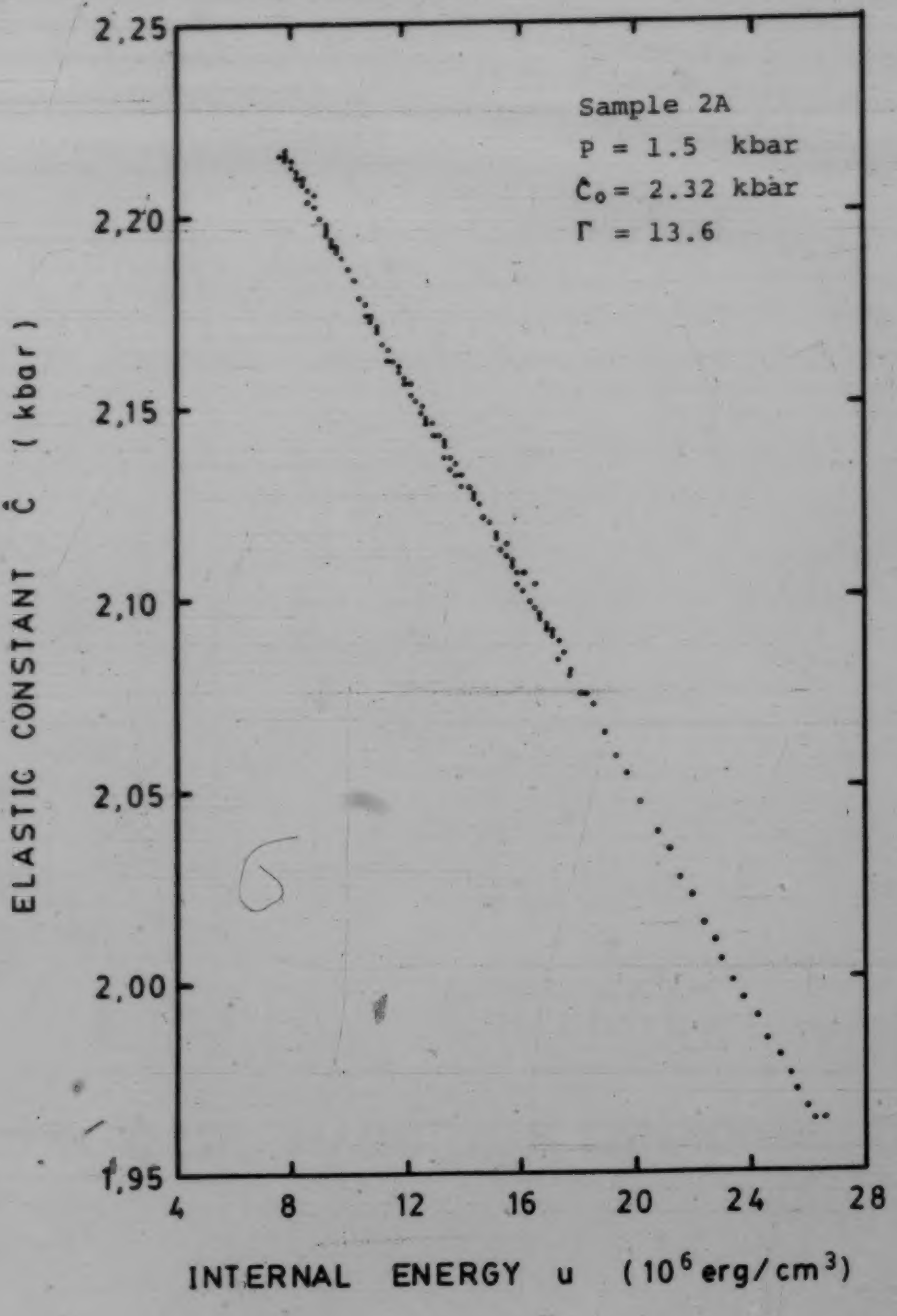

Fig. 4.9 Ĉ Dependence on u(T) in Sample 2A

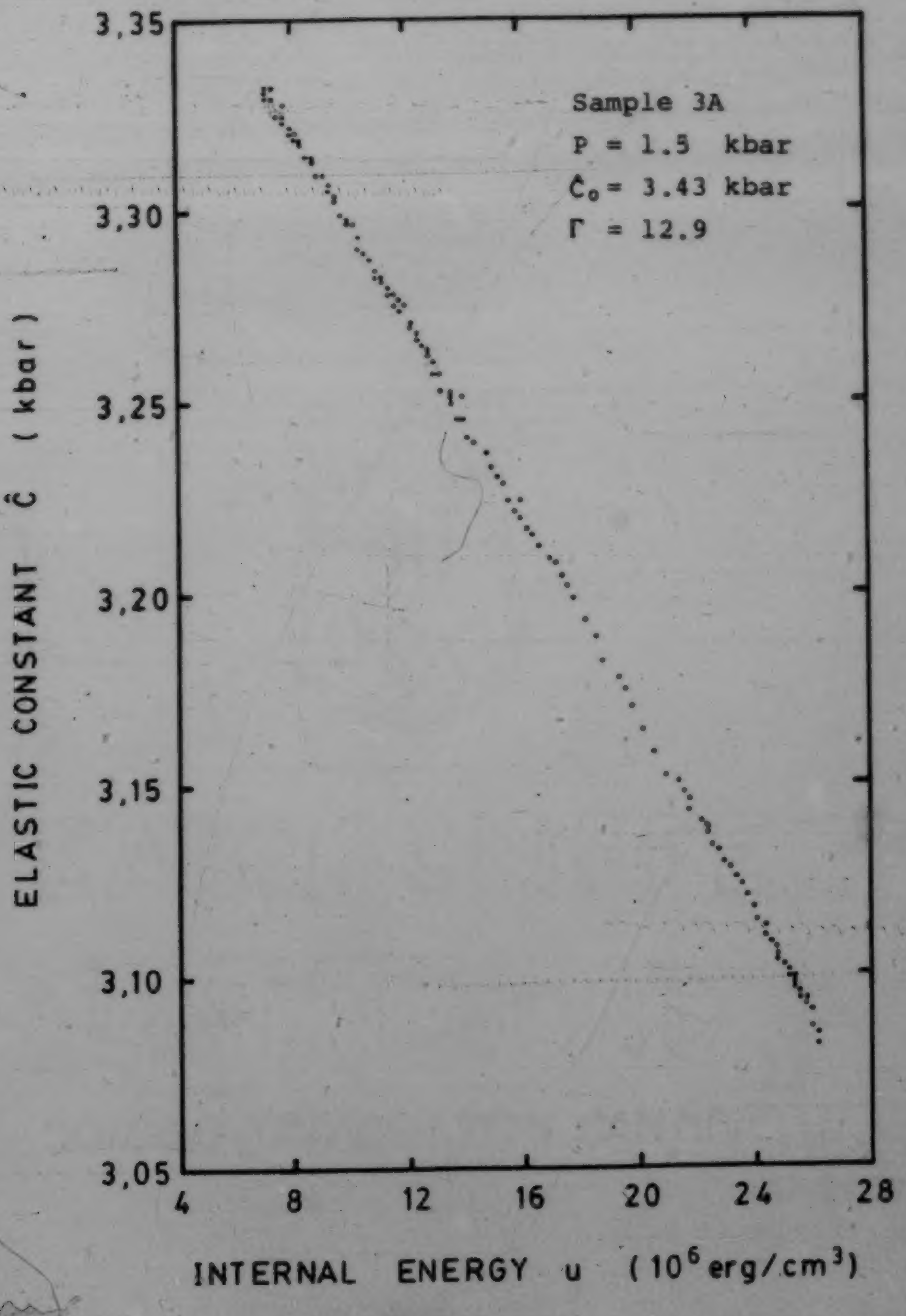

Fig. 4.10 – Ĉ Dependence on u(T) in Sample 3A

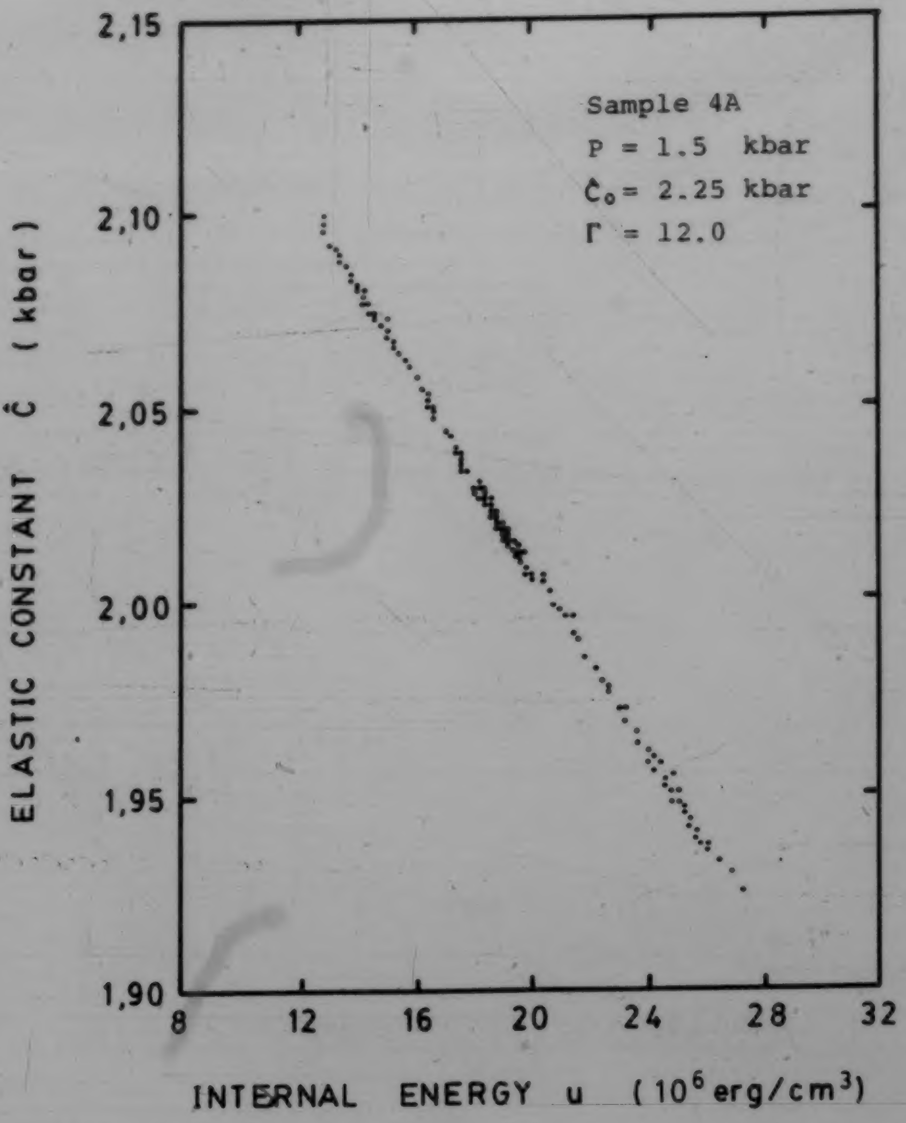

Fig. 4.11 $\hat{C}$ Dependence on u(T) in Sample 4A

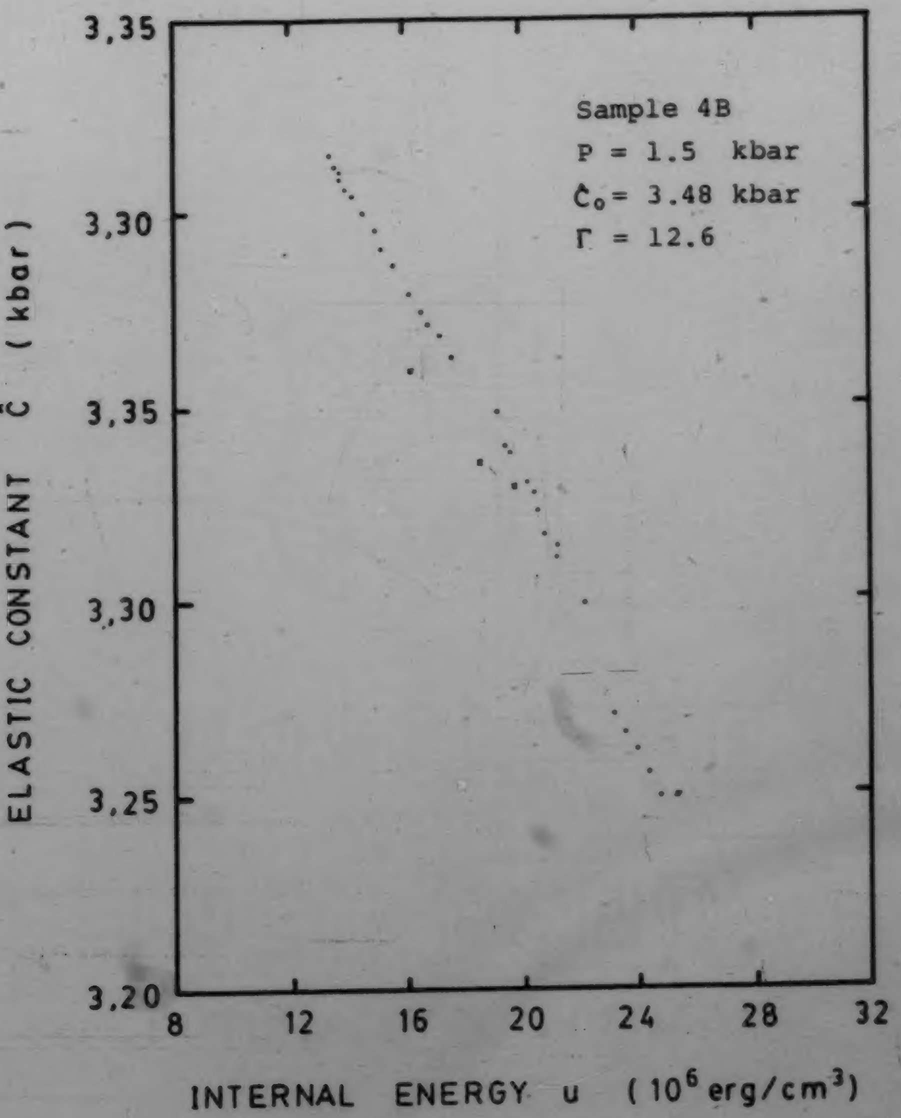

Fig. 4.12 Ĉ Dependence on u(T) in Sample 4B

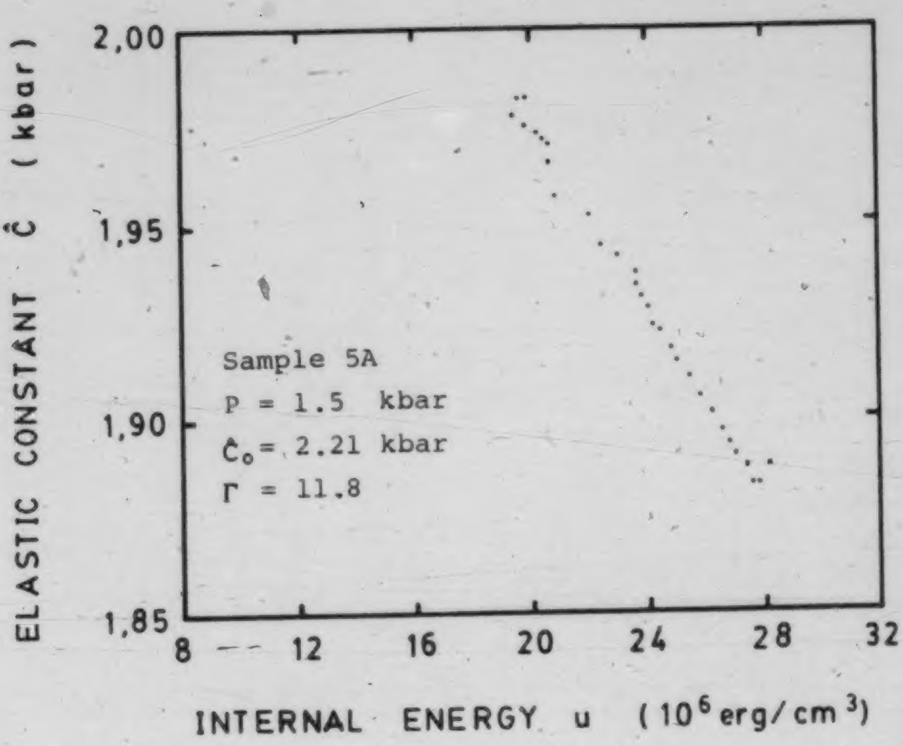

Fig. 4.13 Ĉ Dependence on u(T) in Sample 5A

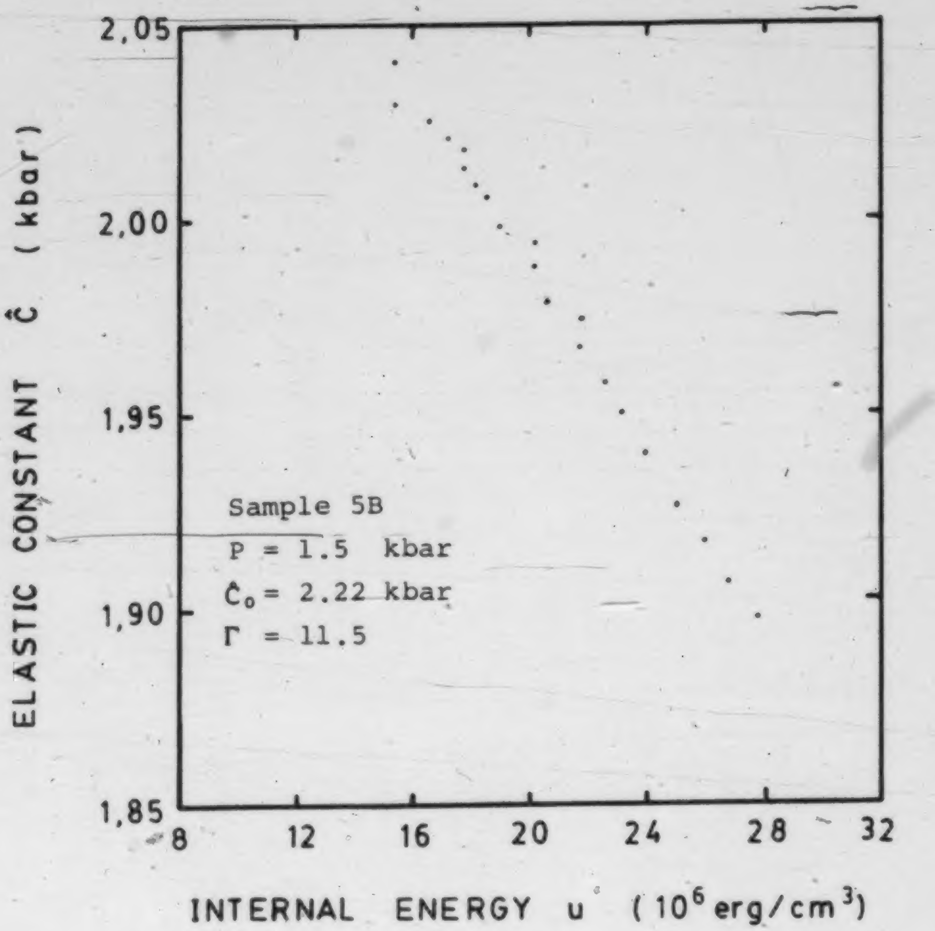

Fig. 4.14 Ĉ Dependence on u(T) in Sample 5B

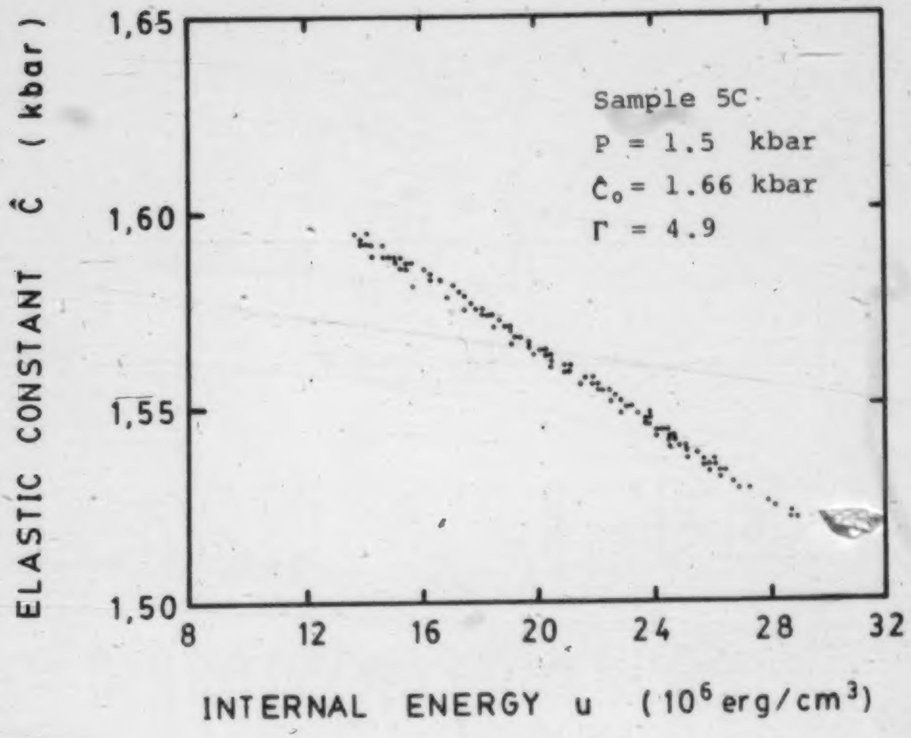

Fig. 4.15 Ĉ Dependence on u(T) in Sample 5C

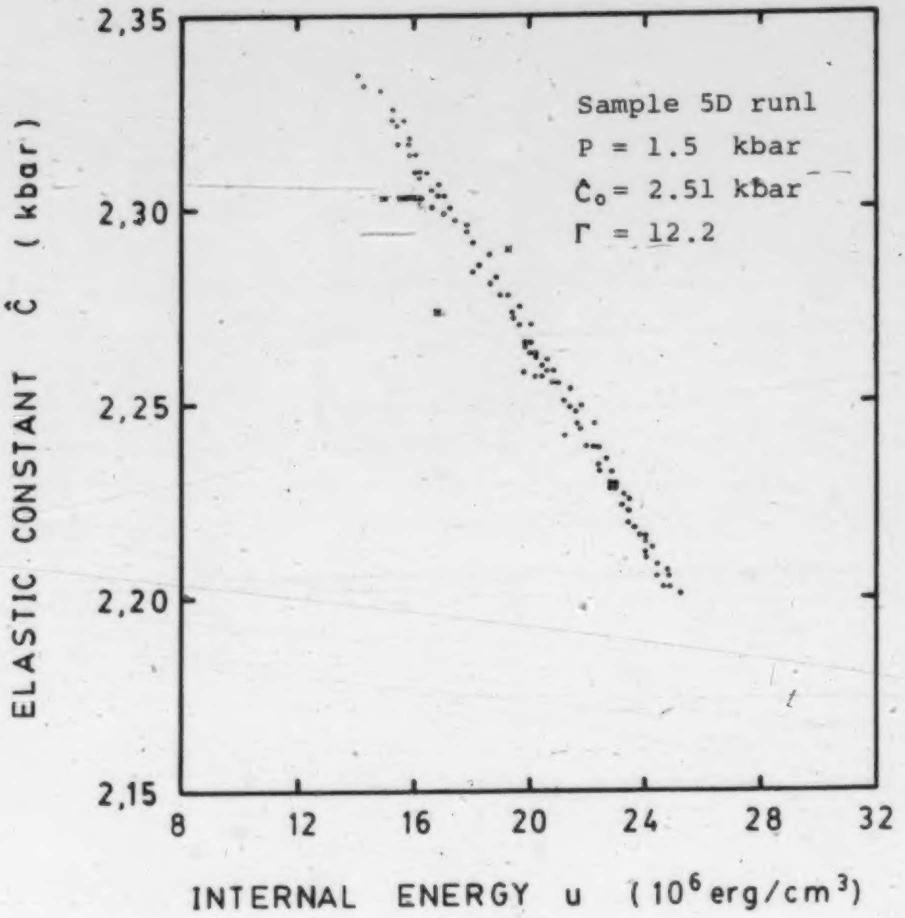

Fig. 4.16 Ĉ Dependence on u(T) in Sample 5D run1

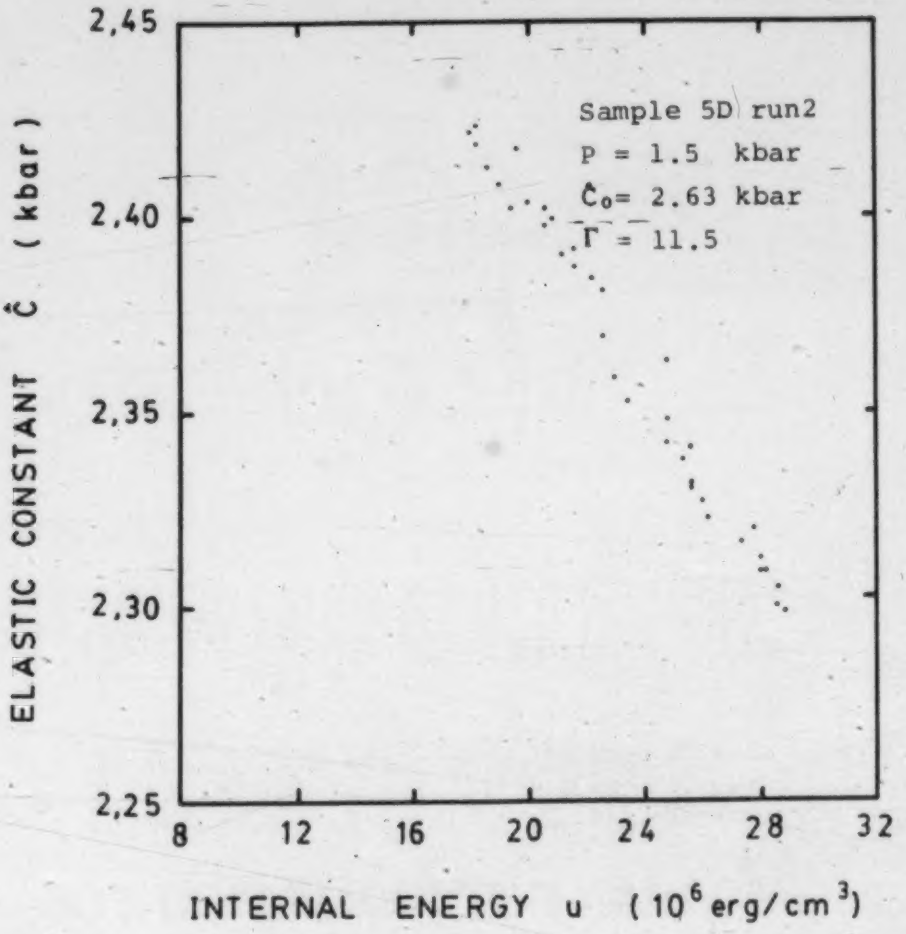

Fig. 4.17 Ĉ Dependence on u(T) in Sample 5D run2

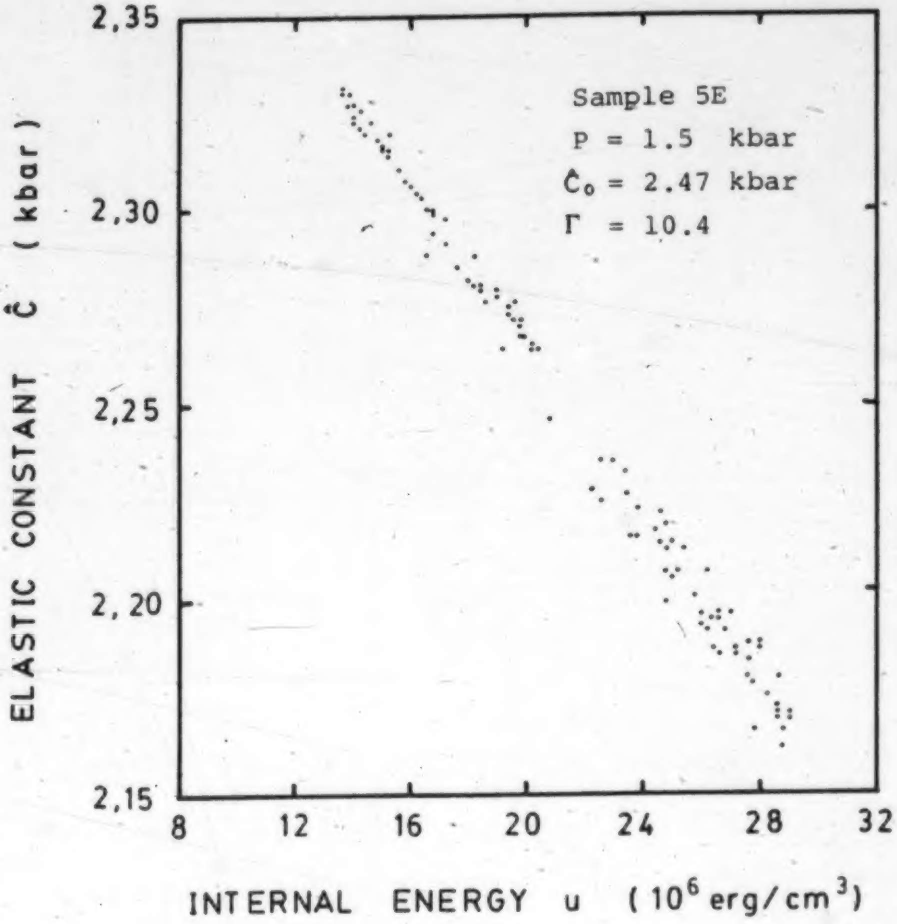

Fig. 4.18 Ĉ Dependence on u(T) in Sample 5E

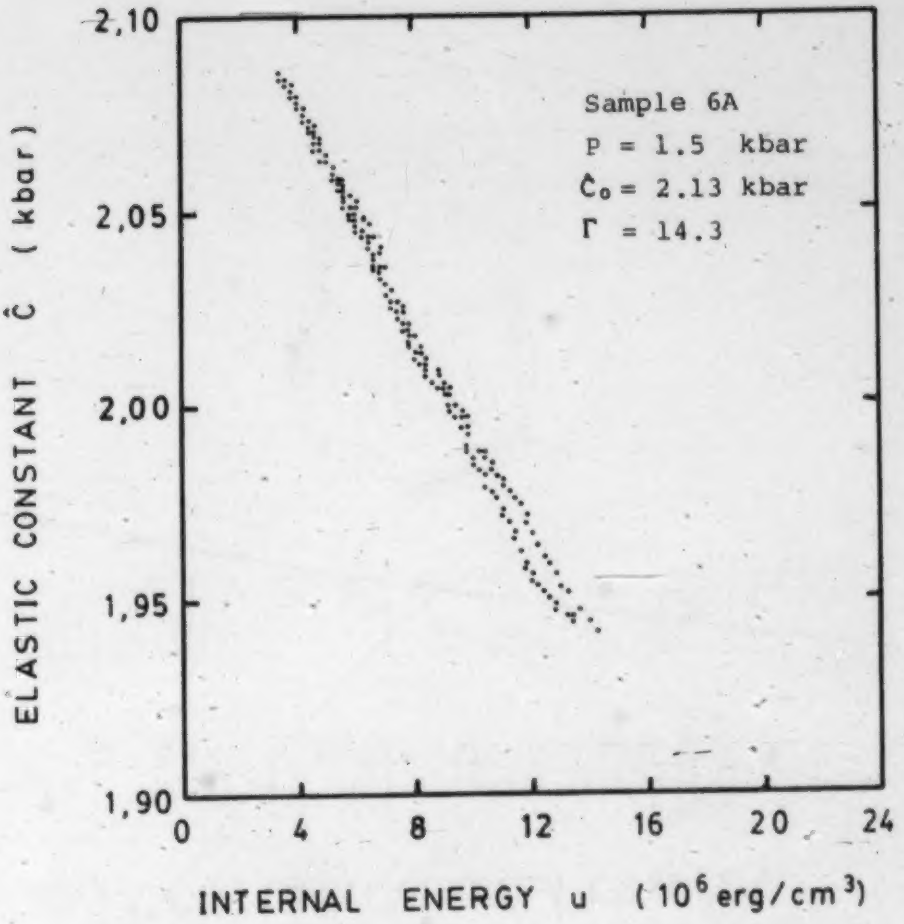

Fig. 4.19 Ĉ Dependence on u(T) in Sample 6A

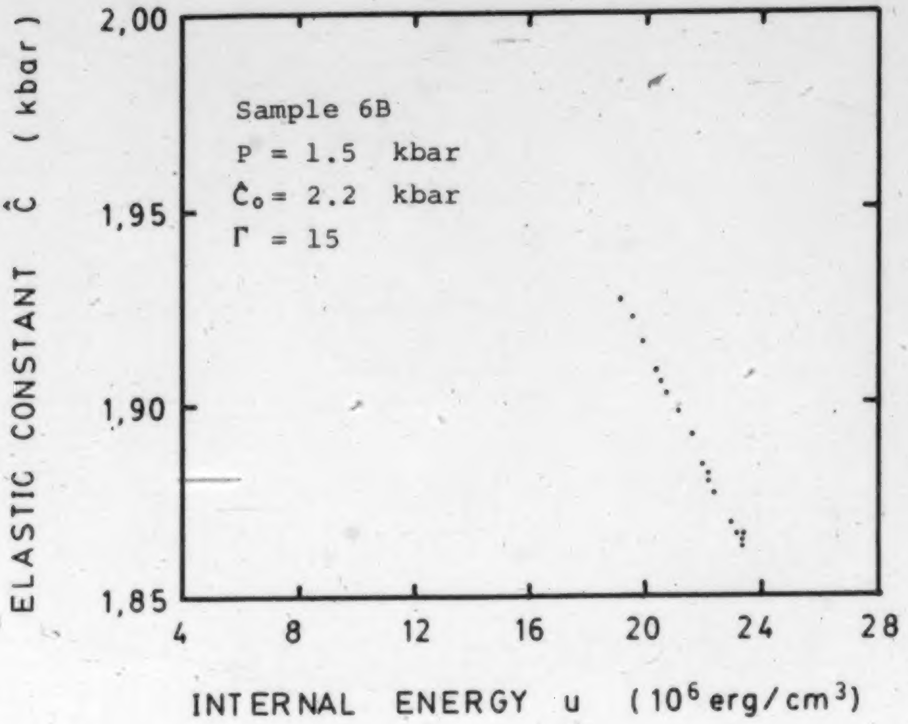

Fig. 4.20 $\hat{C}$ Dependence on u(T) in Sample 6B

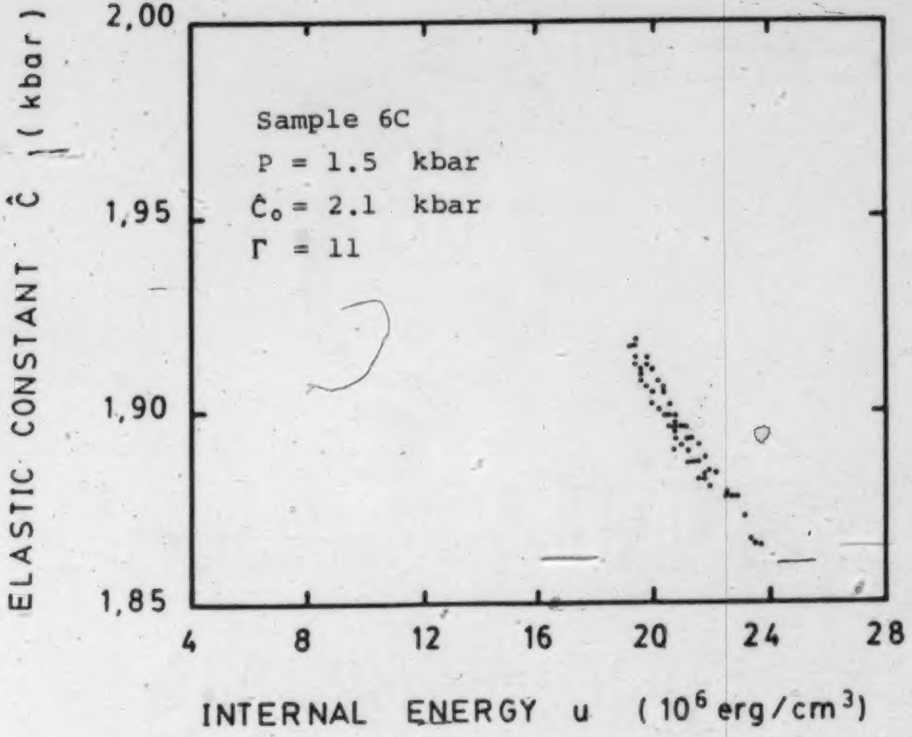

Fig. 4.21 Ĉ Dependence on u(T) in Sample 6C

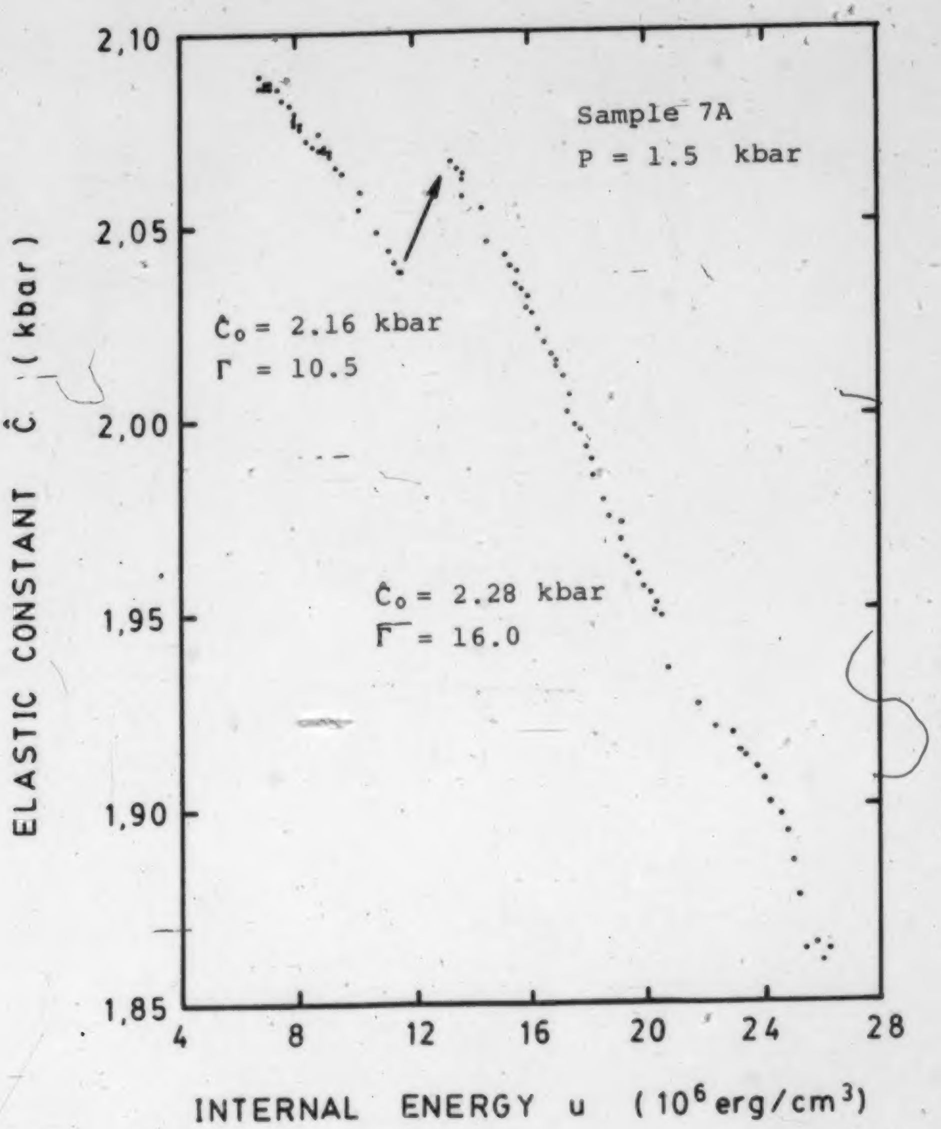

Fig. 4.22 Ĉ Dependence on u(T) in Sample 7A

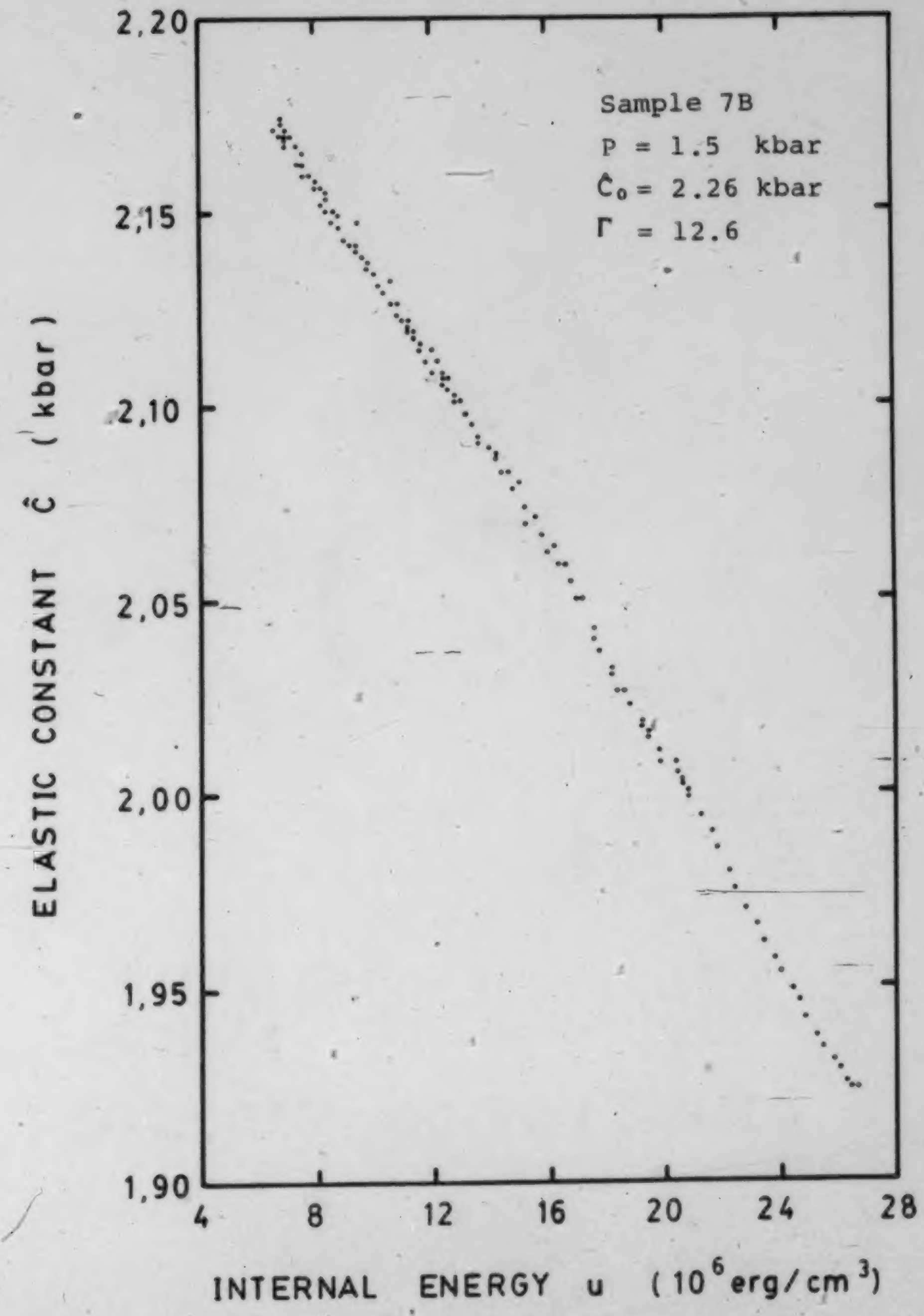

Fig. 4.23 $\hat{C}$ Dependence on $\underline{u}(T)$ in Sample 7B

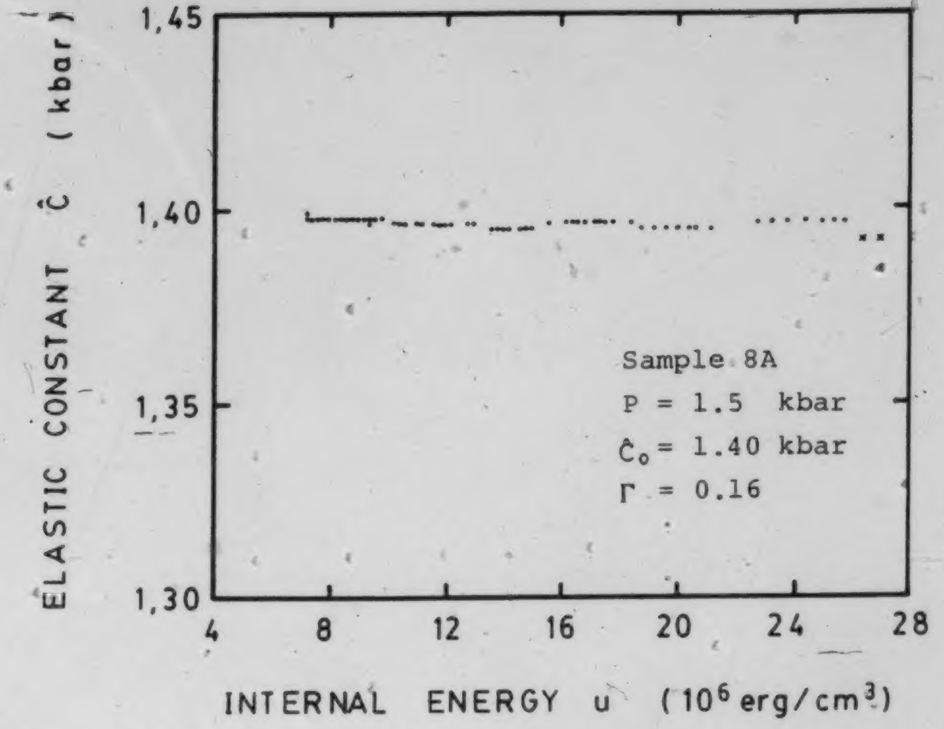

Fig. 4.24 $\hat{C}$ Dependence on u(T) in Sample 8A

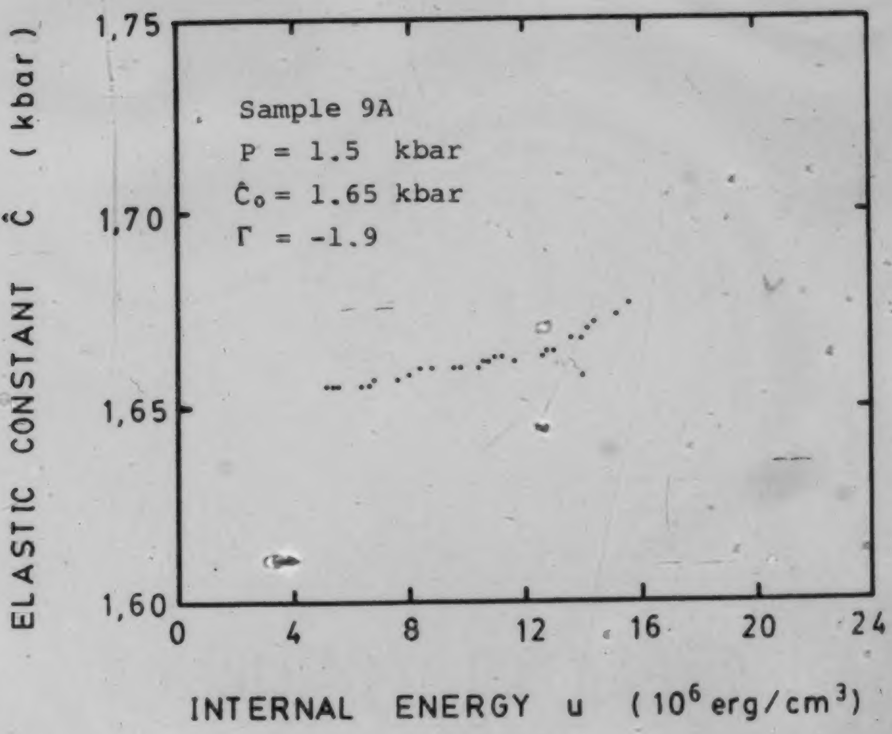

Fig. 4.25 $\hat{C}$ Dependence on u(T) in Sample 9A

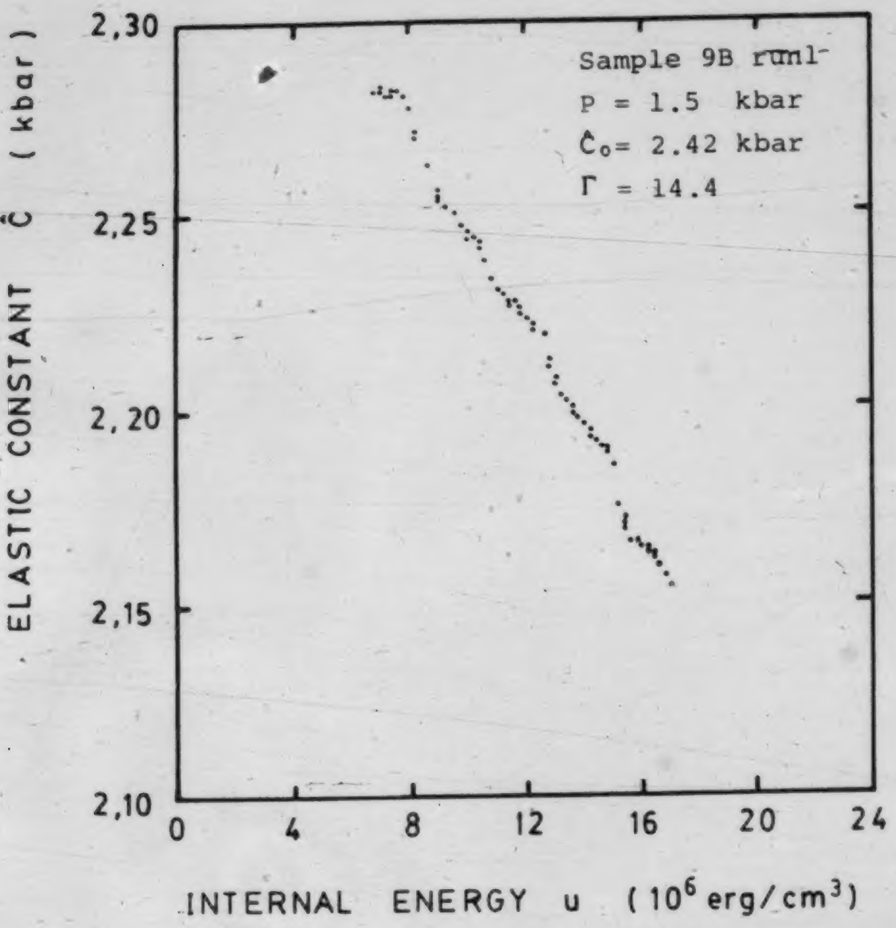

Fig. 4.26 Ĉ Dependence on u(T) in Sample 9B run1

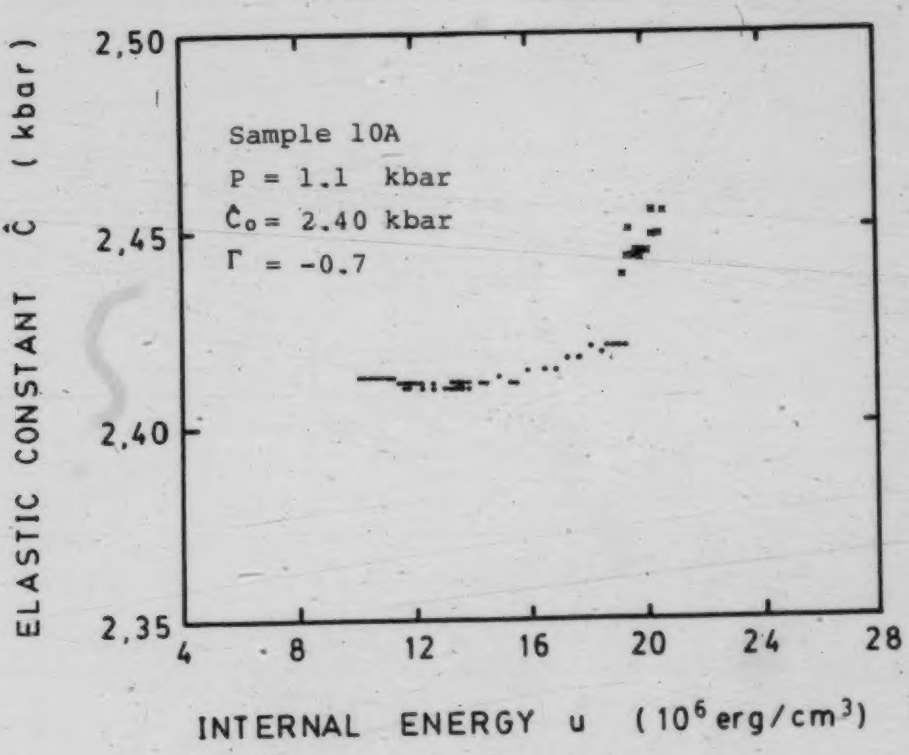

Fig. 4.28 $\hat{C}$ Dependence on u(T) in Sample 10A

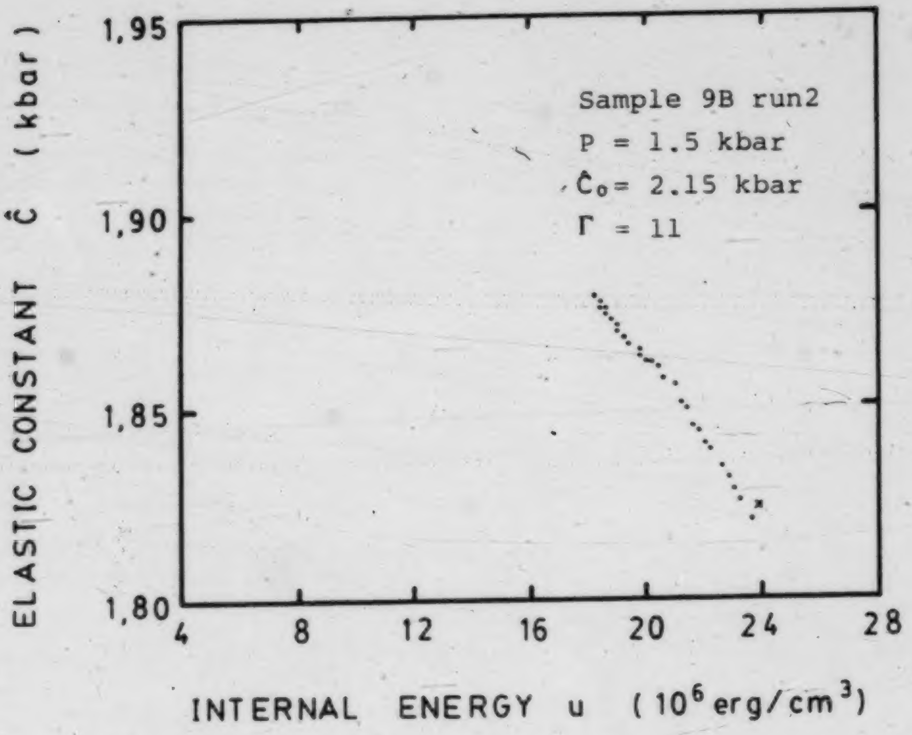

Fig. 4.27 Ĉ Dependence on u(T) in Sample 9B run2

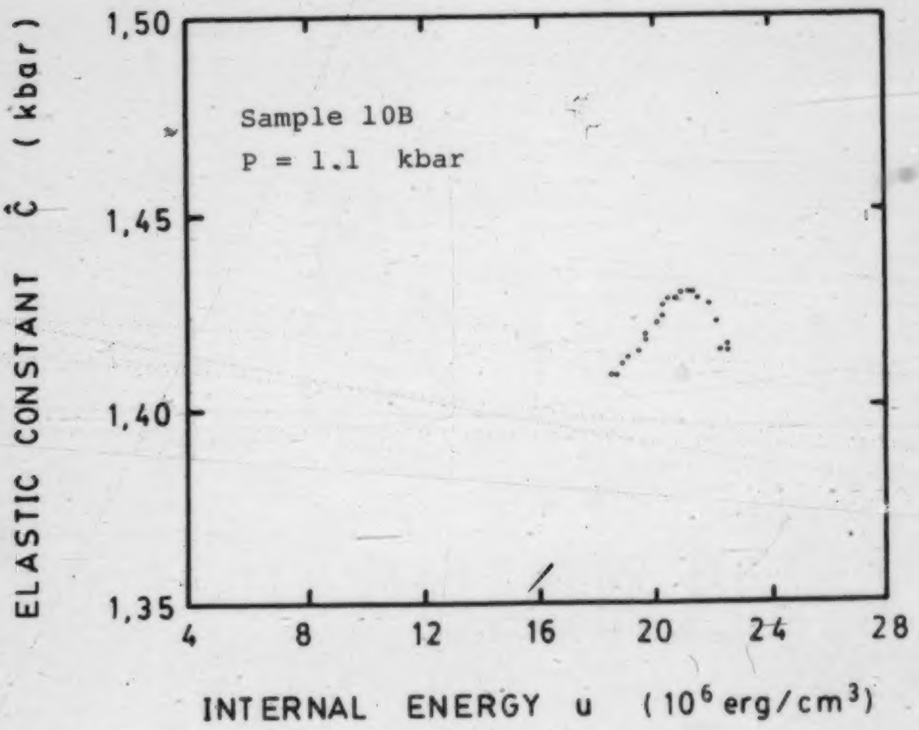

Fig. 4.29 Ĉ Dependence on u(T) in Sample 10B

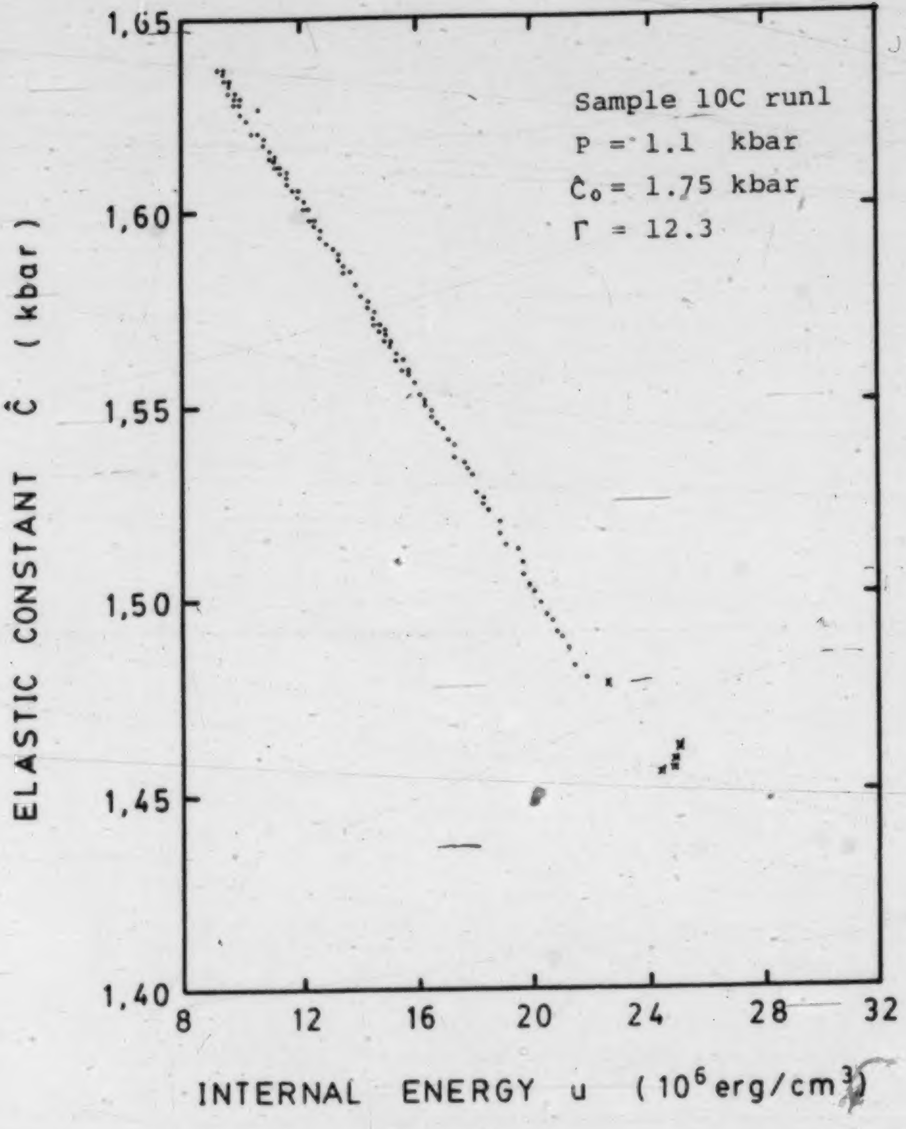

Fig. 4.30 Ĉ Dependence on u(T) in Sample 10C run1

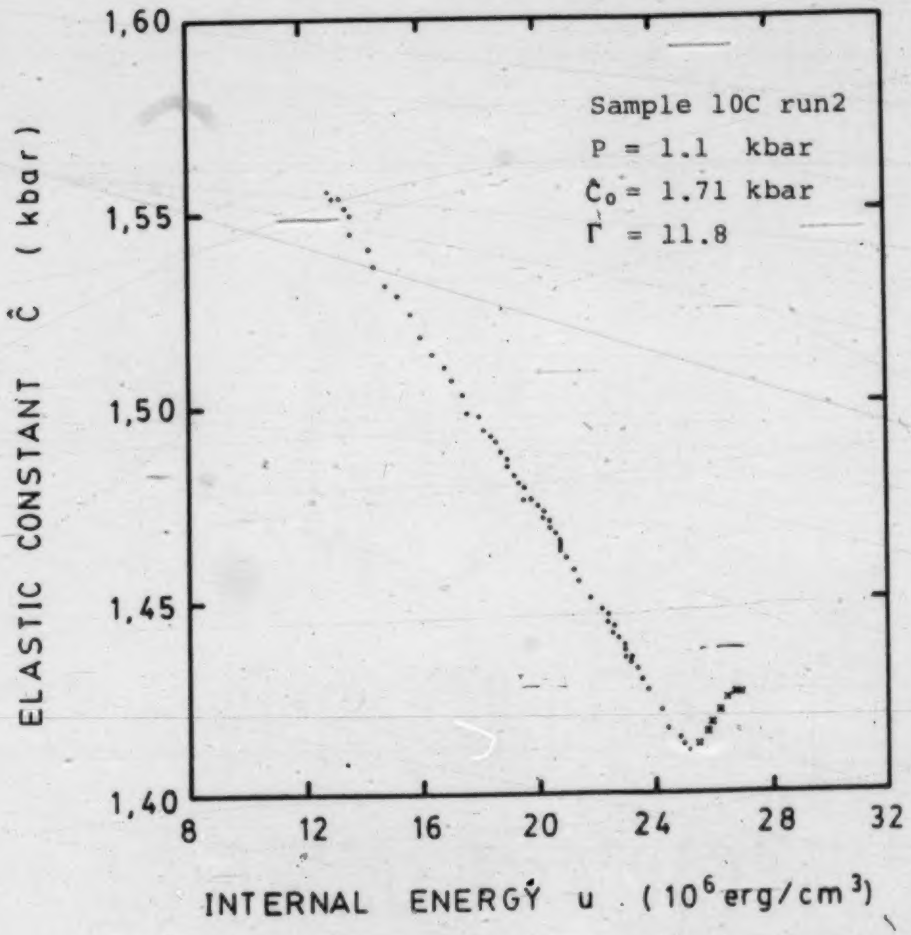

Fig. 4.31 $\hat{C}$ Dependence on u(T) in Sample 10C run2

Table 4.1

Measured Values of $\hat{C}_0$ in Γ in hcp ^{4}He

sample	$\hat{C}_0$	error	Γ	error
1A run1	2.2494	.0005	13.42	.02
1A run2	2.2488	.0008	13.27	.03
1B	2.246	.004	13.2	.2
2A	2.321	.003	13.59	.10
3A	3.425	.003	12.88	.08
4A	2.248	.009	12.0	.2
4B	3.48	.02	12.6	.5
5A	2.21	.08	11.8	1.7
5B	2.22	.05	11.5	1.2
5C	1.663	.006	4.93	.15
5D run1	2.51	.06	12.2	1.3
5D run2	2.63	.10	11.5	2.1
5E	2.47	.02	10.4	.6
6A	2.133	.002	14.34	.12
6B	2.2	.1	15	2
6C	2.1	.2	11	4
7A run1	2.16	.03	10.5	1.6
7A run2	2.28	.04	16.0	.9
7B	2.261	.004	12.61	.13
8A	1.399	.009	0.16	.03
9A	1.649	.008	-1.9	.3
9B run1	2.422	.013	14.4	.5
9B run2	2.15	.10	11.2	2.4
10A	2.403	.014	-0.7	.5
10C run1	1.752	.004	12.29	.13
10C run2	1.707	.009	11.8	.2

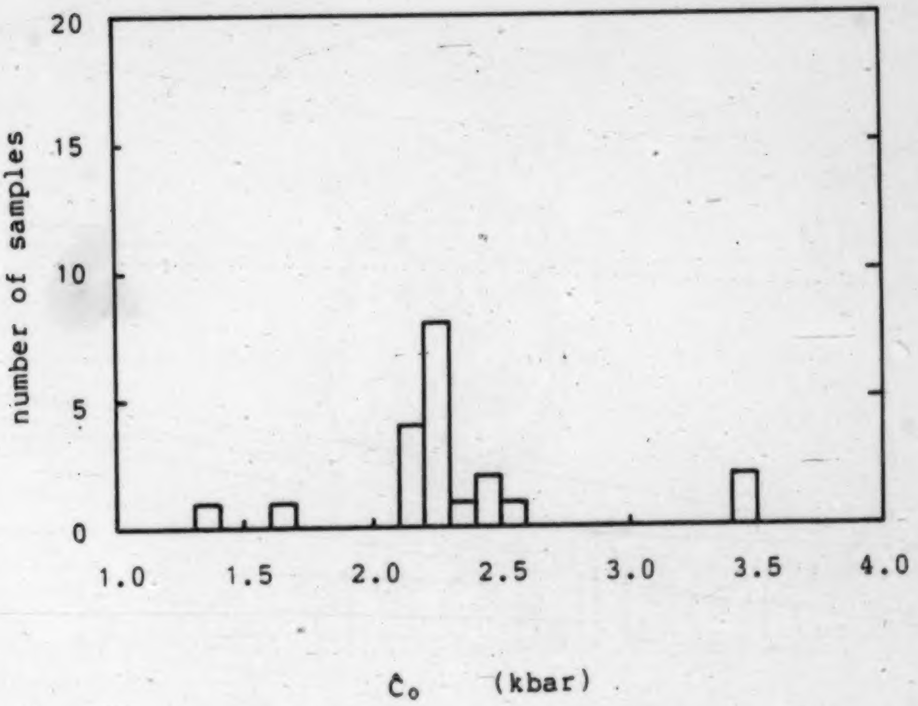

Fig. 4.32 Distribution of Values of $\hat{C}_0$ in ^4He at 1.5 kbar

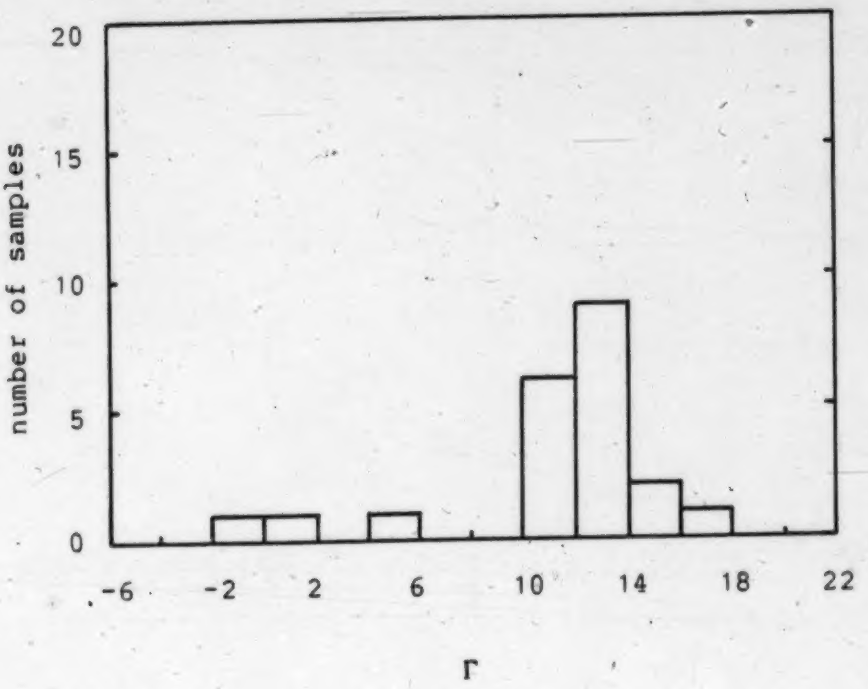

Fig. 4.33 Distribution of Values of Γ in ⁴He at 1.5 kbar

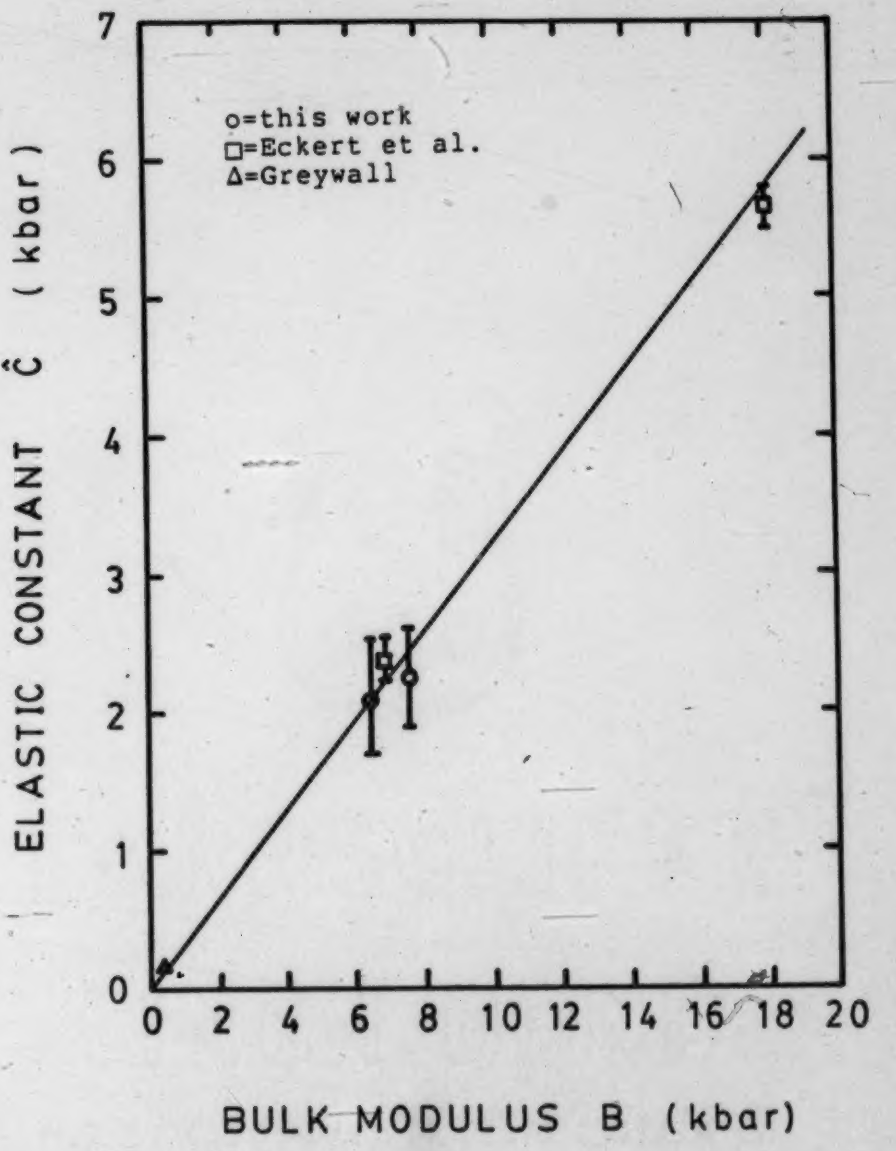

Fig. 4.34 Transverse Mode Elastic Constant in ⁴He at Several Pressures

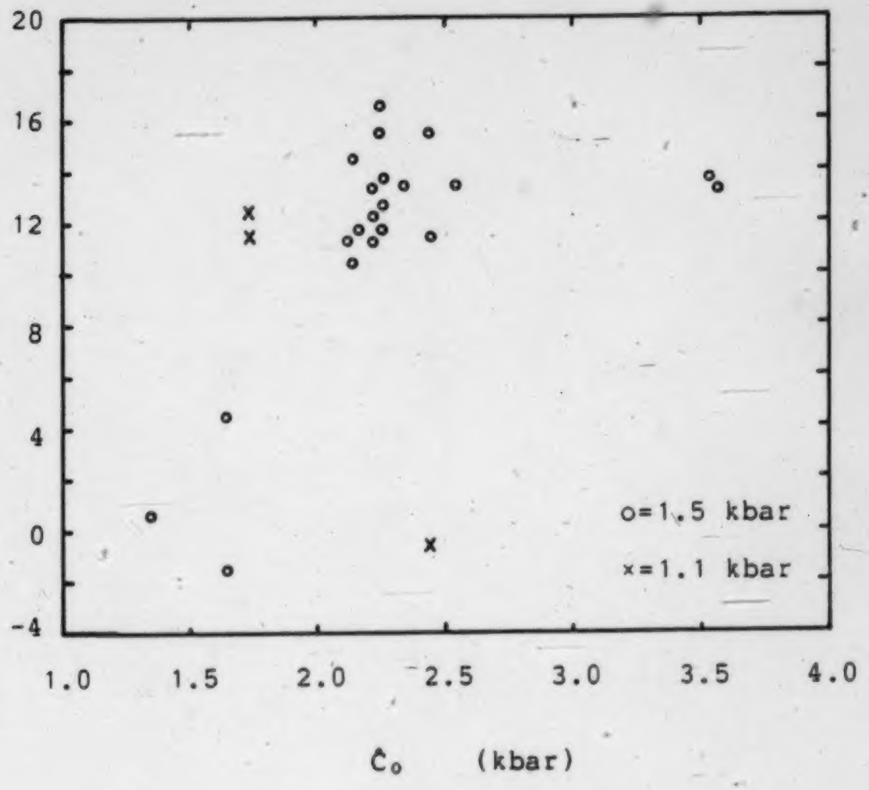

Fig. 4.35 $\hat{C}_0$ Dependence on Γ in ^{4}He at 1.1 and 1.5 kbar

Table 4.2

Values of $\Gamma_{\alpha\beta}$ in hcp Materials

	Γ_{11}	Γ_{44}	Γ_{66}	Debye Temp. (K)	P (bar)	ref.[a]
Be	45	24	20	1780	1	1
Mg	12	6	4	394	1	2
Zn	27	13	13	318	1	3&4
Cd	37	10	17	216	1	5
Y	21	10	9	262	1	6
H_2[b]	29			115[f]	65	7
H_2[b]		27	27	116[f]	72	7
D_2[c]	24[h]			107[f]	99	7
D_2[d]		20	20	106[f]	95	7
^{4}He	26±8			26	40	8
^{4}He[e]	23±10			26	40	9
^{4}He	23±3			36	120	10
^{4}He		12±8	12±8	96	1500	11
^{3}He	31±8			42[g]	140	12
^{3}He	27±8			49[g]	180	12

[a] The references are listed on the next page.

[b] para-H_2.

[c] ortho-D_2 with 2% para-D_2.

[d] ortho-D_2 with 5% para-D_2.

[e] with 1% ^{3}He.

[f] The Debye temperature was interpolated from the data of reference 7.

[g] Interpolated from the data of reference 13.

[h] This is a better estimate of Γ_{33} than Γ_{11} since $\hat{k}$ was only 15° off the c-axis.

References for Table 4.2

1) F.J. Smith & C.L. Arbogast, J. Appl. Phys., 31, 99 (1960).

2) L.J. Slutsky & C.W. Garland, Phys. Rev., 107, 972 (1957).

3) C.W. Garland & R. Dalven, Phys. Rev., 111, 1232 (1958).

4) G.A. Alers & J.R. Neighbours, Phys. & Chem. Solids, 7, 58 (1958).

5) C.W. Garland & J. Silvermann, Phys. Rev., 119, 1218 (1960).

6) J.F. Smith & J.A. Gjevre, J. Appl. Phys., 31, 645 (1960).

7) R. Wanner & H. Meyer, J. Low Temp. Phys., 11, 715 (1972).

8) I. Iwasa, H. Suzuki, & K. Araki, J. Phys. Soc. Jpn., 46, 1119 (1979).

9) I. Iwasa & H. Suzuki, J. Phys. Soc. Jpn., 49, 1722 (1980).

10) D.I. Calder: Ph.D. Thesis, University of Alberta, Edmonton Canada, (1977, unpublished).

11) This work

12) J.R. Beamish, Ph.D. Thesis, University of Alberta, Edmonton Canada, (1982, unpublished).

13) H.H. Sample and C.A. Swenson, Phys. Rev., 158, 188 (1967).

G. BIBLIOGRAPHY

Ahlers, G., Phys. Rev. A, 2, 1505 (1970).

Alers, G.A, and Neighbours, J.R., Phys. & Chem. Solids, 7, 58 (1958).

Barford, N.C., Experimental Measurements: Precision, Error and Truth, (Addison-Wesley, Don Mills, Canada, 1967).

Beamish, J.R. and Franck, J.P., Phys. Rev. Lett., 47, 1736 (1981).

Beamish, J.R., Ph.D. Thesis, University of Alberta, Edmonton Canada, (1982, unpublished).

Beattie, J.A., J. Math. and Phys., 6, 1 (1926-1927).

Boyer, H.E. and Gall, T.L. eds., Metals Handbook (Desk Edition), (Ameican Society for Metals, Metals Park, Ohio, 1985), P. 1.44.

Breazeale, M.A., Cantrell, J.H. Jr. and Heyman, J.S., in Methods of Experimental Physics ed. Edmonds, P.D., (Academic Press, New York, 1981), vol. 19, P. 67.

Calder, I.D. and Franck, J.P., Phys. Rev. B, 15, 5262 (1977).

Calder, I.D., Ph.D. Thesis, University of Alberta, Edmonton Canada, (1977, unpublished).

Crepeau, R.H. and Lee, D.M., Phys. Rev. A, 6, 516 (1972).

Crepeau, R.H., Heybey, O., Lee, D.M., and Strauss, S.A., Phys. Rev. A, 3, 1162 (1971).

Driessen, A.,van der Poll, E., and Silvera, I.F., Phys. Rev. B, 33, 3269 (1986).

Dugdale, J.S. and Franck, J.P., Phil. Trans. Roy. Soc. (London), A257, 1 (1964).

Eckert, J., Thomlinson, W., and Shirane, G., Phys. Rev. B, 18, 3074 (1978).

Faulk, F., J. de Physique, sup. 12, C4-3 (1982).

Franck, J.P., Phys. Rev. Lett., 11, 208 (1964).

Garland, C.W. and Dalven, R., Phys. Rev., 111, 1232 (1958).

Garland, C.W. and Silvermann, J., Phys. Rev., 119, 1218

(1960).

Granato, A.V., Lucke, J., J. Appl. Phys., *27*, 583 (1956).

Granato, A.V.,Schwarz, R.R., and Kneezel, G.A., J. de Physique, *42*, sup. 10, C5-1055 (1981).

Granato, A.V., and Kneezel, G.A., J. de Physique, *42*, sup. 10, C5-1061 (1981).

Greywall, D., Phys. Rev. A, *3*, 2106 (1971).

Gunton, D.J., and Saunders, G.A. Solid St. Commun., *14*, 865 (1974).

Hiedemann, E.A. and Hoesch, K.H., Z. Phys., *90*, 322 (1934).

Iwasa, I., Suzuki, H., and Araki, K., J. Phys. Soc. Jpn., *46*, 1119 (1979).

Iwasa, I., and Suzuki, H., J. Phys. Soc. Jpn., *49*, 1722 (1980).

Leibfried, G., and Ludwig, W., in *Solid State Physics*, eds. F. Seitz & D. Turnbull, (Academic Press, New York, 1961), vol. 12, P. 275.

May, J.E. Jr., IRE Nat. Conv. Rec., *6*, Pt. 2, 134 (1958).

Minkiewicz, V.J., Kitchens, T.A., Lipchultz, F.P., Nathans, R., and Shirane, G., Phys. Rev., *174*, (1968).

Musgrave, M.J.P., *Crystal Acoustics*, (Holden-Day, San Fancisco, 1970).

Nakanishi, N., Progress in Materials Science, *24*, 143 (1979).

Perkins, A.J., Scripta Met., *8*, 31, (1974).

Reese, R.A., Sinha, S.K., Brun, T.O., and Tilford, C.R. Phys. Rev. A, *3*, 1688 (1971).

Sample, H.H. and Swenson, C.A., Phys. Rev., *158*, 188 (1967).

Slutsky, L.J., and Garland, C.W., Phys. Rev., *107*, 972 (1957).

Smith, F.J., and Arbogast, C.L., J. Appl. Phys., *31*, 99 (1960).

Smith, F.J., and Gjevre, J.A., J. Appl. Phys., *31*, 645 (1960).

Tsymbalenko, V.L., Sov. Phys. J.E.T.P., *60*, 537 (1984).

Wallace, D.C., Thermodynamics of Crystals, (John Wiley & Sons, New York, 1972).

Watson, G.H. and Daniels, W.B., Phys. Rev. B, 31, 4705 (1985).

Wanner, R. and Franck, J.P., Phys Rev. Lett., 24, 365 (1970).

Wanner, R., Mueller, K.H., and Fairbank, H.A., J. Low Temp. Phys., 13, 153 (1973).

Wanner, R. and Meyer, H., J. Low Temp. Phys., 11, 715 (1973).

Wanner, R., Meyer, H. and Mills, R.L., J. Low Temp. Phys., 13, 337 (1973).

Wanner, R., Iwasa, I. and Wales, S., Solid State Commun., 18, 853 (1976).

Zener, C., Phys Rev., 49, 122 (1936).

V. ATTENUATION OF TRANSVERSE SOUND AND THE fcc-hcp ^{4}He TRANSFORMATION

A. INTRODUCTION

As it propagates, sound diminishes in amplitude by the factor $e^{-\alpha x}$, where x is the distance that the sound has propagated and α is the attenuation coeficient. Attenuation in solids may result from crystal defects that scatter or absorb energy from the sound field. Attenuation changes preceding some martensitic transformations have been associated with the dynamics of the transformation.[38] [39] [40]

It was of interest to determine if attenuation changes near the fcc-hcp ^{4}He transformation were associated with the dynamics of the transformation. This study constitutes the first investigation of the attenuation in ^{4}He near the fcc-hcp phase line.

B. EXPERIMENT

The acoustic high pressure cell, thermometry, pressure system, helium supply, and cryogenic equipment for this experiment were the same as that for the velocity measurements described in chapter IV,

The basic pulse echo technique for attenuation measurement[41] was used. A train of ultrasonic echoes was produced in solid helium and the signal from the echoes was displayed on an oscilloscope. The technique for doing this was the same as described for the relative velocity measurements described in chapter IV.

---

[38] N. Nakanishi, Progress in Material Science, 24, 143, (1979).
[39] A.V. Granato, R.R. Schwarz and G.A. Kneezel, J. de Physique, 42, sup. 10, C5-1055 (1981).
[40] R. Wanner, H. Meyer and R.L. Mills, J. Low Temp. Phys., 13, 853 (1976).

A video camera monitored the oscilloscope that displayed the echo train. A second video camera monitored the solid helium with the intensity contrast method described in chapter III. The two video images were mixed with a special effects generator and recorded on a video cassette recorder. During some transitions, the image of the computer screen, which displayed the cell temperature, was also mixed into the video image and recorded.

After data acquisition was complete, the tape was replayed and held in freeze frame in many places. In each freeze frame the height of the echo signals on the oscilloscope image were recorded. The peak heights were fit to:

$$h = h_0 \exp(-\alpha d(2n-1)) \qquad (5.1)$$

where h is the height of the n^{th} received acoustic pulse, h_0 is the height of the initial pulse, d is the separation of the transducers and α is the attenuation.

---

[41] M.A. Breazeale, J.H. Cantrell Jr. and J.S. Heyman, in Methods of Experimental Physics ed. P.D. Edmonds (Academic Press, New York, 1981) Vol. 19, P. 67.

When the attenuation was less than .4 cm^{-1}, over ten echoes could be observed and the attenuation measurement accuracy was about 10%. The accuracy was limited by the fact that the echo envelope did not perfectly follow eq. 5.1. When the attenuation was more than 1 cm^{-1}, the shapes of the echoes were very irregular. Typically two echoes could be observed through the "noise background". The accuracy of these measurements was limited to about 50% by the uncertainty in the determination of the height of an irregularly shaped echo.

The samples were assumed to be single crystals, or at least consist of large grains, because visual observations (see chapter III) indicated that ^{4}He generally forms single crystals or large grain samples.

C. RESULTS

Attenuation of transverse sound was measured for for 21 hcp and 21 fcc samples of ^{4}He at 1.5 kbar. A sample was slowly solidified and cooled into the hcp phase. Subsequent samples were produced by passing through the fcc-hcp transformation. The solid was not melted during the course of the experiment. The attenuation in the fcc phase was generally much higher the the attenuation in the hcp phase. This is illustrated in the distribution of measured attenuation values shown in fig. 5.1. The attenuation in hcp ^{4}He was typically .4 cm^{-1} and the attenuation in fcc ^{4}He was typically 1 cm^{-1}.

The attenuation in the samples changed little between transformations, but changed dramatically during a transformation. For most transformations, the attenuation change was primarily monotonic and had only small attenuation fluctuations superimposed on the monotonic attenuation change. During a few transformations, the attenuation fluctuations were more pronounced. In a few cases, the attenuation clearly went through a minimun during the transformation.

D. DISCUSSION

The attenuation was generally much higher in the fcc than in the hcp phase. This result can be compared with the result in solid H_2. In solid H_2, the attenuation in the cubic phase is higher than the attenuation in the hcp phase.[42] In H_2, the cubic phase occurs at a lower temperature than the hcp phase. The attenuation change has been attributed to the dynamics of the phase transformation[43] in the following way: The first cooling transition introduces lattice defects that remain in the crystal after the completion of transformation. These defects increase the attenuation. The reverse transformation (the first heating transformation) removes the defects and results in a decrease in attenuation.

---

[42] R. Wanner, H. Meyer and R.L. Mills, J. Low Temp. Phys., 13, 853 (1976).

[43] R. Wanner, H. Meyer and R.L. Mills, J. Low Temp. Phys., 13, 853 (1976).

In solid helium the situation is different. The first cooling transition causes a decrease in attenuation. Since it is unlikely that the first cooling transition would remove defects, the attenuation change appears to be unrelated to the dynamics of the transformation. Rather, it appears that the higher attenuation in the fcc ^{4}He phase is directly due to the different crystal structures. Perhaps higher attenuation of the fcc phase is connected to the fact that the fcc phase has slip planes ({111}) in four orientations and the hcp phase has slip planes ({0001}) in only one orientation. Perhaps different attenuations in solid H_2 are also directly due to the different crystal structures rather than the transformation dynamics.

E. SUMMARY

The attenuation of transverse sound was measured in ^{4}He at 1.5 kbar. The attenuation was generaly higher in the fcc phase than in the hcp phase. The difference in attenuation appears to be directly due to the difference in the crystal structure and not related to the dynamics of the formation of the crystal.

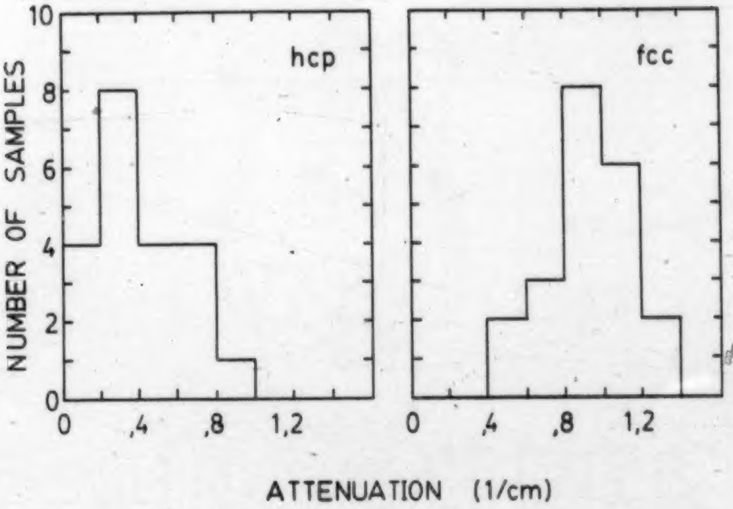

Fig. 5.1 Distribution of Measured Values of Attenuation of Transverse Sound
a) (left) in hcp ^{4}He
b) (right) in fcc ^{4}He

F. BIBLIOGRAPHY

Breazeale, M.A., Cantrell,J.H., Jr. and Heyman, J.S., in Methods of Experimental Physics ed. P.D. Edmonds (Academic Press, New York, 1981) Vol. 19, P. 67.

Nakanishi, N., Progress in Material Science, 24, 143, (1979).

Granato, A.V., Schwarz, R.R. and Kneezel, G.A., J. de Physique, 42, sup. 10, C5-1055 (1981).

Wanner, R., Meyer, H. and Mills, R.L., J. Low Temp. Phys., 13, 853 (1976).

VI. CONCLUSIONS

Four approaches were taken to investigate the dynamics of the fcc-hcp ^{4}He transformation.

A kinetic study was done in which temperature oscillations (of amplitude smaller than the temperature hysteresis) about the equlibrium temperature were produced. When an fcc-hcp interface was present in the sample during the temperature oscillations, it was found that the temperature oscillations produced oscillations in the interface. This demonstrated that interface was very mobile. The high interface mobility shows that the transformation is a thermoelastic martensitic transformation. If the progress of the transformation was interrupted, it became more difficult to bring the interface into motion again. After holding the interface for several minutes, the interface was made to move only when the solid was superheated to a temperature near A_s or supercooled to a temperature near M_s. These observations indicated that the transformation kinetics are dominated by the activation barrier that the interface must surmount before it can become glissile. The activation barrier was estimated (for a 1.2 kbar ^{4}He sample) to be 10^3 erg/cm^3. The elastic force opposing the transformation (although present) was much less than the activation barrier. This categorizes the transformation as a Class I thermoelastic martensitic transformation.

A study of the fcc-hcp ^{4}He transformation morphology was made. The visual method for this investigation used the optical birefringence of the hcp phase to distinguish it from the optically isotropic fcc phase. The fact that metallurgists have have been able to determine much about transformation dynamics from morphological observations, lent hope that this investigation would lead to a better understanding of the transformation dynamics. The transformation appeared to be heterogeneously nucleated. For some transformations, the progress of the interface was hindered by defects in the solid. The interaction of the interface with crystal defects is the most direct evidence that the transformation is indeed martensitic. There were several observations of transformations occurring by the passage of a single planar interface across the entire sample. This indicates that the samples produced were single crystals or at least consisted of large grains. This is strong evidence that the transformation is a thermoelastic martensitic transformation. The hcp orientation was reproduced in consecutive transformations. This supports previous evidence of a lattice orientation relation. A preferred orientation for the interface was observed; however, the preferred orientation did not appear to be unique. During some transformations, the interface rotated about a pivot. The pivot was the site of a defect in the crystal to which the interface was pinned. Bands sometimes appeared in the solid helium image when the helium was rapidly cooled or heated near the transformation temperature. These bands may have indicated the presence of different hcp variants formed either by twinning or by the fcc→hcp transformation.

A new model was presented for the interface structure. In the model, the interface consistsd of a coupled Shockley partial dislocation array (CSPA). The coupling of the partials results from having an equal number of the three partials Aδ, Bδ and Cδ on any small portion of the interface. The model predicts no net deformation to occur during the advance of the interface. The model also predicts that the interface would have a preferred orientation with three-fold degeneracy. The model allows the interface to travel outside of the preferred orientation if the interface is pinned along one line. All the morphological observations, except for the production of bands, were explained in terms of this model.

The observations that the transformation is a thermoelastic martensitic transformation suggested that the transformation may have mode softening associated with the dynamics of the transformation. To determine if mode softening occurs in ^{4}He, measurements of the transverse sound velocity near the fcc-hcp ^{4}He phase line were made. The transverse sound velocity was found to decrease as much as 7% as the hcp→fcc transformation was approached. The temperature dependence of the sound velocity was explained very well by the quasi-harmonic approximation. This theory predicts that the elastic constant depends linearly on the thermal component of the internal energy of the solid. The derivative of the elastic constant with respect to internal energy, Γ, was found to be mode dependent and usually about twelve. This value for Γ was found to be nearly the same in all hcp materials. This is truly remarkable since the elastic constants in the hcp materials for which Γ was calculated varied by a factor of 9000. To my knowledge, the universality of Γ has not been pointed out. The transverse sound modes did not soften sufficiently for homogeneous nucleation by a phonon nucleation mechanism to be possible.

No evidence was found of the sound velocity being affected by oscillations in the thickness of extended dislocations.

Acoustic attenuation changes have been associated with the transformation dynamics in some martensitic transformations. Attenuation of transverse sound was measured in ^{4}He to determine if the transformation dynamics affected the attenuation. The attenuation was found to be much higher in the fcc phase (typically 1 cm^{-1}) than in the hcp phase (typically .4 cm^{-1}). Attenuation differences appeared to be directly related to the difference in the crystal structures and not related to the dynamics of the transformation.

VII. APPENDIX: Energy of a Dislocation Assembly

The elastic strain energy, which makes up most of the dislocation energy, of a single dislocation is given by[44]:

$$U = A\,b^2 \tag{A.1a}$$

where b is the Burgers vector and A is given by:

$$A = \frac{GL\,\ln(R/r_0)}{4\pi(1-\nu)}\,(1-\nu\cos^2\alpha) \tag{A.1b}$$

where G is the shear modulus, L is the dislocation length, ν is the Poisson ratio, R and r_0 are the outer and inner radii of the cylindrical region over which the elastic approximation for the strain field is valid, and α is the angle between the dislocation line and the Burgers vector. R may be taken to be the radius of the grain and r_0 may be taken to be on the order of b. Careful estimation of R and r_0 is not necssary because U is not sensitive to their values. Since ν is about 1/3, the value of $(1-\nu\cos^2\alpha)$ will vary by less than a factor of two. Therfore, within a factor of two, A is independent of the Burgers vector, b.

The energy of an assembly of dislocations that are so widely separated that their elastic strain fields do not interact significantly will be given as:

---

[44] D. Kuhlmann-Wilsdorf, "Dislocations", in Physical Metallurgy, R.W. Cahn ed, (John-Wiley & Sons, New York, 1965).

$$E = \Sigma U_i = A \Sigma b_i^2 \qquad (A.2)$$

where U_i is the energy of the i^{th} dislocation and b_i is the magnitude of the Burgers vector of the i^{th} dislocation.

At the other extreme, the separation between the dislocations in an assembly may be so small that the strain field of each dislocation may be approximately centered on the same line. A Burgers circuit about this line will give the total Burgers vector, $\underline{b}^T$, where:

$$\underline{b}^T = \Sigma \underline{b}_i \qquad (A.3)$$

and the energy of the group of dislocations can be calculated from eq. A.1 as:

$$E = A (\underline{b}^T)^2 = A (\Sigma \underline{b}_i)^2 \qquad (A.4)$$

In summary, an assembly of widely separated dislocations has an energy approximately proportional to the sum of the squares of the Burgers vectors, and an assembly of dislocations in close proximity has an energy approximately proportional to the square of the sum of the Burgers vectors.